Drug Research Program
Division of Pharmaceutical Chemistry and Technology
Faculty of Pharmacy
University of Helsinki
Finland

IMMOBILIZED ENZYME MICROREACTORS IN DRUG METABOLISM RESEARCH

Iiro Kiiski

ACADEMIC DISSERTATION

To be presented, with the permission of the Faculty of Pharmacy of the University of Helsinki, for public examination in lecture hall 1041, Biocenter 2,
on the 12th of February, 2021 at 13 o'clock

Helsinki 2021

ISBN 978-951-51-6923-5 (paperback)
ISBN 978-951-51-6924-2 (PDF)
ISSN 2342-3161 (print)
ISSN 2342-317X (online)
https://ethesis.helsinki.fi/

The Faculty of Pharmacy uses the Urkund system (plagiarism recognition) to examine all doctoral dissertations

Published in
Dissertationes Scholae Doctoralis Ad Sanitatem Investigandam Universitatis Helsinkiensis

Unigrafia, Helsinki 2021

Supervisor	Associate Professor Tiina Sikanen Drug Research Program Division of Pharmaceutical Chemistry and Technology Faculty of Pharmacy University of Helsinki Finland
Co-Supervisors	PhD (Pharm.) Päivi Järvinen Drug Research Program Division of Pharmaceutical Chemistry and Technology Faculty of Pharmacy University of Helsinki Finland
	PhD Ville Jokinen Department of Materials Science and Engineering School of Chemical Engineering Aalto University Finland
Reviewers	Professor Polona Žnidaršič-Plazl Faculty of Chemistry and Chemical Technology University of Ljubljana Slovenia
	Professor Vincenza Andrisano Department for Life Quality Studies University of Bologna Italy
Opponent	Professor Nicolas Szita Department of Biochemical Engineering University College London United Kingdom

Abstract

Drug metabolism is an enzyme-catalyzed process that has major implications for a drug's safety and efficacy. Consequently, evaluating the metabolic properties of a new drug candidate is of paramount importance already in the preclinical phase of drug development.

Although the available *in vitro* techniques for drug metabolism research have improved over recent years, the state-of-the-art methodology relies on enzyme assays conducted in static conditions, with limited spatiotemporal control of assay variables. Conducting metabolic assays under flow-through conditions could pave the way for more in-depth understanding of the mechanistic basis underlying drug-enzyme and drug-drug interactions. This, however, requires that drug-metabolizing enzymes be immobilized onto a solid support material without compromising protein folding or enzyme function. Although a wealth of different enzyme immobilization strategies are currently available, most of them are not amenable to immobilization of the microsomal, drug-metabolizing enzymes.

The aim of this thesis was to establish immobilized enzyme microreactor (IMER) platforms for studying drug metabolism under flow conditions, thereby improving the *in vitro-in vivo* prediction of the metabolic fate of new drug candidates. The use of microfluidics and microfabrication technology facilitated the straightforward implementation of flow-through assays and furthermore allows their multiplexing (parallelism) and integration with other operational units on a single platform, minimizing both reagent consumption and dead volumes.

In the first sub-project (publication I), a novel strategy for the immobilization of the membrane-bound enzymes cytochrome P450 (CYP) and UDP-glucuronosyltransferase (UGT) was designed and implemented on microreactors fabricated from off-stoichiometric thiol-enes (OSTE). The strategy was based on biotinylation of human liver microsomes via biotin-tagged fusogenic liposomes, and utilized the tunable surface chemistry of OSTEs to allow easy functionalization of the microreactor surface. The IMER platform was preliminarily characterized to ascertain enzyme stability and preservation of key enzyme kinetic parameters, with an emphasis on CYP-mediated (phase I) oxidoreductive reactions.

In the second sub-project (publication II), the feasibility of the IMER platform for studying the kinetics of UGT-mediated drug conjugation (phase II) was assessed, with an emphasis on the mechanistic basis for the pronounced underestimation of *in vivo* clearance kinetics by the currently available static *in vitro* techniques. In particular, the effect of membrane disruption and fatty-acid inhibition on UGT-kinetics *in vitro* was studied in detail. The kinetics of zidovudine glucuronidation (the model reaction used in this study) under flow-through conditions was shown to be in good agreement with that obtained using microsomal incubations in static conditions without the need for added pore-forming agents such as alamethicin.

In the third sub-project (publication III), the technology was further developed by incorporating a highly overlooked dimension in the assay design: the impact of oxygen partial pressure on the metabolic fate of drug candidates. This was achieved by exploiting the unique material-induced oxygen scavenging property of thiol-ene polymers. The developed chip design allowed the rapid and simple control of oxygen concentration in enzymatic assays, which is difficult to achieve with conventional static assay methods.

Overall, the developed methodology was shown to retain enzyme activity and native enzyme kinetic parameters of both CYP and UGT enzymes, an unconditional prerequisite for drug metabolism assays. With the immobilization method utilizing membrane biotinylation via liposome fusion, common problems (such as diffusion-limited kinetics and enzyme inactivation) associated with conventional immobilization approaches were circumvented. Furthermore, the universal applicability of the immobilization method for all membrane-bound enzymes was preliminarily demonstrated with recombinant CYP enzymes in sub-project/publication I.

The methodology developed here also enabled mechanistic studies focused on the alamethicin-induced membrane disruption (commonly used in UGT assays to overcome mass transfer limitations) and the proposed inhibitory effects of fatty acids, which may shed light on the foundations behind the poor *in vivo* correlation associated with UGT reactions *in vitro*.

The material-induced oxygen scavenging facilitated by OSTE polymers, together with microfluidic actuation, was shown to be an easily controllable approach for adjusting the oxygen partial pressure on demand. The advantage of this approach is that, unlike in typical approaches, complex chip designs or pressurized compartments are not needed. Beyond the demonstrated feasibility of the IMER platform for studying the impact of NADPH-cytochrome P450 oxidoreductase (POR)-mediated metabolism, the theoretical framework established here for OSTE-enabled oxygen control in microfluidic assays is likely to find many applications, particularly in organ-on-a-chip research.

In conclusion, the microreactor platform developed in this thesis offers an enabling toolbox for conducting *in vitro* drug metabolism assays under flow conditions that circumvents many of the key shortcomings of current state-of-the-art (static) *in vitro* enzyme assay methodology, as well as those of previously reported IMER platforms. At the time of publication, the methodology developed herein has already been utilized in several follow-up studies and has shown utility in diverse applications beyond this work.

Preface

This work was carried out at the Division of Pharmaceutical Chemistry and Technology, Faculty of Pharmacy, University of Helsinki during the years 2017–2020. The work was funded by the Doctoral Programme in Drug Research (DPDR), University of Helsinki.

First and foremost, I want to thank my supervisors Associate Professor Tiina Sikanen, Dr. Päivi Järvinen and Dr. Ville "Joksa" Jokinen. I am grateful for Tiina for constantly showing faith in me ever since I started working in her lab as an intern in 2015. Tiina, if in all these years I have managed to absorb even a fraction of your brilliance and tenacity, I am sure I will do well in life. Päivi, thank you for all the kind support and advice, and the (occasionally) fun times in the cell lab. Joksa, besides being one of the sharpest scientific minds I know, you are also a phenomenal pedagogue, and I have had the pleasure to learn a lot from you (Joksa is also most excellent company on conference trips!). I am also grateful for Professor Ryuji Kawano (Tokyo University of Agriculture and Technology) and Professor Shuhei Furukawa (Kyoto University) for all the hospitality (including karaoke, obviously) during my unforgettable research visit to Japan in spring 2019.

My sincerest thanks are also due to all the co-authors for their valuable contribution to this work. I wish to thank Tea Pihlaja, Lauri Urvas, Sanna Artes and Elisa Ollikainen from the Division of Pharmaceutical Chemistry and Technology for their help in the laboratory. Dr. Joanna Witos and Docent Susanne Wiedmer are acknowledged for their expertise in lipid chemistry.

I want to also thank all my (ex-) colleagues at the Division of Pharmaceutical Chemistry and Technology for creating a warm and inclusive work atmosphere. In particular, Erkka Järvinen is acknowledged for convincing me to apply for the DPDR salaried position, which proved out to be a worthwhile endeavor. Loving thanks to all the former and present members of our very own "CheMiSys" family. Having such nice people around has made all the work so much easier, and our shared coffee breaks have always been something to look forward to. In particular, I want to acknowledge Markus Haapala for his out-of-this-world BBQ skills, and Gowtham Sathyanarayanan and Kati Piironen for the moral support in the moments when things just were not going according to plan (which would be 90% of the time).

There is so much more to life than science and my friends have always been there to remind me of this fact when I have needed it the most. A page or two won't suffice to name all the people the company of which I've had the pleasure to enjoy on this journey, but I want to especially acknowledge all the fine gentlemen associated with the acronyms YJS and FAB4.

I certainly would not be where I am without my family. I do not have the words to tell how grateful I am to my parents, Sari and Markku, for their unwavering love and support during my entire life. Last, thank you Reetta, for being a shining beacon of love and compassion during the darkest of storms.

Helsinki, January 2021

Contents

List of original publications

This thesis is based on the following publications:

I **Iiro Kiiski**, Tea Pihlaja, Lauri Urvas, Joanna Witos, Susanne Wiedmer, Ville Jokinen, Tiina Sikanen. Overcoming the pitfalls of cytochrome P450 immobilization through the use of fusogenic liposomes. *Advanced Biosystems*, 3, 2019, 1800245 (6 pp). DOI: 10.1002/adbi.201800245

II **Iiro Kiiski**, Elisa Ollikainen, Sanna Artes, Päivi Järvinen, Ville Jokinen, Tiina Sikanen. Drug glucuronidation assays on human liver microsomes immobilized on microfluidic flow-through reactors. *European Journal of Pharmaceutical Sciences,* 158*,* 2021, 105677 (9 pp). DOI: 10.1016/j.ejps.2020.105677

III **Iiro Kiiski**, Päivi Järvinen, Elisa Ollikainen, Ville Jokinen, Tiina Sikanen. The material-enabled oxygen control in thiol-ene microfluidic channels and its feasibility for subcellular drug metabolism assays under hypoxia in vitro. *Manuscript*

The publications are referred to in the text by their corresponding roman numerals.

Author's contribution to the publications included in the doctoral thesis:

Publication I

The microchip fabrication was carried out by the author, with the exception of the SU-8 cleanroom master fabrication, which was carried out by Dr. Ville Jokinen. The immobilization protocol was conceived by the author. Experiments were designed by the author together with Dr. Susanne Wiedmer and Dr. Tiina Sikanen. The experimental work was executed by the author with contributions from others: Tea Pihlaja contributed to the optimization of the immobilization protocol, water contact angle measurements, and characterizing immobilized recombinant proteins; Lauri Urvas contributed to the characterization of recombinant CYP-IMERs; and Dr. Joanna Witos contributed to the characterization of liposomes. The publication was written by the author with contributions from co-authors.

Publication II

The microchip fabrication was carried out by the author, with the exception of the SU-8 cleanroom master fabrication, which was carried out by Dr. Ville Jokinen. The experiments were designed by the author with Dr. Ville Jokinen, Dr. Päivi Järvinen and Dr. Tiina Sikanen. Experiments were conducted by the author with contributions from others: Sanna Artes contributed to the characterization of immobilized UGT enzymes and Elisa Ollikainen contributed to the mass spectrometric analysis of glucuronide samples. The publication was written by the author with contributions from co-authors.

Publication III

The microchips and experiments were designed by the author together with Dr Ville Jokinen, Dr. Päivi Järvinen and Dr. Tiina Sikanen. Microchips were fabricated in full by the author. The experimental work was executed by the author, with Elisa Ollikainen contributing to the mass spectrometric analysis of drug metabolites. The publication was written by the author with contributions from co-authors.

List of additional publications

Additional publications closely related to the thesis work, but not included in the experimental part of this thesis:

1. Gowtham Sathyanarayanan, Markus Haapala, **Iiro Kiiski**, Tiina Sikanen. Digital microfluidic immobilized cytochrome P450 reactors with integrated inkjet-printed microheaters for droplet-based drug metabolism research. *Analytical and Bioanalytical Chemistry*, 410, 2018, 6677–6687.

2. Eveliina Jutila, Risto Koivunen, **Iiro Kiiski**, Roger Bollström, Tiina Sikanen, Patrick Gane. Microfluidic lateral flow cytochrome P450 assay on a novel printed functionalized calcium carbonate-based platform for rapid screening of human xenobiotic metabolism. *Advanced Functional Materials*, 28, 2018, 1802793.

The work presented in this thesis has also been presented in the following international peer-reviewed conference proceedings:

1. **Iiro Kiiski**, Sari Tähkä, Gowtham Sathyanarayanan, Markus Haapala, Ville Jokinen, Tiina Sikanen. Immobilized cytochrome P450 microreactors with integrated heaters. *Proceedings of the 20th International Conference on Miniaturized Systems for Chemistry and Life Sciences (MicroTAS 2016)*, Dublin, Ireland, 2016, 645–646.

2. **Iiro Kiiski**, Tea Pihlaja, Lauri Urvas, Ville Jokinen, Tiina Sikanen. Immobilization of membrane-bound enzymes on micropillar arrays via fusogenic liposomes. *Proceedings of the 22nd International Conference on Miniaturized Systems for Chemistry and Life Sciences (MicroTAS 2018)*, Kaohsiung, Taiwan, 2018, 2121–2123.

3. **Iiro Kiiski**, Sanna Artes, Ville Jokinen, Päivi Järvinen, Tiina Sikanen. Microfluidic immobilized enzyme reactors for prediction of drug clearance in vivo. *Proceedings of the 23rd International Conference on Miniaturized Systems for Chemistry and Life Sciences (MicroTAS 2019)*, Basel, Switzerland, 2019, 744–745.

4. **Iiro Kiiski**, Päivi Järvinen, Ville Jokinen, Tiina Sikanen. Mechanistic study of oxygen-scavenging properties of off-stoichiometric thiol-enes. *Proceedings of the 24th International Conference on Miniaturized Systems for Chemistry and Life Sciences (MicroTAS 2020)*, Online conference, 2020, 402–403.

Symbols and abbreviations

AMT	3’-amino-3’-deoxythymidine
b-FL	biotinylated fusogenic liposome
b-HLM	biotinylated human liver microsome
BSA	bovine serum albumin
CE	capillary electrophoresis
CL_{int}	intrinsic clearance
CYP	cytochrome P450
CLEA	cross-linked enzyme aggregates
CLEC	cross-linked enzyme crystals
DLS	dynamic light scattering
DMSO	dimethyl sulfoxide
DNTB	5,5′-dithiobis(2-nitrobenzoic acid), Ellman’s reagent
DOPE	1,2-dioleoyl-*sn*-glycero-3-phophoethanolamine
DOTAP	1,2-dioleoyl-3-trimethylammonium-propane
EC	electrochemical detection
ER	endoplasmic reticulum
EOF	electroosmotic flow
ESI	electrospray ionization
FL	fusogenic liposomes
HLM	human liver microsome
[I]	inhibitor concentration
IC_{50}	half maximal inhibitory concentration
IMER	immobilized enzyme (micro)reactor
k	reaction rate constant
K_I	enzyme-inhibitor complex dissociation constant
K_M	Michaelis constant
LC	liquid chromatography
LC-MS/MS	liquid chromatography–tandem mass spectrometry
μTAS	micro total analysis system
MS	mass spectrometry
MS/MS	tandem mass spectrometry
NADPH	β-nicotinamide adenine dinucleotide phosphate
NCE	new chemical entity
OSTE	off-stoichiometric thiol-ene
OSTE+	off stoichiometric dual-cure thiol-ene-epoxy system
PBS	phosphate buffered saline
PDMS	poly(dimethyl siloxane)
PEG	poly(ethylene glycol)
PECVD	plasma-enhanced chemical vapor deposition
PI	photoinitiator
POR	NADPH-cytochrome P450 oxidoreductase
PMMA	poly(methyl metacrylate)

[S]	substrate concentration
SEM	scanning electron microscope/microscopy
StrA	streptavidin
SU-8	trademark name of a commercial epoxy-based polymer by Microchem Corp.
T_g	glass transition temperature
TQ-S	triple quadrupole mass spectrometry
UDP	uridine 5'-diphosphate
UDPGA	uridine 5'-diphospho-glucuronic acid
UGT	uridine 5'-diphospho-glucuronosyltransferase
UPLC	ultra-performance liquid chromatography
UV	ultraviolet
v_0	initial velocity
V_{max}	maximal enzyme activity
WCA	water contact angle

1 Introduction

Drug development is a notoriously risky and costly undertaking. The process from discovery of a hit molecule to commercial launch of a drug typically takes over 10 years, with costs reaching $1 billion for each successful drug that enters the market.[1] A drug candidate can fail at any stage of the development pipeline, and most do: About 90% of drugs that reach the clinical trial phase never make it to the market.[2,3]

Drug metabolism is an enzyme-catalyzed biotransformation process that plays a major role in both the efficacy and safety of a drug *in vivo*. For example, a drug could be metabolized too rapidly for any therapeutic effect to occur. Alternatively, drug metabolism could result in the generation of toxic metabolites, or two concomitantly administered drugs metabolized via same pathways could interfere with each other's metabolism, resulting in drastic changes in drug exposure. Consequently, the evaluation of the metabolic properties of a new drug candidate is of paramount importance and should occur as early as possible in the drug development pipeline in order to pinpoint unsuitable candidates before undertaking time- and cost-intensive clinical trials.

The current state-of-the-art methodology in drug metabolism research involves enzyme assays conducted in static conditions on a well-plate platform, with limited spatiotemporal control of assay variables. The development of immobilized enzyme microreactors (IMER) by the immobilization of drug-metabolizing enzymes would benefit the field of *in vitro* metabolism research in many ways. Most importantly, microreactors allow the possibility of performing experiments under flow-through conditions. This enables the precise spatiotemporal control of reaction conditions by simply altering the chemical composition of the flow, which facilitates determination of enzyme kinetic parameters and mechanistic studies of time-dependent drug-drug and drug-enzyme interactions. However, the immobilization of membrane-bound enzymes such as members of the cytochrome P450 (CYP) and UDP-glucuronosyltransferase (UGT) enzyme families (which constitute the majority of enzymes responsible for human drug metabolism) has proven difficult: current immobilization approaches are not well-suited for these membrane proteins and often result in unwanted alterations in enzyme function.

Since the advent of microfluidics some 30 years ago, microfluidic applications have found their way into virtually every imaginable field of research, drug development included. The ever-increasing interest in microfluidics is based on the intrinsic benefits of miniaturization. The manipulation of minute volumes within micrometer or nanometer scale channels decreases reagent consumption and produces less waste. With modern microfabrication technologies, several unit operations can be easily integrated into one microfluidic chip to create so-called micro total analysis systems (μTAS), the ultimate goal of which is to create a streamlined "sample in/answer out" system.

This thesis will discuss the state-of-the-art in the development of flow-through microreactors for drug metabolism research, with an emphasis on enzyme immobilization and available manufacturing materials and methods. The thesis will also review assay design principles, setting the scene for the development of microfluidic flow-through immobilized enzyme reactors, the overall aim of this thesis work.

2 Review of the literature

2.1 Human drug metabolism

In order for a drug to have any clinical effect, it must be absorbed by the body in sufficient amounts and distributed across biological barriers to reach therapeutic concentrations in the target organ. This is why the majority of clinically used drug molecules are lipophilic in nature. Once absorbed in the body, lipophilic substances tend to accumulate in body tissues, and thus cannot be straightforwardly excreted from the body via the kidneys or intestines. Consequently, the main objective of drug metabolism is to render exogenous substances more hydrophilic, thus facilitating their elimination through urine or feces. Drug metabolism is often associated with loss of pharmacological potency, but can in some cases result in the production of toxic or pharmacologically potent metabolites.[4]

The metabolic pathway of a drug is usually divided into distinct phases. Phase I reactions include a variety of functionalization reactions, mostly oxidative in nature, that are catalyzed by various classes of enzymes, particularly those of the cytochrome P450 (CYP) superfamily.[5] Phase I reactions are typically regarded as a preparatory step followed by conjugation (phase II) of the newly formed functional group to a hydrophilic moiety (e.g., glutathione, glucuronic acid, or sulfate) that further enhances drug hydrophilicity, thus facilitating excretion through urine or bile. It should be noted, however, that many drugs are metabolized only *via* phase I or phase II reactions, or sometimes even in reverse order. More recently, as the importance of biological barriers and membrane transporters in drug efficacy and metabolism has become increasingly appreciated, phases 0 (active drug uptake by transporters) and III (active drug export by efflux pumps) have been added to the overall metabolism scheme.[6] As CYPs and UDP-glucuronosyltransferases (UGTs) together are responsible for approximately 90% of the metabolism of marketed drugs,[7,8] these enzymes were selected as the focal point of this thesis and were used as the target enzymes for immobilization.

Figure 1 depicts the metabolism of the opioid analgesic drug codeine. The metabolism of codeine is a typical example of a metabolic pathway involving both phase I and II reactions, and also showcases the importance of metabolism in drug therapy. Codeine is first transformed into morphine in a CYP2D6-catalyzed demethylation reaction. Morphine is the metabolite responsible for the analgesic effect of codeine, which itself is rather pharmacologically inert.[9] Patients' allelic variants of CYP2D6 can have a drastic effect on the success of codeine therapy: Those with alleles that dampen CYP2D6 activity will be poor metabolizers who experience a lack of analgesic effect; those with alleles that increase CYP2D6 activity will be rapid metabolizers who could accumulate hazardous concentrations of morphine. Morphine further undergoes phase II metabolism into two glucuronide conjugates, morphine-3-glucuronide and morphine-6-glucuronide, that are then excreted out of the body through the urine. Interestingly, morphine-6-glucuronide is an even more potent analgesic than morphine.[10]

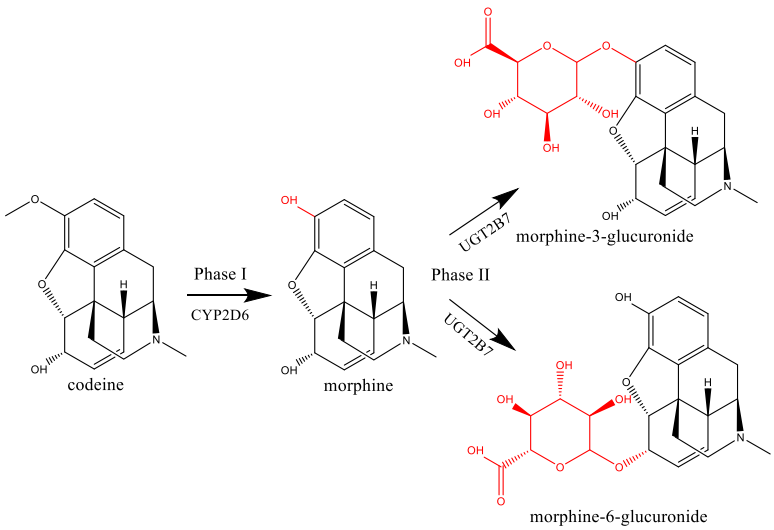

Figure 1. *Metabolic pathway of the opioid analgesic codeine.*

CYP enzymes are undoubtedly the most important group of drug metabolizing enzymes, comprising approximately 75% of metabolism of all marketed drugs.[7,8,11] CYPs are heme-containing monooxygenases that catalyze the oxidation of substrates with an oxygen atom derived from molecular oxygen (O_2), while reducing the remaining oxygen atom into water.[12,13] The electrons needed for this reduction reaction are usually supplied in the form of nicotinamide adenine dinucleotide phosphate (NADPH), which acts as the co-substrate in CYP reactions. The electron transport in CYP reactions is mediated by an auxiliary protein called NADPH-cytochrome P450 oxidoreductase (POR), which is obligatory for CYP activity.[13,14] The heme-containing protein cytochrome b_5 is also associated with CYP modulation, but its precise role remains unclear.[14,15] CYPs, as well as these auxiliary proteins, are membrane-bound enzymes located primarily in the endoplasmic reticulum (ER) of hepatocytes. The lipid membrane environment is integral to CYP function, affecting enzyme conformation and the interaction between CYPs and their redox partners.[16]

UDP-glucuronosyltransferases (UGTs) are the most prominent class of enzymes that catalyze phase II reactions.[7,8] UGTs catalyze the conjugation of a glucuronic acid moiety, derived from the cofactor UDP-glucuronic acid (UDPGA), into a suitable functional group on a substrate molecule by a glycosidic bond. Similar to CYPs, UGTs are also membrane proteins located mainly in the ER of the liver.[17] However, unlike CYPs, which reside on the cytosolic side of the membrane, the active site of UGTs is located on the luminal side of the ER. This complicates the evaluation of data obtained *in vitro* experiments in ways that will be discussed in more detail in section 2.1.2.

2.1.1 Metabolism in preclinical drug development

When discovering new chemical entities (NCE), the primary goals of preclinical *in vitro* drug metabolism studies are: (1) the assessment of metabolic stability (i.e. susceptibility of the NCE to metabolism in general); (2) identification of principal metabolites and the enzymes involved in their generation and the kinetics thereof; and (3) assessing the potential for drug-drug interactions.[18,19] The information gathered from *in vitro* studies is then integrated with *in vivo* data from animal models to predict the fate of the NCE in the human body so that no unpleasant surprises—such as toxic metabolites or potentially hazardous drug interactions—are encountered during clinical trials. This chapter briefly discusses the rationale behind the evaluation of *in vivo* drug metabolism and interaction potential based on *in vitro* experimental data.

Metabolic reactions, like any other enzyme-catalyzed reaction, are usually characterized by parameters derived from fitting experimental data into a nonlinear kinetic model, the most commonly the Michaelis-Menten model.[20] Under steady-state conditions (i.e., no appreciable depletion of substrate during the reaction and thus no change in the concentration of the enzyme-substrate complex[20]), a reaction obeying Michaelis-Menten kinetics can be described by the Equation 1:

$$(1) \qquad v_0 = \frac{V_{max}[S]}{K_M + [S]}$$

Where v_0 is the initial reaction velocity, [S] is the substrate concentration, and K_M and V_{max} are reaction-specific constants defining the reaction kinetics. K_M, also called the Michaelis constant, is determined as the substrate concentration at which half of the maximum reaction velocity (V_{max}) is reached. Once the major enzymes responsible for the elimination of the NCE have been elucidated and the respective kinetic parameters determined, the intrinsic clearance (CL_{int}) of the drug can be calculated (assuming non-saturating substrate concentrations, i.e. $[S] << K_M$) using Equation 2[21,22]:

$$(2) \qquad CL_{int} = \frac{V_{max}}{K_M}$$

To evaluate *in vivo* hepatic clearance, the *in vitro* CL_{int}, expressed in units of L/min/mg enzyme (or number of cells in the assay), is first multiplied by a scaling factor to normalize the rate of metabolism with respect to the amount of liver tissue in the body. An estimate of total hepatic clearance is achieved when the *in vivo* CL_{int} value is substituted into a liver model that takes into account physiological phenomena such as blood flow and mass transfer inside the liver.[21,22] In addition to hepatic clearance, a drug could have extrahepatic elimination routes (such as renal excretion of unchanged drug), and these should be taken into consideration in total-body clearance, obtained as a sum of all alternative elimination routes.[22,23]

Drug-drug interactions occur when concomitantly administered drugs interfere with one another's metabolism. Most commonly, one drug inhibits the metabolism of another drug,

resulting in increased plasma concentrations of the latter, possibly leading to toxic side effects.[24,25] The CYP enzyme family is particularly prone to interactions owing to their broad substrate spectrum combined with narrow substrate specifity.[26] Several CYP-inhibiting drugs have been removed from the market due to severe adverse drug reactions.[27,28] Therefore, increasing emphasis has been put on identifying possible risks for adverse drug-drug interactions already in the preclinical phase of drug development. Enzyme inhibition can be either reversible or irreversible. Reversible inhibition is the more common mechanism of the two, and can be further divided into three modalities—competitive, noncompetitive, and uncompetitive inhibition—depending on whether the inhibitor binds directly to the enzyme's active site (competitive) or elsewhere (non- or uncompetitive) on the enzyme.[8,29] In irreversible inhibition, the inhibitor covalently bonds to the enzyme's apoprotein or the heme group, resulting in total loss of enzyme function. In this circumstance, enzyme function can only be restored by *de novo* synthesis of new enzyme. Therefore, irreversible enzyme inhibition is an especially unwanted property in an NCE. Besides inhibition, drugs can also cause enzyme induction by acting as activators of transcription factors regulating the expression metabolic enzymes.[30]

The simplest and most common way to assess the interaction potential of an NCE is by conducting an half maximal inhibitory concentration (IC_{50}) assay, where varying concentrations of a test compound are tested for their propensity to inhibit a model reaction and the concentration causing 50% of maximal inhibition is reported as the IC_{50} value.[31,32] However, IC_{50} depends on the substrate concentration used in the assay and does not discern between different inhibition modalities.[33] For a more detailed and unambiguous characterization of inhibition, usually further along in the drug development pipeline, the dissociation constant of the enzyme-inhibitor complex, K_i, should be determined using a range of substrate and inhibitor concentrations. With K_i determined, it is possible to predict the effect of an inhibitor on the intrinsic clearance using the Equation (3) (shown as an example for competitive inhibition):

$$CL_{int(i)} = \frac{V_{max}}{K_m(1+(\frac{[I]}{K_i})} \quad (3)$$

Here, [I] represents the concentration of inhibitor at the enzyme active or modulatory site. Even if free plasma concentrations of the drug are known, estimating this parameter can be challenging because especially lipophilic drugs might concentrate in hepatocytes, far exceeding the concentrations found in blood.[18]

To differentiate between reversible and irreversible (also called mechanism-based) inhibition, the inhibitor is preincubated with the enzyme of interest across different time intervals.[34] If the magnitude of inhibition changes over time, the inhibition is referred to as time-dependent inhibition, which often suggests that the inhibition is also mechanism-based, i.e., irreversible. At this stage, additional experiments are needed to conclusively verify the mechanism-based and irreversible nature of the inhibition. For example, unlike inhibition due to a competitive inhibitor with extremely high affinity or a more potent inhibitory metabolite, mechanism-based inhibition cannot be recovered by dialysis.[35]

2.1.2 *In vitro* models

The extrapolation of drug metabolism results from preclinical *in vivo* animal studies is difficult and prone to misinterpretations, given the fundamental differences in metabolism between species.[36] Specifically, drug metabolism in animal models often results in disproportional metabolite ratios or the appearance of completely different metabolites compared to what is observed in humans. This is particularly critical when human metabolism of a drug results in a toxic metabolite that is not observed in the animal model. Consequently, *in vitro* experiments with models based on human-derived material are an integral part of preclinical drug metabolism studies. Since metabolism mainly takes place in the liver due to its high expression levels of drug metabolizing enzymes, most *in vitro* metabolism models are based on liver-derived cells or tissue.[19,23,37] It should be noted, however, that drug metabolism also takes place in other organs and tissues—particularly the lungs, kidneys and intestines—that may play a major role in the metabolism of a given drug, depending on its characteristics and route of administration.[38]

The *in vitro* models used in preclinical studies can be categorized as subcellular, cellular, and tissue models. All of the available models have a unique set of pros and cons in terms of *in vivo* resemblance, availability, simplicity and economic feasibility, (Table 1).

Table 1. *Advantages and disadvantages of different human-derived model systems for the study of drug metabolism* in vitro.

In vitro model	Advantages	Disadvantages
Subcellular fractions	• Simple • Low cost • Established protocols	• All metabolic enzymes not present • Lack of cell functions (e.g. no induction) • Toxicity assays not applicable
Cell lines	• Good availability • Intact cells • Easy to culture	• Poor expression of some metabolic enzymes • Dedifferentiation
Primary hepatocytes	• All metabolic enzymes present • Good *in vivo* correlation	• Limited availability • High cost • Challenging culture protocols • Limited viability
Intact tissue	• Complete tissue architecture	• Limited availability • Limited viability

Subcellular fractions—in particular human liver microsomes (HLM)—are considered the industry standard model for pre-clinical metabolic profiling and drug interaction studies because of their relative affordability, availability, and acceptable *in vivo* resemblance.[31,32,39,40] HLM consist of vesicles of hepatocyte endoplasmic reticulum prepared by differential centrifugation.[41] HLM contain all the endogenous enzymes localized in the ER, namely CYPs, UGTs and flavin monooxygenases (FMOs). Even though

these enzymes carry out the majority of human drug metabolism, any metabolites produced by other systems (e.g. sulfotransferases, SULTs) cannot be studied with HLM. Furthermore, enzymatic activity of HLM can vary substantially between donors, but this problem can be overcome by using a pool of liver samples from several donors. For distinguishing which enzymes participate in the biotransformation reactions of a given drug, microsomal vesicles of isolated, recombinant human enzymes produced in insect cells (marketed under the names baculosome or supersome) are commonly used. However, because subcellular fractions lack the active gene expression that occurs in intact cells, they cannot be used for studying enzyme induction.

The study of UGT-mediated metabolism using subcellular fractions has certain complications, that make it more difficult to extrapolate *in vivo* metabolism from *in vitro* studies.[42,43] Namely, because the active sites of UGTs are located on the luminal side of microsomes, the membrane forms a physical barrier to the drug substrates and cofactors, resulting in underestimation of glucuronidation rates (a phenomenon referred to as latency).[42,44] This problem can be overcome by disrupting the membrane, for example by using a pore-forming agent like the peptide antibiotic alamethicin.[45] Free fatty acids leaching from the microsomal preparations during incubations have also been shown to inhibit UGT enzymes, resulting in dramatically altered kinetic parameters.[46–48] This inhibition can be counteracted by sequestering the inhibitory moieties with the addition of albumin to the incubation mixture. Even with these modifications to the experimental protocol, cell-based methods are often more successful—albeit not perfect—in predicting *in vivo* clearances of glucuronidated drugs.[49] When using cell models, care should be taken that competing metabolic pathways, such as those involving CYPs, do not interfere with the study of the glucuronidation reaction of interest.[40]

The most significant advantage of cell models is that they contain the complete molecular machinery of the cell— including the presence of all drug-metabolism enzymes, active gene expression, and intact transport processes—allowing the study of metabolic phenomena on a detailed level that is not feasible in subcellular models. Primary hepatocytes isolated directly from the human liver are widely used as a model system, owing to their strong *in vivo* resemblance. Cryopreserved primary hepatocytes are also commercially available, although they are considerably more expensive than subcellular matrices or cell lines. With modern culturing techniques, primary hepatocytes can be cultured for several weeks, but cultured cells often suffer from loss of differentiation and decline in enzyme expression levels over time.[50] Transformed cell lines, either artificially transformed or derived from tumor tissue, can be used as a cheaper and more easily manageable alternative to primary hepatocytes. However, cell lines often suffer from dedifferentiation, which can result in impaired expression of drug-metabolizing enzymes, potentially undermining their applicability in the assessment of drug metabolism.[51] It should be noted however, that novel culturing methods, such as organ-on-a-chip approaches, have been shown to prevent cell dedifferentiation and improve the expression of drug-metabolizing enzymes in long-term cell cultures.[52,53]

Intact liver tissue can also be used as an *in vitro* metabolism model. By definition, tissue-based models are the most *in vivo*-like of all the available model systems. Besides enzyme-containing hepatocytes, tissue models also contain all the non-parenchymal cell types as

well as intact cell-to-cell contacts, both of which both are important regulators of tissue function.[54] The most commonly used tissue model is liver slices prepared with high-precision tissue slicers.[55] The major disadvantage of tissue models is, quite understandably, their poor availability, and this is further hampered by the lack of reliable cryopreservation procedures.[32] As with cell models, the activity of metabolic enzymes also declines in tissue slices upon culturing.[56]

For drugs metabolized primarily by CYPs, the use of hepatocytes does not necessarily offer a significant advantage over subcellular models.[57,58] However, for UGT metabolism, cell models have been more successful in predicting *in vivo* drug clearances.[42,49] This might be related to the more complicated disposition of highly hydrophilic glucuronides—which involve active efflux and influx processes (i.e., metabolic phases 0 and III)—in cell models.[59] Despite their undeniable advantages, cell-based models are always to some extent "black boxes," where the influence of different mechanistic aspects (i.e., metabolism, membrane permeation) on the total outcome cannot always be disentangled.

One relevant shortcoming common to all conventional *in vitro* models is that the assays are performed under an atmospheric, non-physiological oxygen environment. Oxygen partial pressure is a crucial factor that affects many biological processes. Oxygen levels in the human body vary greatly, with the most oxygenated tissues experiencing oxygen partial pressures between 10-13% and the least oxygenated tissues (like the liver and colon) experiencing partial pressures of approximately 5%.[60] Despite the importance of the oxygen microenvironment, most *in vitro* assays are performed under ambient air (21% O_2), with oxygen partial pressures not encountered even in the most oxygenated human tissues.[60] The use of non-physiological oxygen conditions is largely due to the difficulty of oxygen control in conventional *in vitro* platforms such as well plates. The use of non-physiological oxygen conditions can have drastic effects on the behavior of biological samples,[61,62] which may lead to erroneous interpretations of drug metabolism assay results. The normoxic oxygen concentration in a healthy liver is around 40 µM (4%).[63,64] For CYPs, oxygen dependency varies across substrates and enzyme isoforms. In general, the K_{O2} values of CYPs (i.e., the oxygen concentration resulting in half maximal enzyme activity), are reported to be in the range of 10 µM (1%).[65–67] This means that under normoxic conditions, most CYPs reactions are oxygen-independent but can become limited by oxygen under conditions of mild hypoxia, known to occur in many physiological conditions. For example, impaired hepatic oxygen uptake has been linked to decreased drug clearance in geriatric patients.[68] Hypoxia is also known to alter the metabolic profile of drugs, as exemplified by the antiviral drug zidovudine, which is increasingly converted to a myelotoxic reductive metabolite in hypoxic conditions.[69] However, the literature on oxygen-dependence of CYP activity is rather scarce, presumably due to the lack of feasible methods for the on-demand control of oxygen partial pressure in enzymatic assays.

The implementation of immobilized enzyme reactors (IMERs) via the affixing of drug-metabolizing enzymes would provide several benefits over conventional assays. First, immobilization allows for the use of flow conditions. Importantly, this enables the spatiotemporal tuning of reaction conditions on demand by simply altering the chemical composition of the flow.[70] For example, by creating concentration gradients of the substrate, its enzyme kinetics can be determined in a single automatable experiment.[71–73] Affixing the

enzyme inside the reactor also facilitates more straightforward downstream processing, such as metabolite purification. The compartmentalized enzyme reaction is also easily combined with additional unit operations, such as on-line metabolite detection or a separate cell compartment for studying metabolite-induced toxicity.[74,75] Given these benefits, the immobilization of drug-metabolizing enzymes has been a subject of keen interest for over four decades.[76,77] However, the fact that the most important classes of drug-metabolizing enzymes—namely CYPs and UGTs—are membrane-bound proteins has posed a formidable challenge to the field because of several shortcomings with conventional immobilization approaches. Enzyme immobilization, both in general and in the special case of membrane-bound drug-metabolizing enzymes, is discussed in more detail in the next chapter.

2.2 Enzyme immobilization

Enzyme immobilization techniques are generally divided into three main categories. Enzymes can either be (i) bound to a support material via physical or chemical interactions, (ii) entrapped inside a porous matrix, or (iii) cross-linked together to form enzyme aggregates or crystals (Figure 2). The pros and cons of each strategy are briefly elaborated below.

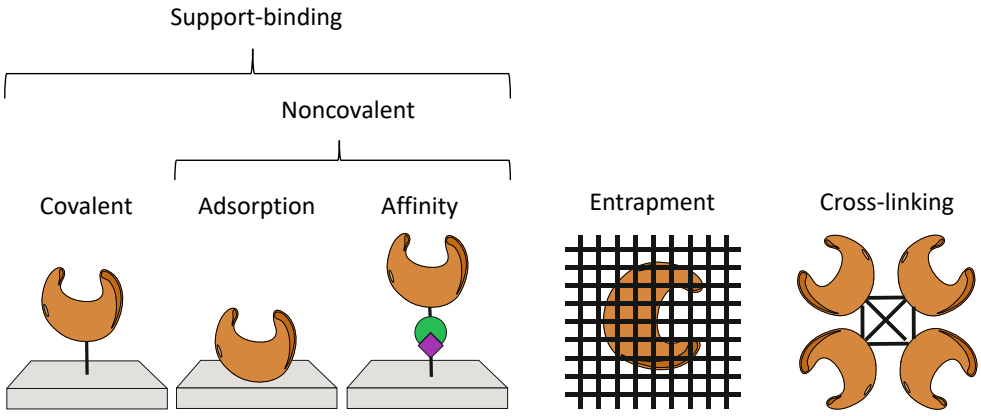

Figure 2. *Schematic representation of different enzyme immobilization approaches (© I. Kiiski 2020).*

Enzymes can be bound on support materials via both covalent and non-covalent bonds. Non-covalent methods can be further divided into physical (hydrophobic and van der Waals interactions), ionic (electrostatic interactions) and affinity-based (e.g. antibody-mediated binding) methods.[78,79]

Owing to their low binding energies, non-covalently bound enzymes are easily washed away from the carrier surface, especially in more demanding conditions, such as elevated temperatures.[78,79] On the other hand, weak interactions do not usually alter the tertiary structure of the enzymes, thereby helping the enzymes to retain their activity.[80] Affinity

immobilization is based on bio-specific interactions between complementary chemical species found on the immobilized molecule and the solid support (e.g., between biotin and avidin or between an antibody and an antigen).[81] While classified as a noncovalent method, affinity immobilization can result in binding energies close to those of covalent bonds.[82] Affinity immobilization results in very specific bonding that is also reversible in nature, which theoretically enables the renewal of the enzyme material. However, affinity-based methods usually require modification of the enzyme to introduce the affinity-tag, which can result in enzyme inactivation.

Covalent bonding allows for more stable anchorage between the enzyme and the carrier surface. When selecting the specific functionality to be used in immobilization, chemical compatibility with both the target enzyme and reactor surface must be taken into account.[83] Common immobilization chemistries include aldehydes, carboxylic acids, primary amines and thiols. All chemistries have specific characteristics (e.g., optimum pH and solubility) and must be chosen based on the requirements of the application.[84] Traditional covalent binding chemistries rely on functional groups naturally present in biomacromolecules (e.g., NH_2 and COOH) so no prior enzyme modification step is needed. As there is no effective control over where the covalent bond between the enzyme and the surface will be formed, covalent binding methods will generate a heterogeneous population of enzyme due to the random orientation of the immobilized biomolecules. This may result in decreased overall activity if the substrate's access to the active site is hindered in some of the immobilized enzymes. The steric hindrance associated with covalent immobilization can be overcome by distancing the enzyme from the support using a spacer molecule.[85] If charged residues are used for immobilization, the alteration of protein surface charge can potentially alter enzyme activity due to detrimental changes in protein folding.[79]

Entrapment approaches involve the physical trapping of the enzyme inside a porous matrix of synthetic or natural origin. The polymer network is cross-linked in the presence of the enzyme, trapping the enzyme inside the matrix due to physical restraints of the polymer pore size. Entrapment enables high volumetric enzyme concentrations with relatively mild immobilization conditions.[86,87] Entrapment can be readily applied to a variety of different enzymes, as it is not based on any enzyme-specific properties. Main disadvantages of entrapment are enzyme leaching and impaired diffusion.[78] Impaired diffusion is due to the steric constraints caused by the matrix that affect substrate diffusion to the active site of the enzyme. Under these circumstances, enzyme kinetics are usually limited by diffusion rather than the velocity of the reaction itself. These alterations should be taken into consideration when using IMERs with entrapped enzymes for enzyme kinetic characterization.

Commonly used entrapment matrices include sol-gels and hydrogels.[88] Hydrogels are more biocompatible than sol-gels and do not require toxic reagents for the polymerization process. Most hydrogels are also transparent, which enables the use of various imaging techniques. Commonly used hydrogels include synthetics like poly(ethylene glycol) and polyacrylamide and natural polymers like chitosan and agarose.

By cross-linking, carrierless macroparticles can be prepared from enzyme aggregates or crystals.[78,88] The advantage of this technique is that the volumetric enzyme concentration is not diluted by the carrier material, as in the case of entrapment techniques. Cross-linking

techniques can be divided into two categories according to the physical state of the enzyme prior to cross-linking. Cross-linked enzyme crystals (CLECs) are prepared from crystallized enzyme with the addition of a bifunctional reagent such as glutaraldehyde. The resulting cross-linked crystals are stable and highly active, and their particle size can be readily controlled. However, protein crystallization is a laborious procedure that requires high-purity enzyme. This drawback of CLECs is avoided when enzyme aggregates are used as a starting material instead. Subsequent cross-linking of these aggregates generates cross-linked enzyme aggregates (CLEAs). As protein precipitation is often used for purification, both purification and immobilization can be combined into a single unit operation that can be used, for example, to immobilize an enzyme directly from a crude fermentation broth. In the context of membrane-bound enzymes, such as CYPs and UGTs, crosslinking is rarely used because the protein is embedded inside a lipid membrane. Approaches that have been successfully applied to membrane-bound drug-metabolizing enzymes are discussed next in more detail.

2.2.1 Immobilization of membrane-bound CYP enzymes

Research on the immobilization of drug-metabolizing enzymes has to-date focused mainly on CYP enzymes, while the immobilization of UGTs has received very little attention. This is presumably due to the enticing challenges related to the immobilization of CYPs. The complex nature of the CYP system, with its multiple membrane-embedded co-operative enzymes, places special demands on the immobilization process. Removing of a protein from its hydrophobic surroundings and reconstituting it into another is a harsh process that is likely to damage the target and result in decreased functionality. With CYPs, this process would have to be performed on several proteins (i.e., CYP and its redox partners) simultaneously, while maintaining their molar ratio and interactions. Several different approaches have been described for immobilizing microsomal vesicles and will be discussed in detail next with examples from the literature. Though this discussion focuses on CYPs, most observations also hold true in the case of any membrane-bound enzyme.

For HLM, entrapment approaches are most commonly used for immobilization.[74,75,89–92] A probable explanation for the preference of entrapment over other strategies is that it has no special demands regarding protein structure and is therefore just as suitable for membrane-bound enzymes as it is for other classes of proteins. It could also be argued that because the membrane-bound enzymes are embedded within the phospholipid membrane, the efficiency of covalent immobilization methods based on the chemistry of amino acids is diminished.

Zguris et al.[89] immobilized human liver microsomes in microfluidic channels by entrapment in poly(ethylene) glycol. The hydrogel matrix was microstructured by photolithography to create CYP arrays that facilitated mass transfer between the flow-through solution and the CYP-matrix. The immobilization process was shown not to disrupt CYP activity. However, the enzyme kinetics of the immobilized CYPs were not studied. It can be hypothesized that in this configuration the hydrogel matrix imposes diffusional constraints that would affect the enzyme kinetics of the immobilized enzymes.

Sakai-Kato et al.[90] used sol-gel chemistry with aqueous silicate as a starting material to entrap human liver microsomes into a microarray on a glass surface. The shelf life of the HLM was drastically improved compared to that of the soluble enzyme (weeks vs. days). The K_M value of testosterone 6β-hydroxylation via CYP3A4 in immobilized HLM was also determined and found to be slightly higher compared to that of nonimmobilized HLM. As explained in the previous chapter, this is likely due to the steric constraints inherent in entrapment-based immobilization.

Wu et al.[93] reported another entrapment strategy in which HLM was immobilized in a microwell interconnected to a microfluidic channel by placing a polycarbonate membrane with 0.4 μm pores on the bottom of the well. The pores were small enough to restrain the microsomes while also permitting molecular transport. The researchers claimed that the physical immobilization procedure did not cause any enzyme inactivation, but the study did not present any data on enzyme stability or kinetics to support this claim.

Besides HLM, similar enzyme entrapment strategies have also been applied to animal-derived enzyme sources. Lee et al.[92,94] immobilized rat liver microsomes inside a poly(dimethyl siloxane) (PDMS) microchannel by embedding an array of PEG-hydrogel pillars inside the channel. As expected, the entrapment of microsomes inside the hydrogel resulted in diffusion-limited enzyme kinetics, increasing the apparent K_M and decreasing the apparent V_{max} of the model reaction. The authors speculated that the limited diffusion could be mitigated by design revision—that is, reducing the hydrogel pillar diameter and increasing the hydrogel porosity. However, no experimental evidence on this was presented and it can be hypothesized that a looser entrapment matrix might result in enzyme leaching out of the microreactor.

Membrane-bound CYPs have also been immobilized on lipid bilayers on solid supports. This approach is similar to entrapment in the sense that it targets the whole microsomal vesicle rather than just the CYP enzyme and does not involve the use of a molecular tag or linker incorporated into the protein structure. Ueda et al.[95] immobilized recombinant CYP microsomal vesicles on the surface of micropatterned lipid bilayer membranes on glass substrates. The patterned lipid surface used for the immobilization was composed of fluid membrane islets confined in a framework of rigid polymerized lipid domains. The microsomal vesicles were immobilized by membrane fusion with the fluid bilayers induced by the lipid composition of the bilayer on the substrate surface. When compared with direct adsorption of microsomes on a glass substrate, the enzymes immobilized on the lipid bilayers showed improved enzymatic activity. However, the long-term stability and kinetic properties of the immobilized enzymes were not studied in detail.

Despite its apparent limitations, immobilization based on covalent modifications of the protein structure has also been used in the immobilization of microsomal constructs. Schejbal et al.[96] immobilized CYP2C9 baculosomes on magnetic particles to create a CYP-IMER for drug metabolite analysis coupled with capillary electrophoresis (CE). The researchers used used covalent bonding for immobilization, utilizing standard carbodiimide-based chemistry.[84] Kinetic parameters for diclofenac were determined with the IMER-CE-setup and shown to be in accordance with the literature. However, the IMER exhibited a rapid loss of enzymatic activity, which needed to be compensated by fitting the results into an exponential decay model.

Nicoli et al.[97] immobilized recombinant human CYP microsomal vesicles on a neutravidin-functionalized liquid chromatography (LC) column by labelling the microsomes with biotin via dialysis. The constructed IMER was used to conduct on-line drug metabolism studies by coupling the system to a mass spectrometer. However, the kinetic parameters of the immobilized enzyme were not assessed. Moreover, the reactions had to be conducted at room temperature because the immobilized enzyme was not stable at elevated temperatures. The immobilization protocol of the microsomes was also rather complex and time-consuming, involving two 2h-long dialysis steps used to remove interfering substances and unreacted material, which can also compromise enzyme stability (Figure 3B). Nevertheless, from the standpoint of kinetic determinations, the support-binding approaches reported by Schejbal et al.[96] and Nicoli et al.[97] represent the state-of-the art in CYP/UGT immobilization in the sense that they are not as prone to diffusional restrictions as scaffold-based systems are.

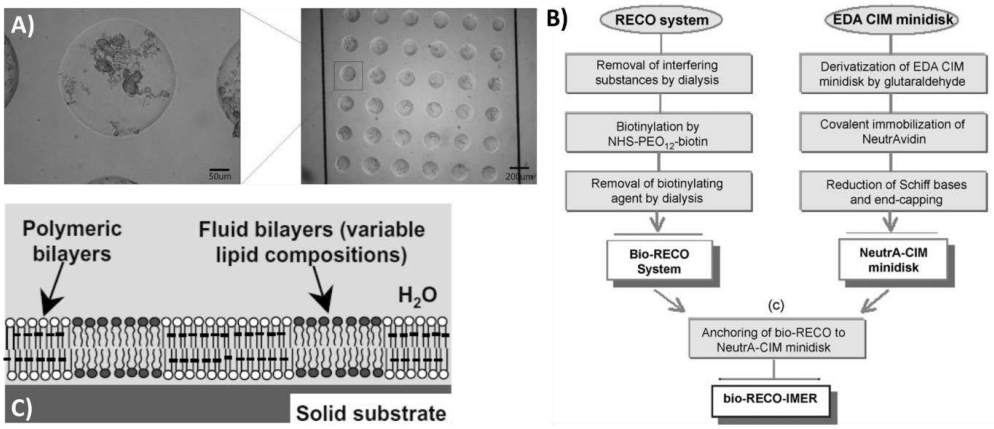

Figure 3. *Immobilization approaches for microsomal drug-metabolizing enzymes. A) Human liver microsomes entrapped inside poly(ethylene glycol) micropillars. Modified and reprinted from ref. 92. © 2013, with permission from Elsevier. B) Schematic of a CYP immobilization procedure based on affinity binding of covalently biotinylated microsomes on a neutravidin-functionalized monolithic mini-column. Modified and reprinted from ref. 97. © 2008, with permission from Elsevier. C) Schematic of a micropatterned lipid membrane used for immobilizing CYP-containing microsomes. Modified and reprinted from ref. 95. © 2007, with permission from Elsevier.*

2.2.2 Immobilization of soluble CYP enzymes

The earliest attempts at immobilizing membrane proteins involved the immobilization of whole-membrane fragments.[98] These approaches often suffered from high levels of nonspecific binding and instability. Consequently, in contemporary techniques, membrane proteins are usually solubilized and reconstituted in detergents or lipids with defined characteristics. CYP enzymes can be rendered soluble by deleting the hydrophobic N-terminus sequence. For soluble CYPs, covalent bonding is more applicable because the

different functional groups of the amino acids are more readily available for bonding using different chemistries; this is likely why covalent immobilization is the method of choice when working with soluble CYPs.[99–101] A drawback of using soluble CYPs is that the auxiliary proteins must be applied in solution along with the substrate for each reaction, which considerably increases operational costs. It is also possible to immobilize the redox partners on the same carrier as the CYPs, but the adjustment of spatial relationships and stoichiometric ratios of the different proteins might prove challenging. In one example of covalent immobilization of recombinant CYPs, Wollenberg et al.[99] immobilized soluble recombinant CYP2C9 using amine-directed coupling to a UV-activated poly(methyl methacrylate) (PMMA) surface. Compared to the soluble enzyme, stability was improved in the immobilized enzyme. However, the costly cofactor POR needed to be supplied alongside the substrate, undermining the economic feasibility of this design.

Cross-linking is not easily implemented for membrane-bound enzymes. Cross-linking microsomal vesicles as such would likely result in enzyme inactivation and uncontrollable aggregation of microsomes, which would in turn limit substrate diffusion. However, soluble bacterial CYP enzymes have been immobilized by cross-linking. Tan et al.[102] immobilized a soluble bacterial CYP with its redox protein partners by supramolecular complex formation, fusing the enzymes to self-assembling protein linkers. The cross-linked enzyme formed a reusable, water-insoluble gel.

CYPs can also be immobilized on electrode surfaces. The use of electrodes can obviate the need for NADPH and auxiliary proteins since electrons can be accepted directly from the electrode surface. This way, CYPs can be used as biosensors by monitoring changes in electrical current when exposing the system to different substrates.

Although technically feasible, immobilization of soluble CYPs is unlikely to meet the needs of *in vitro* drug discovery because of this technique's poor correlation with *in vivo* clearance.[103] Because of this, this thesis focuses mainly on methodology applicable to membrane-bound enzymes.

2.3 Microfluidic systems in drug metabolism research

The concept of micro total analysis systems (μTAS), enabled by the utilization of microfabrication and microfluidics, was first coined in a seminal paper by Andreas Manz and colleagues in 1990.[104] Since then, microfluidic systems have found use in practically all fields of chemistry and biology, ranging from simple point-of-care diagnostic devices[105] to intricate body-on-a-chip systems[106] that emulate human physiology.

In pharmaceutical sciences, microfluidic systems have gained attention as novel tools that could potentially speed up the cumbersome drug development process.[107] The manipulation of minute volumes within micro- or nanometer-sized channels, results in decreased consumption of expensive bioreagents (such as the cofactors of enzymatic reactions). Owing to the short distances and high surface-to-volume ratios in microfluidic channels, mass and heat transfer occur rapidly, which both facilitate precise control of experimental parameters and reduces total analysis time.[108,109] One key advantage of microfluidic systems, made possible by their small size and the utilization of modern

microfabrication processes, is the integration of several functional units (e.g. reaction, separation and detection) on one integrated microchip. The implementation of immobilized enzyme microreactors in the microscale also benefits from the same advantages. This chapter focuses on different aspects of microsystem design, with a focus on miniaturization of immobilized enzyme reactors.

2.3.1 Microfabrication

Microfabrication encompasses all technologies intended to structures at or below the micrometer scale. Microfabrication processes were originally developed by the semiconductor industry for the creation of integrated circuits in silicon. In recent decades, these processes have been also adopted by the microfluidics community. In addition, several methodologies have been developed solely for purpose of fabricating microfluidic devices.

First-generation microfluidic chips were made from silicon and glass using standardized photolithography methods initially developed for silicon.[110] More recently, polymer materials have rapidly replaced glass and silicon in microfluidic applications. This is due to a multitude of reasons. While silicon was an obvious choice of material for microelectronics given its semiconductive properties, it is not as suitable for the manufacturing of microfluidic systems for applications in chemistry or life sciences. For example, microchip capillary electrophoresis requires high voltages that simply cannot be generated on a conductive material. The immense range of polymer materials, on the other hand, represent a cornucopia of physico-chemical and mechanical properties so that the most feasible material can be chosen based on the specific requirements of each application. Fabrication of glass and silicon is costly and typically requires hazardous chemicals and clean room facilities,[111] whereas polymer fabrication is often a less demanding process. In particular, the 1998 introduction of soft lithography-based prototyping of PDMS microstructures by George Whitesides' laboratory[112,113] paved the way for the efficient utilization of polymer materials. PDMS soft lithography enables replication of silicon microstructures in PDMS itself, but also allows the use of PDMS as an intermediate mold for replication of high-definition microstructures in practically any heat- or light-curable polymer material under normal laboratory conditions, as will be described later. Given the prevalence of polymers in microfluidic applications, the remainder of this chapter will focus solely on polymers.

Polymer microfabrication techniques can be divided into two categories: (i) direct machining methods, including micromachining and lithography, and (ii) replication methods, including embossing and casting. Most thermoplastic materials can be patterned with both direct machining and replication methods, whereas elastomer patterning is done mostly by casting and thermoset patterning via UV lithography.[111] All microfabrication techniques have different limitations with respect to feature resolution and accuracy, and these must be considered on a case-by-case basis. In general, lithography offers the highest accuracy and feature resolution, but elastomers casted on master structures defined by photolithography can also produce relatively high resolution patterns.[112] Casting and photolithography, both exploited in this thesis, are discussed next in more detail.

Photolithography is the process of exposing a photosensitive material to (UV-)light through a photomask that defines the patterned shape.[114] Photolithography lies at the heart of the semiconductor industry, where it is routinely used in the fabrication of common electronic components. In this context, photolithography is utilized in the direct processing of silicon, whereas in the microfluidics field photolithography is also used as an intermediate step in creating high-definition molds for use in polymer replication.[111,112] In the photolithographic process (Figure 4), the substrate is first coated with a light-sensitive photoresist. Next, the photoresist is exposed to UV-light through a photomask selectively exposing some parts of the resist, defining the pattern to be fabricated. After exposure, the photoresist is developed using a solvent. Depending on the polarity of the resist, either the exposed parts (positive resists) or the unexposed parts (negative resists) are dissolved in the developer solution. In silicon processing, the underlying silicon layer is then selectively etched before removing the photoresist. Many photoresists have rather low viscosity, resulting in very thin layers (on the order of a few microns), thereby restricting their use in microfluidic applications that require the manipulation of cells, or volumes at the microliter scale. Some photoresists, such as the epoxy-based negative tone photoresist SU-8, can be used for the fabrication of layers that are hundreds of micrometers in depth, which is why it is widely used in the microfluidics field both for the creation of standalone devices[115,116] and as a mold for replication of high-aspect ratio structures.[113,117]

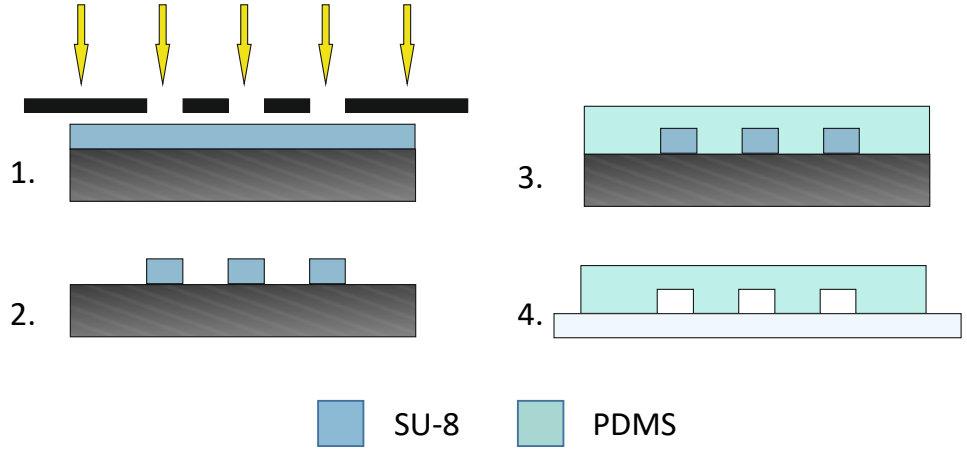

Figure 4. *Schematic illustrating the soft lithography processing of PDMS negative photoresist. The process consists of 1) patterning of the negative photoresist SU-8 through a photomask, 2) developing the exposed photoresist, 3) replica casting of PDMS using the SU-8 layer as a master structure, and 4) bonding the obtained PDMS layer on a substrate (e.g., glass) to create microchannels.*

In all replication methods, structures defined by a master mold are replicated on a polymer substrate. The material requirements of the master mold depend on the replication method used, but common desirable attributes include high precision of the structures, minimal surface roughness, and inert interfacial chemistry between the substrate and the mold.[111] In

techniques like injection molding,[118] where thermoplastics are structured by elevated heat and pressure, the structural demands for the mold are more strict, making the mold fabrication more expensive and time-consuming. Many replication methods, such as injection molding and hot embossing,[119] also require specialized machinery. Owing to its simplicity, casting is often the replication method of choice especially in low-cost preliminary prototyping, when new designs are revised on a regular basis. Replication by casting is a straightforward process where the liquid polymer mixture is simply poured on top of a master mold (typically fabricated from SU-8), cross-linked using heat or UV-light, and detached from the mold. The aforementioned PDMS soft lithography process is a typical example of such a replication process, and owing to its many beneficial qualities (see section 2.3.2), PDMS is by far the most widely used material in casting.[120] Because the elasticity of PDMS facilitates the detachment of even very rigid polymers from the mold, PDMS is the most commonly used negative mold material for replicating the master structures on other polymers curable by heat or light.[121]

2.3.2 Materials

As manufacturing materials, polymers offer a wide-range of physico-chemical as well as mechanical properties, and can be classified into three main categories: thermosets, thermoplastic materials, and elastomers.[111,122] Thermosets, such as the photoresist SU-8, are materials that can be cross-linked using heat or radiation, generating a relatively hard and inflexible molecular network. This process is irreversible, and the material cannot be reshaped after curing. Thermoplastic materials, such as poly(methyl methacrylate) (PMMA) show a distinct softening at their glass transition temperature, which permits processing using replication methods. Thermoplastics do not cure *per se*, so they can be reshaped by reheating. Elastomers, such as PDMS, contain long molecular chains that are physically entangled rather than chemically linked. Elastomers characteristically have a low Young's modulus and can return to their original shape after external stress is removed.

The aforementioned simplicity and low cost of PDMS fabrication—along with many beneficial properties, including optical transparency, high oxygen permeability, and inherent cell compatibility—often make PDMS an optimal material, especially for many organ-on-a-chip applications. However, PDMS also has several limitations, including limited solvent tolerance and the tendency to swell upon exposure.[123] PDMS rapidly becomes hydrophobic as it ages, which often causes unwanted adsorption and absorption of hydrophobic molecules on the chip surface and bulk, respectively, altering solute concentrations and inducing cross-contamination between repeated experiments.[124,125] PDMS surfaces can be rendered hydrophilic by plasma oxidation, but the process is reversible and the surface will regain its hydrophobicity with time.[113,126] To overcome the limitations of PDMS, several alternative polymers have been introduced in the literature, including but not limited to PMMA,[127] polycarbonate,[128] and thiol-enes.[129]

The surface chemistry of the microreactor plays a key role, especially in covalent immobilization. The surface must contain a suitable functional group to facilitate immobilization.[130] Most polymer materials, such as PDMS[131] and PMMA[132] are relatively

inert, and the suitable chemistry must be introduced in a separate functionalization step, for example by using ionized gas,[133] wet chemical treatments[132] or UV-induced reactions.[134] These steps often involve the optimization of several inter-dependent parameters, including processing time and temperature, to ensure replicable results.[133]

Since their introduction in the early 2010's,[135] off-stoichiometric thiol-enes (OSTE) have gained increasing attention in the microfluidics community, owing to their tunable physico-chemical and mechanical properties. In general, thiol-enes are a family of thermoset polymers made up of two monomers, each containing at least two thiol or allyl groups.[136] The monomers polymerize via a fast UV-induced click chemistry reaction,[137] leading to high monomer conversion with high selectivity. A key feature of OSTEs is the ability to easily tune the bulk and surface properties of the polymer by simply changing the ratio of the thiol and allyl monomers. The thiol-ene click reaction proceeds through a step-growth polymerization mechanism, consuming both monomers in equal amounts.[137] Using off-stoichiometric compositions will thus result in an excess of one functional group on the polymer surface as well as in the bulk.[138] This feature of the material offers some advantages for the back-end processing steps of microfluidic systems, such as bonding and surface functionalization. Thiol-enes can be fabricated by replica molding,[121,135] which makes them well suited for fast prototyping purposes. Thiol-enes also lend themselves to photolithographic processing with good structural quality.[139] As a result, OSTE have been successfully applied to a variety of different applications including but not limited to microchip electrophoresis,[140] cell culturing,[141] and microreactors.[121,142,143]

In terms of functionalization, OSTE surfaces are intrinsically rich in either free allyl or thiol groups, both of which lend themselves to straightforward bioconjugation via click chemistry reactions.[144–146] Since the thiol-ene reaction is photoinitiated, the bioconjugation can also be spatially controlled by using a photomask.[147] The tunable surface chemistry makes OSTE an excellent material for applications where enzyme immobilization is needed, as evidenced by numerous recent reports on OSTE-based microreactors.[121,142,148,149]

In addition to surface functionalization, bonding is often another stumbling block in the fabrication of sealed microdevices, including flow-through microreactors.[150] OSTE microstructures can be sealed easily by using opposite excesses of thiol and allyl monomers in the layers to be bonded.[135] Instead, most polymer materials lack suitable, reactive surface chemistry to facilitate bonding of two polymer layers. Chemically inert thermoplastics are typically bonded by thermal fusion bonding or adhesive bonding. Fusion bonding is based on heating substrates above their glass transition temperature and pressing the pieces together, effectively "melting" the two layers into one.[150] The resulting seal is rather strong, but the applied heat and pressure may result in simultaneous microchannel deformation. Using an intermediate adhesive layer allows for straightforward bonding of practically any two materials at low temperatures and pressures.[151] However, as it is challenging to apply a uniform and thin layer of the adhesive, the bonding often results in clogging of the channels.[150] Owing to its conformity, PDMS can spontaneously seal against itself or any other smooth surface, without the need for adhesives or special instrumentation.[113] The bonding of native PDMS is reversible and cannot withstand high pressures, but irreversible seals can be made by treating the surface with plasma prior to bonding. From this perspective, the covalent bonding of two OSTE surfaces fabricated using off-stoichiometric

monomer ratios is extremely straightforward and can be done without any surface activation or adhesives.[135] The only caveat of OSTE bonding is that only surfaces with opposite surface chemistries can be bonded together, resulting in varying surface properties in the microstructures. Novel OSTE compositions (marketed under the name OSTE+) containing an additional epoxy component can be bonded using a second heat-initiated thiol-epoxide polymerization step.[152] Another way of circumventing the need for surfaces with opposite chemistries is omitting the photoinitiator from the monomer mixture. In the presence of a photoinitiator, polymerization results in fully polymerized and inert surfaces.[153] Without the initiator, reactive functional groups remain on the surface, allowing strong bonding of the layers, even if they are of the same composition.[140,154] Under these circumstances, bonding strength is mainly defined by the bulk polymer rigidity.[154]

From a material standpoint, the flow-through microreactors used in drug metabolism studies are not the most demanding application, since high pressures are not needed. However, some special characteristics must be considered when selecting a suitable fabrication material. Solvent compatibility is not an issue, since drug metabolism assays are conducted in aqueous buffer solutions. However, solvents may be needed for surface functionalization before enzyme immobilization, depending on the chemistry involved. Operational temperatures are also rather low, but the material should be able to withstand physiological temperatures (i.e., 37 °C). Attention should, however, be paid to a well-known issue common to most polymer materials: the impacts of non-crosslinked monomers or additives possibly leaching out of the bulk polymer.[155,156] These leaching moieties can interfere with the enzymatic reactions of interest, and their effects should be carefully examined to ascertain material inertness in the context of drug metabolism applications.

2.3.3 Design considerations for immobilized enzyme microreactors

As discussed in Chapter 2.2, enzyme immobilization based on solid support binding is likely the most feasible approach for applications involving kinetic characterization to eliminate the diffusional constraints in enzyme kinetic determinations (an inherent challenge with immobilization strategies based on entrapment). In addition to the chemistry used for enzyme immobilization, the amount of immobilized enzyme depends largely on the total available surface area of the reactor. When immobilizing enzymes inside microreactors, the reactor walls rarely provide a high enough surface-to-volume ratio for producing detectable concentrations of metabolites. Various techniques can be utilized to maximize the catalytic surface area of an enzyme reactor, namely packing the reactor with microparticles (Figure 5A),[96,157] polymerizing a porous monolith structure inside the reactor using heat- or UV-light-curable polymers (Figure 5B),[142,158] or fabricating micropillar arrays as solid supports (Figure 5C).[121,159] The pros and cons of these different approaches are discussed in more detail below.

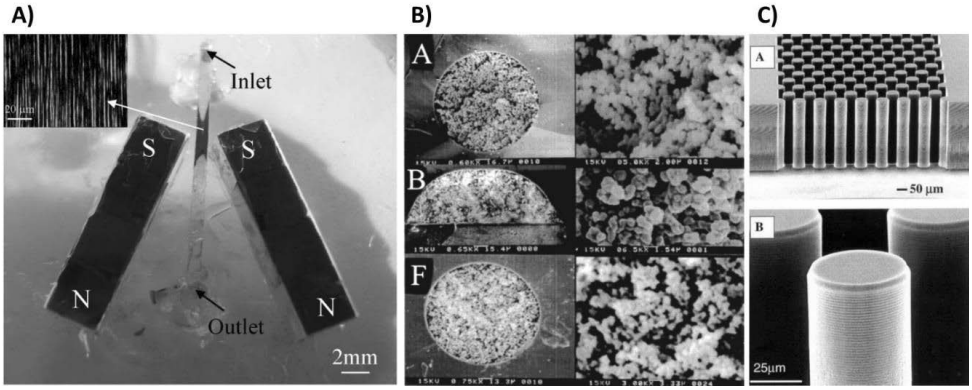

Figure 5. *Microreactor packing strategies. A) Microreactor comprising a plug of magnetic beads maintained between two external magnets. Reproduced from ref. 160 with permission from The Royal Society of Chemistry. B) SEM micrographs of the internal structure of monolithic structures with different polymeric compositions. Reprinted with permission from ref. 158. © 2002 American Chemical Society. C) Microfabricated silicon micropillar structures. Reprinted with permission from ref. 161. © 2002 IEEE.*

A wide range of microparticles are commercially available, featuring different surface chemistries made from various polymers or inorganic materials. Particle packing is relatively straightforward, as the particles can be introduced into the microreactor simply by injection. To prevent particle leakage, a frit structure is usually included in the reactor design.[162] When using magnetic particles, external magnets can also be utilized to hold the particles in place.[160] When using porous particles, mass transport can become an issue as it is restricted by molecular diffusion.[163,164] Tight packing of microparticles can also generate significant back pressure within the system, compromising the sealing of the microdevice.

A porous monolith is usually produced from a single mass of polymeric or inorganic material that is cross-linked *in situ* inside a reactor space.[163] The monolithic material comprises a highly interconnected network of pores facilitating mass transfer by convection. In addition to efficient mass transfer, advantages of monolithic structures over particles include lower back pressures and more stable structures with no risk of solid phase leakage.[163,164] Depending on the starting material, polymerization can be induced by either heat or UV light. When using UV light, monolith formation inside the reactor can be spatially defined by photomasking if the chip material is UV-transparent. Controlling the size and uniformity of the monolith pores and total surface area can be challenging and requires extensive process optimization. Moreover, the porous monolith may introduce diffusional constraints in the same way that scaffold-based immobilization does.

The main advantage of microfabricated micropillars as a solid support is their highly reproducible manufacturing and high degree of design freedom to avoid diffusional constraints. Compared to porous monoliths, the total surface area of micropillar arrays can be kept constant much more easily. This can be of great importance if the amount of immobilized enzyme needs to be precisely controlled and quantitated, as is the case when determining pharmacokinetic constants. Furthermore, compared to a reactor packed with

particles, the perfectly ordered conformation of the pillar array also makes the mass transfer and fluid dynamics in the channel more predictable. Additionally, since the micropillars can be patterned simultaneously with the channel network, no post-processing steps (such as particle packing) are needed.[121]

In addition to the actual microreactor, several auxiliary elements are needed to create a complete analytical setup. Most relevant ones in the microreactor context include flow actuators and detector elements. These additional elements can either be integrated onto the microchip or used as external pieces of equipment. Actuation and detection are discussed in more detail below, as examples of IMER design considerations to evaluate.

In IMERs, reaction time is defined by the flow rate inside the reactor. To enable the accurate determination of enzyme kinetics, the flow rate must be controlled with high accuracy. The most common modes of actuation in microfluidics are electro-osmotic flow (EOF) and pressure-driven flow.[165] EOF occurs when an electric field is applied across a microchannel. It is caused by an electric double layer forming at the interface of the channel and the electrolyte solution that fills the channel. When an electric potential is applied, this mobile layer of ions will induce a bulk flow of solute inside the channel.[166] EOF is a relatively easy way to implement flow actuation, and lends itself to automation via a programmable voltage source. The resulting flow also has a very uniform velocity distribution across the channel cross-section, which is beneficial for certain analytical applications, such as microchip electrophoresis.[167] Because EOF is induced by the interactions between the electrolyte and the channel surface, it is highly dependent on the channel surface chemistry.[166,167] Electro-osmotic pumping is rarely used in IMER applications because enzyme immobilization almost always involves some chemical manipulation of the reactor surface, which could lead to unpredictable changes in EOF velocities. By far the most common actuation method for microfluidic systems is pressure-driven flow.[168] The pressure can be generated either by micropumps integrated on-chip,[169] or by external devices, such as syringe pumps or pneumatic pressure generators. Integrated pressure sources offer minimal dead volumes[170] and integrated fabrication, though at the cost of complexity and inflexibility of the chip design. Off-chip sources provide a simple, universal method of actuation that is compatible with almost any microfluidic device. The caveat of external actuation is the fluidic coupling of the pressure source to the device, which often results in vastly increased dead volumes.

Many chemical reactions need elevated temperatures to reach a sufficient reaction rate, while at the same time many enzymes are easily denatured by elevated temperatures. In particular, CYPs are very sensitive to temperature changes and have a very narrow optimal temperature range (near 37 °C),[171] placing demands for efficient and accurate temperature control. The simplest way to implement microreactor heating is to place the whole setup inside an incubator. However, the spatiotemporal control of heating can be improved by using integrated heating elements with an automated feedback control unit.

The choice of analyte detection method depends primarily on the analytical task at hand. In drug development, pro-fluorescent or pro-luminescent probe substrates are often used in preliminary screening applications because they enable the use of simple workflows compatible with high-throughput well plate protocols.[31] However, due to insufficient enzyme selectivity, these probes do not allow the use of HLM and are instead used mainly

for DDI screening with recombinant enzymes. For most other analytical applications in *in vitro* metabolism studies, liquid chromatography–tandem mass spectrometry (LC-MS/MS) is the industry gold standard due to its universality. The most common detection methods used in microfluidic applications include optical methods based on absorbance or fluorescence, electrochemical detection (EC), and mass spectrometric (MS) analysis. Again, these can be performed either as an integrated unit operation on-chip or by using conventional analytical platforms such as well-plate readers or liquid chromatographs off-chip. In general, miniaturization raises challenges for analyte detection since the number of molecules to detect naturally decreases with smaller volumes. Absorbance detection is particularly affected by miniaturization due to the direct proportionality of the analyte signal to the length of the detection pathway, which is intrinsically small in microfluidic systems.[172] Consequently, electrochemical detection and fluorescence detection with high-power excitation sources (i.e. lasers) are more often used in microfluidic systems. EC is a good fit for microfluidic analysis as detection sensitivity is unaffected by miniaturization. Moreover, miniaturization often results in lower background signals and thus improved signal-to-noise ratios.[173] EC electrodes can be easily implemented on-chip via established microfabrication protocols.[174] Fluorescence detection can offer high sensitivity and can be used for *in situ* detection as well, as long as an optically transparent chip material (such as PDMS or OSTE) is used. However, many analytes—including many metabolites—are not intrinsically electroactive or fluorescent, nor are they chemically suitable for conjugation with electroactive or fluorescent moieties. Of all detection methods, MS offers the best sensitivity and selectivity, while also enabling the identification of unknown compounds in metabolic profiling. Consequently, mass spectrometric detection coupled with LC separation is clearly the most commonly used analysis method in microreactor research. Microfluidic systems have been successfully coupled with MS analysis using several approaches,[175,176] but the integration of on-chip ion sources or chip-to-MS interfacing in general requires special expertise and is by no means a routine task. In practice, the integration of detection methods in drug analysis applications is further complicated by the fact that substrates and metabolites are usually highly chemically similar molecules and can interfere with each other's detection. In addition, other assay constituents, such as enzyme cofactors present in high concentrations, are often fluorescent and interfere with analyte detection via fluorescence. Therefore, a separation step (for example by capillary electrophoresis) is often needed before analyte detection, unless pro-fluorescent probe compounds are used. Given these complications, sample fractions are usually collected out of the microreactor and analyzed off-chip.

2.3.4 Current state of the art in microfluidic drug metabolism studies

Amidst a vast amount of literature on microreactors, those using immobilized CYP or UGT enzymes are under-represented. This is presumably in large part because of the lack of suitable immobilization methods for membrane-bound enzymes. The literature to-date is two-fold, including studies focused on the implementation of enzyme immobilization and studies using IMERs as a part of a highly integrated lab-on-a-chip system (Figure 6).

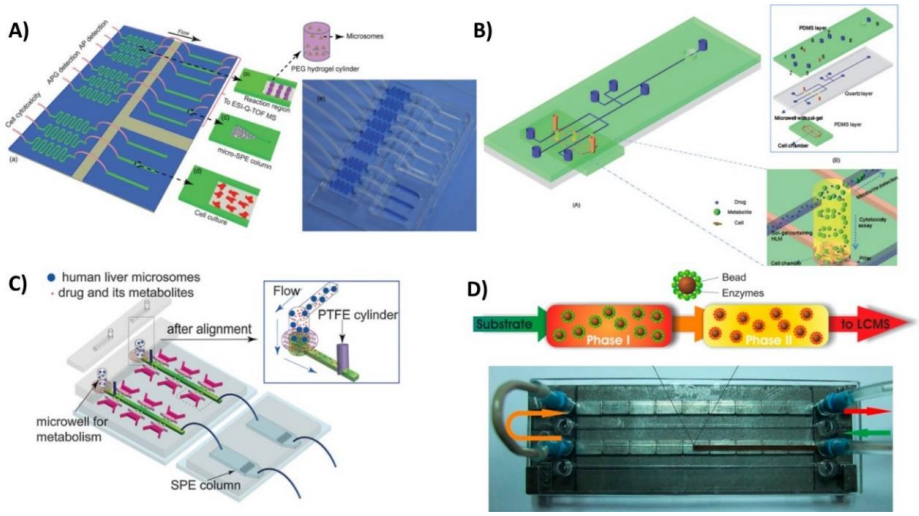

Figure 6. *Integrated microfluidic systems comprising microreactors with immobilized HLM. A) Integrated microfluidic system containing immobilized HLM interconnected to an on-chip SPE-column for pretreatment prior to analysis with ESI-MS, with simultaneous cell toxicity assay with on-chip cultured HepG2 cells. Reproduced from ref. 74 with permission from The Royal Society of Chemistry. B) A microfluidic chip with sol-gel entrapped HLM interfaced with a cell culture chamber and microchip capillary electrophoresis for metabolite analysis. Reproduced from ref. 75 with permission from The Royal Society of Chemistry. C) Schematic drawing of an integrated microfluidic system comprising immobilized HLM for drug metabolism, cell cultivation modules for toxicity assay and sample pretreatment column prior to analysis with ESI-Q-TOF MS Reproduced from ref. 93 with permission from The Royal Society of Chemistry. D) A schematic and a photograph of a modular microfluidic system for the study of coupled phase I–phase II metabolic reactions. Reprinted with permission from ref. 157. © 2014 American Chemical Society.*

Previous studies on microreactors comprising drug-metabolizing enzymes focus mainly on CYP metabolism. In the case of UGTs, studies are limited to only a handful of proof-of-concept studies implemented in conventional capillary-based systems, which do not lend themselves to integration in the same manner as microfluidic systems.[177–179] The drawback of most reported CYP microreactors to-date is that they settle for a brief demonstration of metabolite production on-chip with a modest increase in enzyme stability,[89,97,99] without properly characterizing enzyme function or challenging the setup with enzyme kinetic experiments. On the other hand, when kinetic parameters have been studied in more detail, issues with diffusion-limited kinetics caused by immobilization arise, indicating that there is still room for improvement in the immobilization of membrane-bound enzymes.[92]

Besides reports on the implementation of IMERs, a few proof-of-concept studies have presented impressive integration of HLM microreactors with additional functional units, such as a cell-based toxicity assays or integrated separation and detection units (Figure 6).[74,75,93,157] Kampe et al.[157] demonstrated that sequential phase I–phase II metabolism in a compartmentalized microreactor system can yield drug metabolites that are not obtained in a one-pot suspension assay. The integration of a microreactor module with a cytotoxicity assay and online metabolite analysis with either electrophoresis[75] or MS[74,93] have also been

reported, and such setups have the potential to significantly streamline preclinical drug research. These studies highlight the fact that microfluidics is a widely enabling technique with a view to drug metabolism research. However, all of these studies emphasize only the technical feasibility of integrating the different functional parts. Consequently, the microreactor segments are somewhat vaguely characterized, and little data on enzyme stability or kinetic characterization is presented. This makes the use of these platforms for in-depth investigation of drug metabolism rather premature.

As is the case with most other biological microfluidic models, and also the prevailing in vitro techniques for drug metabolism studies, the impact of oxygen is a completely neglected dimension in microreactor development. All of the previously reported IMER platforms were operated under ambient air, with no capabilities to control oxygen levels inside the reactor. Recently, OSTE polymers were reported to have an inherent oxygen scavenging capability.[180]—a truly unique material property linked with the oxidation of the thioether-linkages in the polymer backbone. The exploitation of material-induced oxygen-scavenging could open new possibilities for implementing metabolism experiments in normoxic conditions using rather simple microchip designs, although for wider exploitation, the mechanistic basis of oxygen scavenging should be examined in greater detail. In conclusion, the current state of the art in microfluidic drug metabolism studies mostly emphasizes the integration of microreactors with other functional units. The microreactor segments themselves remain rather poorly characterized with little data on enzyme stability or kinetics, which undermines their applicability for in-depth investigation of drug metabolism. Consequently, there is a need for a well-characterized, robust, and easily integrated microreactor platform for drug metabolism studies that does not compromise enzyme stability or kinetic properties.

3 Aims of the study

The overall aim of this thesis work was to investigate the applicability of microreactor technology in the study of drug metabolism. To this end, the main technical aim of this thesis was to transfer *in vitro* drug metabolism assays into flow-through conditions by establishing a microfluidic reactor platform incorporating major human drug-metabolizing enzymes. To achieve this goal, both the manufacturing method and the subsequent functionalization and enzyme immobilization steps were carefully examined. The specific aims of the work, and the particular publication (I-III) in which these aims are addressed, were as follows:

- The identification of a suitable fabrication material and surface functionalization strategy for immobilized enzyme reactors (I)
- Development and characterization of an immobilization method for membrane-bound enzymes that does not compromise their activity or kinetic properties (I)
- Validation of the developed methodology in terms of enzyme stability and kinetic parameters of CYPs (I) and UGTs (II)
- Identification and elimination of possible material interactions that could affect metabolic reactions (II, III)
- Understanding the mechanistic basis of material-induced oxygen-scavenging of OSTE (III) and utilizing this phenomenon to control the oxygen partial pressure in microfluidic channels (III)
- Introducing oxygen-control as an integral part of microreactor-based metabolic assays (III)

4 Experimental

This section briefly describes the most relevant chemicals and materials, instrumentation, processes and analytical methods used in this study. More detailed descriptions are found in the respective original publications (I-III).

4.1 Chemicals and materials

Chemicals and commercial materials used in the study are listed in Table 2 and Table 3, respectively. All chemicals were of analytical grade unless otherwise noted. Chemicals and materials used in the fabrication of microchips are listed in Table 4.

Table 2. *Chemicals and reagents used in the study.*

Reagent/solvent	Manufacturer/ supplier	Note	Publication
1,2-dioleoyl-3-trimethylammonium-propane (chloride salt) (DOTAP)	Avanti Polar Lipids, Alabaster, AL	Reagent	I-III
1,2-dioleoyl-*sn*-glycero-3-phophoethanolamine (DOPE)	Avanti Polar Lipids, Alabaster, AL	Reagent	I-III
1,2-dioleoyl-sn-glycero-3-phophoethanolamine-N-(Cap biotinyl) (sodium salt) (biotin-cap-DOPE)	Avanti Polar Lipids, Alabaster, AL	Reagent	I-III
1,2-dioleoyl-sn-glycero-3-phosphoethanolamine-N-(lissamine rhodamine B sulfonyl) (ammonium salt) (Lissamine Rhodamine B-DOPE)	Avanti Polar Lipids, Alabaster, AL	Reagent	I-III
1,2-dipalmitoyl-sn-glycero-3-phosphoethanolamine-N-(cap biotinyl) (sodium salt) (biotin-cap-DPPE)	Avanti Polar Lipids, Alabaster, AL	Reagent	I
2-propanol	Sigma-Aldrich, Steinheim, Germany	Solvent	I-III
3'-amino-3'-deoxythymidine (AMT)	Toronto Research Chemicals, Ontario, Canada	Metabolite	III
5,5-dithio-bis-(2-nitrobenzoic acid)	Sigma-Aldrich, Steinheim, Germany	Reagent	III
6-α-hydroxypaclitaxel	Toronto Research Chemicals, Ontario, Canada	CYP metabolite	II
7-hydroxycoumarin	Sigma-Aldrich, Steinheim, Germany	CYP metabolite	I

8-hydroxyquinoline	Sigma-Aldrich, Steinheim, Germany	UGT substrate	II
8-hydroxyquinoline-glucuronide	Sigma-Aldrich, Steinheim, Germany	UGT metabolite	II
Acetonitrile	Sigma-Aldrich, Steinheim, Germany	Solvent	II
β-nicotinamide adenine dinucleotide 2'-phosphate reduced tetrasodium salt hydrate (NADPH)	Sigma-Aldrich, Steinheim, Germany	Cosubstrate	I-III
Biotin-PEG$_4$-alkyne	Sigma-Aldrich, Steinheim, Germany	Reagent	I-III
Chloroform	Sigma-Aldrich, Steinheim, Germany	Solvent	I-III
Coumarin	Sigma-Aldrich, Steinheim, Germany	CYP substrate	I
Dimethyl sulfoxide	Sigma-Aldrich, Steinheim, Germany	Solvent	I-III
Ethylene glycol	Sigma-Aldrich, Steinheim, Germany	Solvent	I-III
Ethyl phenyl(2,4,6-trimethylbenzoyl)phosphinate (Irgacure® TPO-L)	BASF, Ludwigshafen, Germany	Photo-initiator	I-III
Magnesium chloride hexahydrate	Sigma-Aldrich, Steinheim, Germany	Reagent	I-III
Methanol	Sigma-Aldrich, Steinheim, Germany	Solvent	I-III
Montelukast	Toronto Research Chemicals, Ontario, Canada	CYP inhibitor	II
Paclitaxel	Toronto Research Chemicals, Ontario, Canada	CYP substrate	II
Perchloric acid	Riedel-de Haën, Seelze, Germany	Reagent	I-II
Phosphate buffered saline	Sigma-Aldrich, Steinheim, Germany	Reagent	I-III
Streptavidin (Alexa Fluor® 488 conjugate)	Life Technologies, Eugene, OR	Reagent	I-III
Tris(hydroxymethyl)amino-methane (Trizma® base)	Sigma-Aldrich, Steinheim, Germany	Reagent	I-III
Uridine 5'-diphosphoglucuronic acid trisodium salt (UDPGA)	Sigma-Aldrich, Steinheim, Germany	Reagent	II
Water (Milli-Q)	Millipore, Molsheim, France	Solvent	I-III
Zidovudine	Toronto Research Chemicals, Ontario, Canada	UGT substrate	II-III

Zidovudine glucuronide	Toronto Research Chemicals, Ontario, Canada	UGT metabolite	II

Table 3. *Commercially available materials and products used in the study.*

Material/product	Manufacturer/supplier	Note	Publication
Corning® Supersomes™, rCYP3A4, rCYP2D6	Corning, Wiesbaden, Germany	Recombinant CYP enzymes	I
Dynabeads® M-280	Life Technologies, Oslo, Norway	Magnetic beads	I
Human liver microsomes (HLM), 20 donor pool	Corning, Wiesbaden, Germany	Contains all endogenous CYP/UGT isoforms	I-III
P450-Glo™ assay	Promega, Madison, WI	CYP luminescence assay	I
Pierce™ BCA Protein Assay Kit	Thermo Fischer Scientific, Rockford, IL	Protein quantitation	II
OXNANO oxygen nanoprobes	Pyro Science, Aachen, Germany	Oxygen sensor indicator	III

Table 4. *Microfabrication materials.*

Material/product	Manufacturer/supplier	Publication
1,3,5-Triallyl-1,3,5-triazine-2,4,6(1H,3H,5H)-trione (≥98.0%) (triallyl)	Sigma-Aldrich Saint Louis, MO	I-III
Trimethylolpropane tri(3-mercaptopropionate) (≥95.0%) (trithiol)	Sigma-Aldrich Saint Louis, MO	I-III
Pentaerythritol tetrakis(3-mercaptopropionate) (≥95.0%) (tetrathiol)	Sigma-Aldrich Saint Louis, MO or Bruno Bock, Marscacht, Germany	I-III
Sylgard 184 base elastomer and curing agent	Down Corning Corporation, Midland, MI	I-III
SU-8 developer mr-Dev 600	Micro resist technology, Berlin, Germany	I-III
SU-8 100 photoresist	Micro resist technology, Berlin, Germany	I-III

4.2 Instrumentation

Commercial instruments used in the study are listed in Table 5, with notes explaining their specific use. In addition to the listed instruments, some standard equipment and devices built in-house were also used.

Table 5. *Commercial instrumentation used in the study.*

Material/product	Manufacturer/ supplier	Note	Publication
Microfabrication			
Dymax 5000-EC series UV flood exposure lamp	Dymax Corporation, Torrington, CT	Curing of thiol-enes	I-III
MA-6 mask aligner	Sûss Microtec, Garching, Germany	SU-8 exposure	I-III
miniFactory 3 3D printer	miniFactory, Seinäjoki, Finland	Chip holder fabrication	I-III
OAI LS 30 NUV collimated light source	OAI, San Jose, CA	SU-8 exposure	III
Plasmalab 80+	Oxford instruments, Bristol, UK	Chemical vapor deposition	I-II
Metabolite analysis			
ACQUITY UPLC™ Liquid chromatograph	Waters, Milford, MA	Sample separation	II-III
Varioskan™ Flash multimode reader	Thermo Fisher Scientific, Vantaa, Finland	Fluorescence, luminescence	I
Varioskan™ LUX multimode microplate reader	Thermo Fisher Scientific, Vantaa, Finland	Fluorescence, luminescence	II-III
Xevo Q-S triple quadrupole mass spectrometer	Waters, Manchester, UK	Mass analysis	II-III
Material characterization			
8101e OxySense® Oxygen Transmission Rate Analyzer	Systech Instruments Ltd, Thame, UK	Oxygen permeability measurements	III
DSC 823e Differential scanning calorimeter	Mettler Toledo, Schwarzenbach, Switzerland	Glass transition temperatures	III
Hamamatsu R5929 photomultiplier tube	Cairn Research, Faversham, UK	Fluorescence quantification	I
Moticam 3500 color CCD camera	Motic, Xiamen, China	Image capture	I
Piccolo2 oxygen meter	Pyro Science, Aachen, Germany	Oxygen measurements	III
PicoScope 2203 AD converter	Pico Technology, St. Neots, UK	Fluorescence quantitation	I
Surface tension meter	KSV Instruments Ltd., Helsinki, Finland	Water contact angle measurements	I

Quanta™ 250 FEG scanning electron microscope	FEI, Hillsboro, OR	Microstructure visualization	I-III
Zeiss AxioScope A1 upright epifluorescence microscope	Zeiss Finland, Espoo, Finland	Surface functionalization characterization	I
Zetasizer APS	Malvern, Worcestershire, UK	Liposome size characterization	I
Zetasizer Nano ZS	Malvern, Worcestershire, UK	Liposome size and zeta potential characterization	I
Other			
11 Elite Syringe pump	Harvard Apparatus, Holliston, MA	Flow actuation	I-III
CMA 470 refrigerated microfraction collector	CMA Microdialysis AB, Kista, Sweden	Fraction collection	II-III

4.3 Microfabrication and chip designs

The microreactors developed in this work were fabricated based on replica molding of off-stoichiometric thiol-enes. The fabrication process comprised four steps: 1) fabrication of an SU-8 master; 2) casting of a poly(dimethyl siloxane) (PDMS) mold using the SU-8 master as a template; 3) UV replica molding of the thiol-ene microchannel and cover layer using the PDMS mold; and 4) bonding of the two thiol-ene layers using lamination and UV light. A schematic overview of the fabrication process is illustrated in Figure 7.

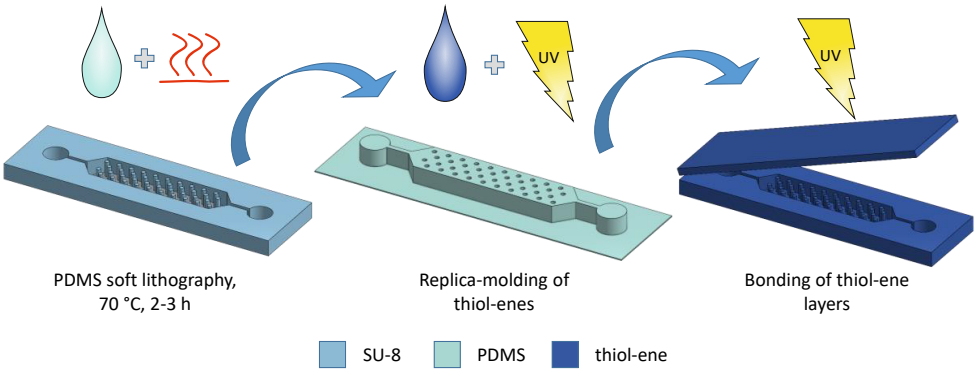

Figure 7. *Schematic of the thiol-ene chip fabrication protocol.*

The microfabrication of the SU-8 masters using UV photolithography was done either in a cleanroom environment (Micronova, Espoo, Finland, Publications I-II) or in a regular wet chemistry laboratory setting (Faculty of Pharmacy, University of Helsinki, Finland, Publication III). Detailed fabrication parameters can be found in the respective original

papers and supporting materials. Briefly, SU-100 negative photoresist was spin coated on a 4 inch silicon wafer substrate and soft baked on a hotplate to yield a 200-µm-thick layer of SU-8. After UV exposure through a photomask, the master was developed by immersion in mr-Dev-600 developer.

The PDMS molds were prepared by mixing the Sylgard 184 base elastomer and the curing agent in a 10:1 ratio (w/w). After degassing in a vacuum for 30 min, the mixture was casted onto the SU-8 master and cured by heat (70 °C for 3 h or 65 °C overnight).

The thiol-ene layers were prepared by mixing trimethylolpropane tri(3-mercaptopropionate) (i.e., "trithiol") or pentaerythritol tetrakis(3-mercaptopropionate (i.e., "tetrathiol") and 1,3,5-Triallyl-1,3,5-triazine-2,4,6(1H,3H,5H)-trione (i.e., "triallyl") monomers (Figure 8) in a defined molar ratio with respect to free functional groups. After pouring the monomer mixture onto the PDMS mold and degassing in a vacuum for approximately 5 min, the thiol-ene was cured under UV light for 5 min (Dymax EC5000 flood exposure lamp, nominal power 225 mW/cm^2). The cured microchannel and lid layers were heated above their glass transition temperature (ca. 70 °C), laminated together, and exposed to UV light for an additional 2 min.

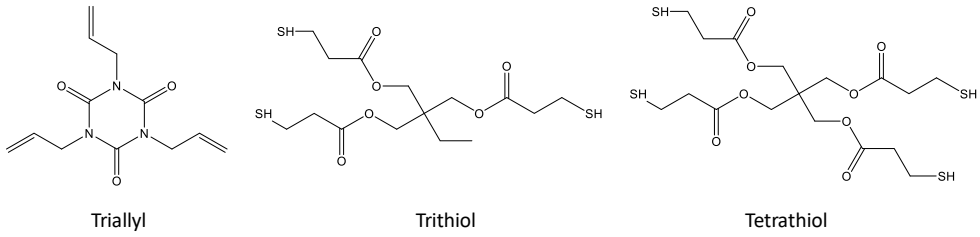

Figure 8. *Chemical structures of the thiol and allyl monomers used for fabricating thiol-ene microreactors.*

The chip designs utilized in this thesis are illustrated in Figure 9. Design 1 involved a single-channel microreactor featuring a dense micropillar array for maximizing the surface area available for enzyme immobilization. Design 2 was an integrated design with the microreactor compartment interfaced with six serially connected micropillar channels responsible for scavenging oxygen out of the feed solution. The micropillar array consisted of an array of approximately 14,400 micropillars (Ø 50 µm) in a hexagonal lattice with an interpillar (center-to-center) distance of 100 µm.

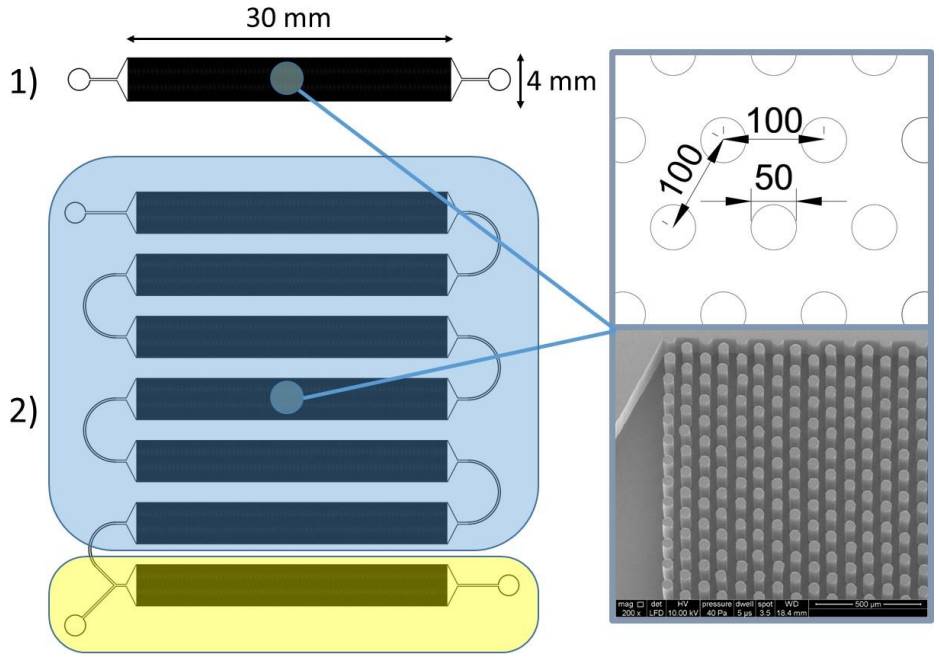

Figure 9. *Schematic drawings of the chip designs used in this work: 1) single-channel microreactor with a micropillar array (publications I and II), and 2) integrated design with the microreactor (highlighted in yellow) interfaced with six serially-connected micropillar arrays for oxygen scavenging (highlighted in blue) (publication III). The inlay shows the detailed dimensions of the micropillar array (in µm), and a SEM image of the pillar array.*

4.4 Immobilization of human liver microsomes

The method for immobilizing membrane-bound enzymes on solid supports developed in this thesis comprised of two steps: 1) biotinylation of membrane constructs comprising the enzymes (i.e. liver microsomes) via spontaneous fusion with biotin-tagged fusogenic liposomes, and 2) immobilization of the biotinylated membrane constructs on avidin-functionalized microreactors made of off-stoichiometric thiol-enes.

4.4.1 Biotinylation of lipid membranes using fusogenic liposomes

The lipid composition of the biotinylated fusogenic liposomes (b-FL) used in this study was modified from previous work.[181,182] The b-FL were prepared by mixing chloroform stock solutions of 1,2-dioleoyl-*sn*-glycero-3-phophoethanolamine (DOPE), 1,2-dioleoyl-3-trimethylammonium-propane (DOTAP), biotin-cap-DOPE (all 10 mg/mL), and lissamine rhodamine B-DOPE (1 mg/mL) in a lipid mass ratio of 1:1:0.1:0.05, respectively. After the bulk solvent was evaporated under a stream of nitrogen, the lipid mixture was kept in

vacuum conditions for an additional 2 h to remove any solvent residues. Next, the dry lipid film was re-solvated in PBS to yield a total lipid content of 2 mg/mL and vortexed for 1 h at room temperature. The resulting multilamellar liposomes were passed through a polycarbonate membrane (pore size = 100 nm) 51 times to yield large unilamellar vesicles (average size 220 ± 25 nm, n=4 batches). Finally, the b-FL (2 mg/mL) and HLM (20 mg/mL total protein) stock solutions were mixed in equal volumes and incubated at 37 °C for 15 min to yield biotinylated HLM (b-HLM). A schematic describing the biotinylation process is presented in Figure 10.

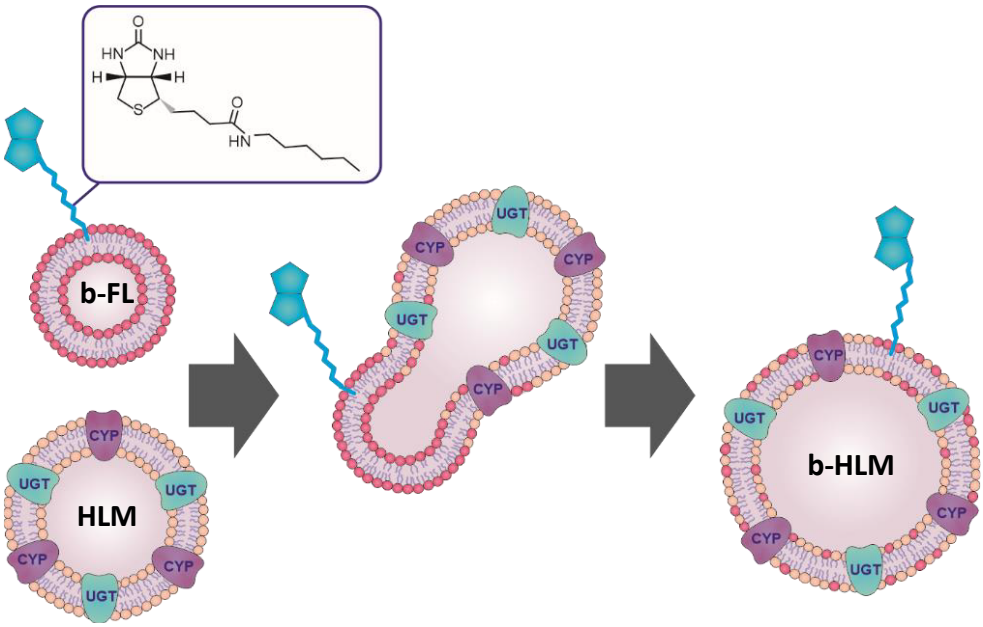

Figure 10. *A schematic describing the biotinylation of human liver microsomes using biotin-tagged fusogenic liposomes. Abbreviations: b-FL, biotinylated fusogenic liposome; HLM, human liver microsome; b-HLM, biotinylated human liver microsome. Adapted with permission from ref. 183. © 2019 John Wiley and Sons.*

4.4.2 Microchip functionalization with avidin and enzyme immobilization

To enable the immobilization of biotinylated HLM inside the microreactor with biotin-avidin chemistry, the microreactor surface was functionalized with streptavidin (Figure 11). First, the reactor was filled with biotin-PEG_4-alkyne (0.1 mM in ethylene glycol with 1% Irgacure® TPO-L as the photoinitiator) and exposed to UV light for 1 min (λ = 365 nm, LED, nominal intensity 14 mW/cm^2). After rinsing with both methanol and water (≥ 5mL each), the channel was filled with 0.5 µg/mL streptavidin (in PBS), incubated at room temperature for 30–45 min and rinsed with ≥ 5 mL PBS. Finally, the reactor was filled with b-HLM (prepared as described in section 4.4.1), the inlets were sealed with Parafilm and

the chips were left to incubate at 4 °C overnight. Before use, the microreactor was rinsed with ≥ 5mL of the run buffer.

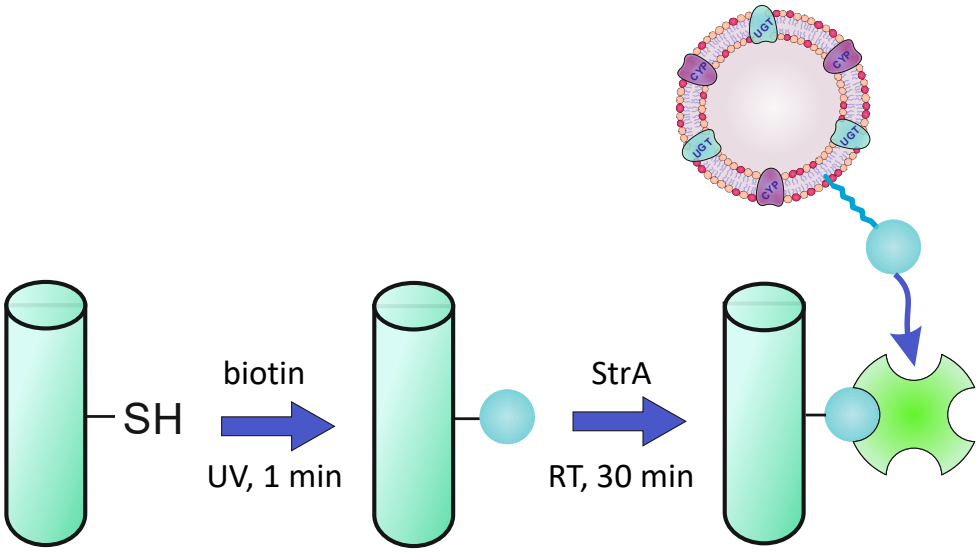

Figure 11. *A schematic describing the microreactor functionalization and enzyme immobilization protocols.*

Streptavidin-functionalized magnetic beads were also used as the immobilization matrix when validating and optimizing the immobilization protocol. Before use, required amount of the superparamagnetic beads pre-functionalized with streptavidin (10 mg/mL, particle diameter 2.8 µm) were pretreated according to the supplier's protocol. Next, the beads were divided into 25 µL aliquots (0.25 mg of beads) and the supernatant was discarded with the help of an external neodymium magnet. The b-HLM (15 µL) was immediately added onto the beads and the suspension was incubated on a tilt rotator for 30 min at room temperature. Next, the supernatant was discarded and the beads were washed 4–5 times with 50 µL PBS. Beads were stored in 50 µL of PBS at 4 °C until use. To serve as a negative control, the beads were also functionalized with biotinylated DOPE or DPPE lipids, followed by native HLM.

4.5 Implementation of flow-through assays

The feed solution was fed through the microreactor with an external syringe pump. The reaction time of the flow-through enzyme assays was adjusted by controlling the linear flow rate of the feed solution. Metabolites were quantified by collecting 50 µL fractions of the output solution either manually or with the help of an automated refrigerated fraction collector. After initiating the flow, one dummy fraction was collected to fill the reactor with

the feed solution. When needed, substrate concentration gradients were created using two interconnected syringe pumps (Figure 12). The chips were heated to physiological temperature (37 °C) by placing an aluminum heating element under the reactor. The temperature on top of the reactor was monitored with a thermocouple and set to 35 °C using a proportional–integral–derivative (PID) controller connected to the circuit. Based on an earlier study,[184] the temperature on top of the channel was assumed to reflect the temperature inside the channel to within 2 °C.

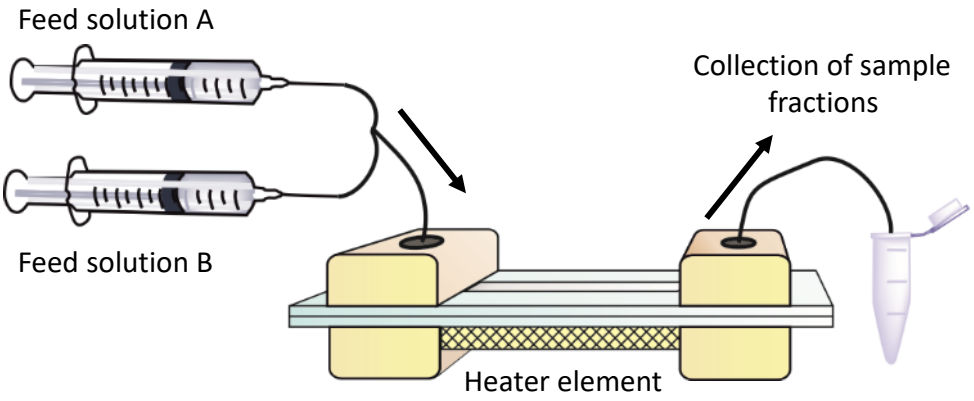

Figure 12. *Schematic view of the implementation of flow-through assays.*

4.6 Model reactions

To evaluate if the immobilization of b-HLM affects CYP or UGT metabolism, the kinetic constants obtained with immobilized enzyme were compared with reference assays performed with non-immobilized HLM in test tubes. The model reactions and assay conditions used for studying CYP and UGT metabolism are summarized in Table 6 and Table 7, respectively.

Table 6. *A summary of CYP model activities and assay conditions used in the study. When studying the effect of immobilization on the kinetic parameters of selected model reactions, b-HLM was immobilized on streptavidin-coated magnetic particles.*

	CYP2A6	CYP2C9	CYP2D6	CYP3A4
Substrate	Coumarin	Luciferin-H	Luciferin-ME EGE	Luciferin-IPA
[S] range for determination of K_M	1-2-4-8-16-32-64 µM	25-50-75-100-150-200-400 µM	7.5-15-22.5-30-45-60-120 µM	2-4-6-8-12-16-32 µM
Metabolite	7-hydroxycoumarin	Luciferin		
Buffer	Tris (0.1 M, pH 7.5) + 3.3 mM $MgCl_2$	Potassium phosphate (0.1 M, pH 7.4)		
HLM (total protein)	0.4 mg/mL	0.4 mg/mL	0.4 mg/mL	0.2 mg/mL
Incubation time	15 min	30 min	30 min	10 min
Stop reagent	4 M perchloric acid (10 µL)	Luciferin detection reactant (100 µL)		
Detection	Fluorescence Ex 325 nm/em 470 nm	Luminescence		

Table 7. *A summary of UGT model activities and assay conditions used in the study. When studying the effect of immobilization on the kinetic parameters of selected model reactions, b-HLM was immobilized inside thiol-ene microreactors.*

	UGT, various isoforms	UGT2B7
Substrate	8-hydroxyquinoline	Zidovudine
[S] range for determination of K_M	n/a	25-50-100-200-400-800-1600-3200-6400 µM
Metabolite	8-hydroxyquinoline glucuronide	Zidovudine glucuronide
Buffer	Tris (0.1 M, pH 7.5) + 5 mM $MgCl_2$	
HLM (total protein)	0.2 mg/mL	0.1 mg/mL
Incubation time	10 min	30 min
Stop reagent	4 M perchloric acid (10 µL)	
Detection	Fluorescence Ex 245 nm/em 475 nm	LC-MS

Control incubations with non-immobilized HLM were conducted in Eppendorf tubes at 37 °C in a total volume of 100 µL. Either NADPH (for CYP enzymes) or UDPGA (for UGT enzymes) was used as a cofactor at a concentration of 1 mM. The incubation buffer, the amount of HLM, and the incubation time were adjusted enzyme-specifically. Prior to initiating the reaction with the addition of the co-substrate, the HLM and the substrate were mixed and preincubated at 37 °C for 5 min. If alamethicin was used in the UGT incubations, the HLM was incubated with alamethicin at 4 °C for 30 min prior to the 5 min preincubation at 37 °C. The reactions were stopped by the addition of 10 µL of ice-cold 4 M perchloric acid, after which the samples were kept on ice for 20 min, centrifuged at 16 000 g for 10 min, and the supernatants were transferred for analysis. Assays conducted using the

commercial luminescent CYP probes were stopped by the addition of the Luciferin detection reagent (100 µL) and incubated at room temperature for 20 min prior to analysis.

4.7 Analytical methods

Fluorescence (umbelliferone and 8-hydroxyquinoline glucuronide) and luminescence (luciferin substrates) detection of drug metabolites was carried out on a Varioskan Flash or a Varioskan LUX multimode microplate reader. Zidovudine-glucuronide and 3'-amino-3'-deoxythymidine (AMT) samples were analyzed with liquid chromatography-electrospray ionization-tandem mass spectrometry (LC-ESI-MS/MS). A Waters Acquity UPLC BEH C-18 reverse-phase column was used for chromatographic separations. Analytes were detected in negative polarity mode using multiple reaction monitoring. Detailed method parameters are outlined in Publications II and III.

4.8 Material characterization

The mechanical and physico-chemical properties of OSTE were characterized in detail using the methods described in this section. The structural quality of the microfabricated structures was evaluated using scanning electron microscopy (SEM). The success of biofunctionalization of thiol-ene surfaces was monitored using both fluorescence microscopy and water contact angle (WCA) measurements. The oxygen scavenging properties of thiol-ene polymers and monomers were characterized optically using an oxygen-sensitive fluorescent dye. To further characterize material properties affecting oxygen diffusion, glass transition temperatures and oxygen permeation of selected thiol-ene compositions were determined.

4.8.1 Structural fidelity

The structural fidelity of the microstructures was assessed by scanning electron microscopy. Samples were attached onto the sample stage with carbon-coated double-sided tape and sputtered with platinum for 25 seconds (30 mA), yielding a 5-nm-thick coating.

4.8.2 Glass transition temperature

Glass transition values for thiol-ene samples were determined by differential scanning calorimetry. The analysis method was comprised of three steps: 1) cooling the sample to -35 °C; 2) a 3-min isothermal sequence; and 3) heating the sample from -35 °C to 100 °C at a rate of 20 °C/min using nitrogen as a purge gas. Glass transition temperatures were determined using STARe software.

4.8.3 Oxygen permeability

To determine the oxygen permeability of different thiol-ene compositions, thin polymer membranes were fabricated by applying a small amount of uncured thiol-ene monomer mixture on a PDMS-coated glass plate, laminating this with another glass plate and curing under UV light for 5 min. The glass slides were separated by pieces of double-sided tape, resulting in a membrane thickness of 100-200 µm. Membrane thickness was measured separately for each sample before the permeability measurement. The oxygen permeability of the samples was determined from two replicate samples using an 8101e OxySense® oxygen transmission rate analyzer equipped with a coulometric detector.

4.8.4 Wettability

The wetting properties of OSTE surfaces after different functionalization steps were characterized using the sessile water drop contact angle method.[185] To determine the water contact angle (WCA), three drops of Milli-Q water were placed randomly over the OSTE surfaces and the contact angle was recorded with an optical contact angle meter and analyzed using Attension Theta software (Version 4.1.0).

4.8.5 Streptavidin binding and enzyme immobilization

The binding of streptavidin on biotin-functionalized thiol-ene surfaces and the immobilization efficiency of b-HLM vesicles on streptavidin-coated thiol-ene microchannels was monitored on a Zeiss AxioScope A1 upright epifluorescence microscope equipped with a Plan-Neofluar 20×/0.4 Corr objective and a HAL100 halogen lamp (100W). The fluorescence signals of Atto 488-labelled streptavidin (ex 488/em 500–700 nm) and lissamine rhodamine B (ex 546±6 nm, em 575–640 nm) were monitored using a Moticam 3500 color CCD camera or quantified using a Hamamatsu R5929 photomultiplier tube equipped with a signal amplifier module and a PicoScope 2203 analog-to-digital (AD) converter.

4.8.6 Material inertness

The amount of thiol monomers leaching out of the cured OSTE microreactors (fabricated with 25% molar excess of tetrathiols) was quantified by titration using Ellman's reagent (5,5′-Dithiobis[2-nitrobenzoic acid], DNTB).[186] First, the free surface thiols were eliminated by incubating a 1 mM DNTB solution inside the channel for 30 min. Next, fresh DNTB solution was incubated inside the channel for different periods of time (10, 20 and 30 min) followed by the quantitation of thiols based on the UV absorbance of the reaction product, 2-nitro-5-thiobenzoate (TNB) (412 nm). For thiol quantitation, a molar extinction coefficient of ε = 14 150 /M cm was assumed for TNB.[187]

4.8.7 Oxygen scavenging

Oxygen levels inside thiol-ene microchannels were monitored using a fiber-optic oxygen meter combined with nanoparticles functionalized with a fluorescent indicator dye. This measurement is based on the oxygen-sensitivity of the fluorescence lifetime of the dye. The nanoparticles were dispersed in de-ionized water at a concentration of 1 mg/mL and the fluorescence signal was measured through the optically transparent thiol-ene top layer. The meter was calibrated with solutions containing 100% and 0% dissolved oxygen. The 100% calibration solution was prepared by repeatedly vortexing a small amount of the nanoparticle solution, opening the tube cap in between vortexes. The 0% solution was prepared by combining 0.1 mg/mL glucose oxidase and 10 mg/mL glucose in to a small aliquot of nanoprobe solution and incubating the sample at room temperature for 10 min.

The effect of polymer composition and different pre-treatments of OSTE on its oxygen scavenging properties were investigated using an array of rectangular OSTE microchannels (2×30×0.2 mm) bonded on top of a glass substrate. The channels (n=4–8 per treatment group) were filled with the nanoprobe solution and the inlets were sealed with Parafilm to prevent evaporation. At each time point, five measurements were taken along each channel's length. Oxygen scavenging under flow conditions was studied by connecting thiol-ene microchannels to a syringe pump filled with the nanoprobe suspension. All measurements were performed at 37 °C, and the temperature was maintained using an aluminum heating block, as with the microreactors.

5 Results and discussion

5.1 Conceptualization

This chapter briefly summarizes the rationale behind the choices made in this study, with respect to microreactor design, materials, and experimental protocols.

With a view to kinetic studies, immobilization approaches based on support binding were mainly considered because they are less prone to diffusion-limited kinetics, as discussed in Chapter 2.2. Micropillars were chosen as the solid support for enzyme immobilization because of two main advantages: 1) the ease of fabrication and operation, and 2) well-defined surface area. Unlike monolith fabrication or particle packing, the fabrication of micropillars is straightforward with no need for additional postprocessing, thereby speeding up the fabrication process. In the author's experience, retaining magnetic particles inside microchannels using external magnets is extremely challenging and difficult to reproduce. Unlike with monoliths, the surface area of the pillar array is precisely defined, facilitating quantitation of enzyme coverage. Furthermore, pillar arrays are not as prone to clogging as monoliths, further streamlining the microreactor operation.

OSTE was chosen as the chip fabrication material because of its many advantageous features, discussed in section 2.3.2. Most notably, these include the tunable surface chemistry that allows the facile functionalization of the microreactor surface and the unique capability of material-induced oxygen-scavenging on-chip. OSTE show very good optical transparency down to the UV-A region (<325 nm).[145] This is especially important when optical detection of analytes is performed on-chip. While in this study the metabolites were analyzed off-chip, this property was nevertheless essential to enable the UV-induced biotinylation step in the microreactor functionalization protocol. No photoinitiator was used in the polymerization, both to ensure that the polymer surfaces had sufficient amount of free, unreacted thiol groups for functionalization and to facilitate the bonding of the chip layers.

Syringe pumps were chosen as the actuation method because of their operational simplicity in comparison to pressure controllers. Using in-house 3D-printed chip holders and commercial capillary connectors, the interfacing of chips and syringes was relatively straightforward with no need for adhesives. The somewhat larger dead volumes compared with integrated actuation solutions did not present a problem since the sample volumes were comparatively large (tens of microliters vs. dead volumes of a few of microliters) and the reaction constituents were inexpensive and readily available.

While it is possible to integrate detection elements with microfluidic chips, the selective detection of metabolites is usually possible only after a separation step, which further complicates the necessary chip design. Consequently, this study focused only on validating of the biological relevance of the developed microreactor platform, and metabolite analysis was done off-chip. The range of studied substrates was very diverse; some substrates were compatible with straightforward fluorescence detection with a well-plate reader (a particularly useful quality for the method development phase), while others required more demanding methods, such as LC-MS/MS analysis. The use of off-chip metabolite detection

offered the needed flexibility for the analysis of a host of different analytes with varying properties.

Given the proof-of-concept nature of this study, integration of different functional units on the chips was kept to a minimum. Additional elements, such as integrated heaters[188,189] or gradient generators.[190] would have inevitably complicated the fabrication process and decreased chip fabrication yields, while not offering any added value at this early stage of development. As a notable exception, the integration of an oxygen-scavenging compartment with the microreactor unit was studied as a means of performing metabolic assays under a controlled oxygen environment (see section 5.5.2).

5.2 Enzyme-immobilization using fusogenic liposomes

5.2.1 Method development

Biotinylation of microsomes

The lipid membrane biotinylation protocol developed in this thesis was based on the spontaneous fusion of biotin-tagged liposomes with lipid bilayers. *In vivo,* membrane fusion is an important phenomenon in processes ranging from exocytosis to protein trafficking and fetal development, and is usually governed by specialized fusion proteins.[191,192] However, specific liposome compositions enable spontaneous lipid bilayer fusion even in the absence of fusion proteins. These fusogenic liposomes (FL) have already been utilized in the functionalization of cell membranes with various chemistries[181,182,193] and as drug nanocarriers for intracellular proteins.[194] The rationale behind the selection of liposome composition is elaborated below.

The ability of lipid bilayers to form fusion intermediate states depends on the lipid composition. The fusion propensity of liposomes is determined by the curvature of the monolayer formed spontaneously by the lipid: Lipids with a positive curvature (monolayers bulged in the direction of the polar heads) tend to inhibit the formation of fusion intermediates, whereas lipids with a negative curvature promote intermediates. Fusion can also be promoted by sufficiently close contact of the two bilayers,[191,192] which can be induced by incorporating positively charged lipids into the liposome composition.[195,196] The close contact of the membranes results in a mutual surface-charge neutralization, and membrane contact is further enhanced by the loss of water molecules bound by hydrogen bonding to the membrane surface.[195] Another factor affecting liposome fusogenicity is liposome size, with the smallest liposomes being the most fusogenic. Increased membrane tension in small liposomes is hypothesized to drive the evolution of intermediary structures into fusion pores.[197,198]

Based on these principles, the liposome lipid composition used in this study was tailored to favor spontaneous fusion with the HLM vesicles. DOPE is a neutral lipid that shows negative curvature and promotes fusion. DOTAP has a net positive charge, promoting close contact between the liposomes and the negatively charged HLM. The fluorescent DOPE

tagged with lissamine rhodamine B serves a dual function. While the fluorescence allows the monitoring of b-HLM immobilization via fluorescence microscopy, the polarization of the delocalized π-electrons in the rhodamine moieties also induces membrane instabilities and disorders that promote fusion.[181,191]

Prior to fusion with HLMs, the multilamellar liposomes (average hydrodynamic radius 493 ± 87 nm, n=4 batches), resulting from re-solvation of the dry lipid film into PBS were extruded to yield unilamellar liposomes with a reduced diameter (220 ± 25 nm, n=4 batches). Upon mixing, the opposite charges of the HLM (-44.3 ± 4.9 mV) and the fusogenic liposomes (69.3 ± 1.8 mV) facilitated fusion by promoting close contact. The occurrence of liposome fusion was verified spectroscopically based on a previously described protocol.[199] Briefly, the rhodamine B fluorophore included in the liposome composition has a self-quenching propensity that is proportional to its surface density. Liposome fusion with unlabeled membranes and the consequential decrease in surface density results in an increase in fluorescence intensity (Figure 13), which can be taken as an indication of successful fusion.

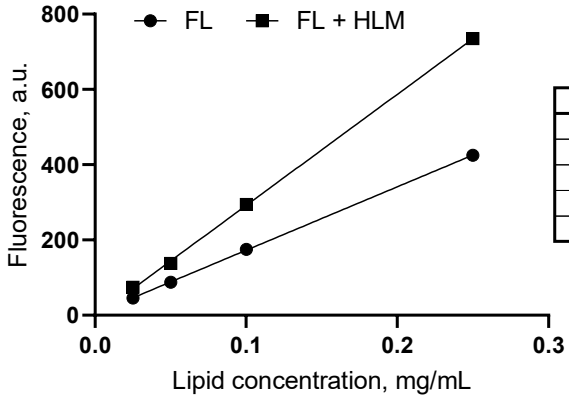

	FL	FL + HLM
Best-fit values		
Slope	1686	2952
Y-intercept	4.187	-3.316
X-intercept	-0.002483	0.001123
1/slope	0.0005932	0.0003387

Figure 13. *Fluorescence signal (ex 560/ em 583) of fusogenic liposomes (FL) with and without the presence of human liver microsomes (HLM) (liposome-HLM ratio 1:10).*

Microreactor functionalization and enzyme immobilization

The robustness of the microreactor functionalization protocol, in terms of the effects of bulk monomer composition and biotin and streptavidin concentrations, was determined by measuring the amount of immobilized streptavidin and b-HLM based on their respective fluorescent tags (Figure 14A-C) (Publication I). Changes in surface properties after each functionalization step were also assessed by changes in water contact angles (Figure 14D). The amount of bound streptavidin increased with increasing amounts of biotin, which could be altered by either the number of free surface thiols or the concentration of the biotin-PEG used for initial surface functionalization. However, the amount of immobilized b-HLM was inversely proportional to the amount of bound streptavidin. Excess streptavidin on the reactor surface likely caused steric hindrance that hindered biotin-streptavidin binding. For

all further experiments, 0.1 mM biotin, 0.5 µg/mL streptavidin, and a 25% molar excess of thiol functional groups were used, as this was shown to result in highest amount of bound b-HLM compared with other tested conditions.

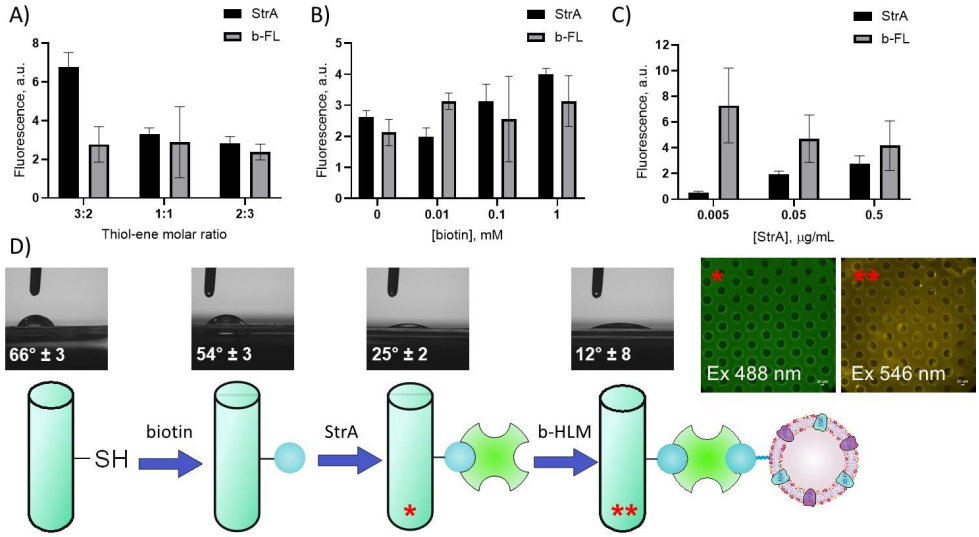

Figure 14. *The effect of A) thiol-ene molar ratio, B) biotin, and C) streptavidin concentration on the binding efficiency of streptavidin (StrA*) and biotinylated fusogenic liposomes (b-FL**) on thiol-ene micropillar surfaces as quantified by fluorescence microscopy (n= 3 IMERs in each case, streptavidin: ex 488/em 500–700 nm; b-FL ex 546/em 575–640 nm). D) A schematic of the functionalization protocol with inlays of fluorescence microscopy pictures and water contact angle measurements of thiol-ene surfaces (25% molar excess of thiol monomers) after each step of the functionalization protocol. Adapted with permission from ref. 183. © 2019 John Wiley and Sons.*

The specificity of the functionalization protocol was verified by sequentially omitting one step of the functionalization and determining the mean cumulative amount of metabolite produced in a 60 min time period from three parallel IMERs. Although some nonspecific binding of both streptavidin and b-HLM can be seen in the fluorescence characterization, the activity of IMERs prepared using the optimized protocol showed significantly higher activity compared to the samples where one or more functionalization steps were omitted ($p < 0.0001$, one-way ANOVA followed by Dunnett's test, Figure 15A). This suggests that the proper binding of b-HLM is contingent on each step of the protocol and any nonspecifically bound enzymes will leak out of the reactor upon the application of flow. The CYP and UGT activities of immobilized b-HLM were also shown to be dependent on the reaction temperature, as expected based on the behavior of native non-immobilized HLM (Figure 15B). To demonstrate the universal applicability of the developed immobilization method, the protocol was also successfully applied to recombinant CYP2D6 and CYP3A4 enzymes expressed in insect cells (Supersomes) (Figure 15C). The average amount of immobilized enzyme was determined by measuring the protein content in the

rinse solution after immobilization using the colorimetric bicinchoninic acid assay,[200] and subtracting this from the amount of protein in the filling solution. Based on the assay, the average amount of immobilized protein was 0.021 ± 0.010 mg (n=4 microreactors).

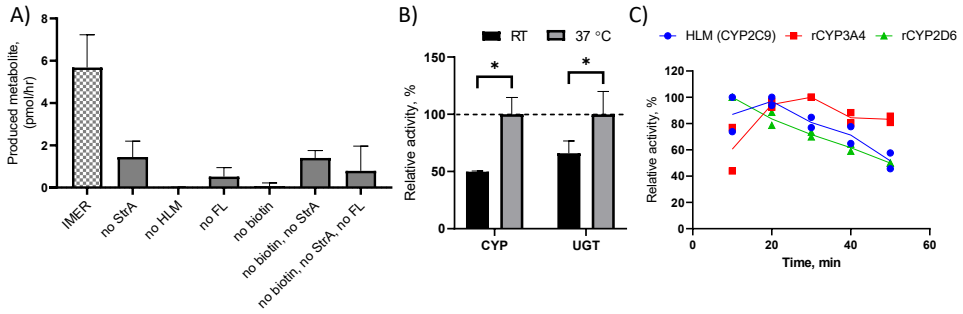

Figure 15. *Characterization of the IMER performance. A) Cumulative metabolite production (over 60 min) of CYP-IMERs prepared by sequentially omitting each of the steps in the functionalization protocol. The model reaction used was Luciferin-H hydroxylation via CYP2C9. Error bars denote the standard deviation between n=3 microreactors in each case. B) Temperature-dependence of CYP and UGT activities of immobilized b-HLM, as assayed using coumarin (CYP2A6) and 8-hydroxyquinoline (multi-UGT substrate) as probe substrates. Activity at 37 °C was set as 100%. Error bars denote the standard deviation between n = 3 IMERs in each case. *p-value < 0.05 (Student's t-test). C) Relative activity of IMERs featuring immobilized HLM or different immobilized recombinant CYP enzymes (rCYP). The specific probe substrates used were Luciferin-H (HLM, CYP2C9), Luciferin-IPA (rCYP3A4), and Luciferin-ME EGE (rCYP2D6) (n=2 IMERs each).*

5.2.2 Protocol validation

For an immobilization method to be truly applicable for the study of drug metabolism the applied processing should not alter enzyme kinetic parameters, otherwise the results cannot be reliably extrapolated to the *in vivo* context. In addition, the immobilization of the enzyme should not compromise enzyme activity or stability. The immobilization method developed in this thesis was validated for both the kinetics and stability of CYP- (Publication I) and UGT-catalyzed (Publication II) reactions.

Enzyme kinetics

The effect of immobilization on enzyme kinetics was evaluated by immobilizing b-HLM on streptavidin-coated magnetic particles as described in section 4.4.2. (Publication I). Only CYP enzymes were investigated in this preliminary characterization in order to focus specifically on the effects of biotinylation and subsequent immobilization on enzyme kinetics. CYPs reside on the cytosolic side of the microsomal membrane[12] and are freely accessible to substrate binding in the absence of steric or diffusional constraints imposed by immobilization. However, the kinetics of UGT enzymes, which reside on the luminal side

of the membrane,[17] are complicated by the mass transfer limitation caused by the intact microsomal membrane. This will be discussed in more detail in section 5.4.

In addition to CYP2A6, which was used for the initial method development, enzyme kinetic parameters were also determined for three CYP isoforms most often involved in the metabolism of pharmaceuticals—CYP3A4, CYP2C9 and CYP2D6[7]—using enzyme-specific substrates. For each enzyme tested, the K_M values of the immobilized b-HLM were comparable to values obtained using native, non-immobilized HLM (Table 8). This confirmed that the developed immobilization strategy does not suffer from impaired diffusion, a typical issue in entrapment approaches that often leads to several-fold increases in apparent K_M.[92] Since the protein itself is not targeted in the biotinylation process, this method also leaves the active sites of the CYPs better accessible compared to other approaches, such as those based on covalent bonding.[96,97]

Table 8. *K_M values determined for different CYP enzymes (±standard error) in non-immobilized HLM or immobilized on commercial streptavidin-coated magnetic beads. In each case, n=2 independent incubations in each case.*

Enzyme	K_M (μM)	
	Nonimmobilized	Immobilized
CYP3A4	5.2 ± 0.5	15.8 ± 1.2
CYP2C9	75.1 ± 5.3	116.4 ± 37.3
CYP2D6	21.0 ± 2.4	32.0 ± 5.2
CYP2A6	2.9 ± 0.3	2.2 ± 0.5

Enzyme stability

Comparison of the enzyme activities of native HLM and b-HLM confirmed that the biotinylation process did not significantly alter the activity of soluble CYP (Publication I) (Figure 16A). This was expected since the biotinylation process does not require any covalent modifications to the enzyme itself, which could result in enzyme inactivation. The stability of immobilized b-HLM was further studied by immobilizing b-HLM on streptavidin-functionalized magnetic particles. No significant loss of CYP activity was observed with immobilized b-HLMs even after two weeks of storage at 4 °C (Figure 16B). By contrast, negative controls prepared by solubilizing non-biotinylated HLMs on lipid-coated magnetic beads lost half of their activity after 6 days. Upon repeated incubations, the CYP activity started to decrease, typically halving after each incubation cycle. This was likely caused by incomplete recovery of the beads during the incubation and washing steps of the assay protocol. Similar loss of activity was also reported by Schejbal et al., when immobilizing recombinant microsomal CYPs on magnetic particles.[96]

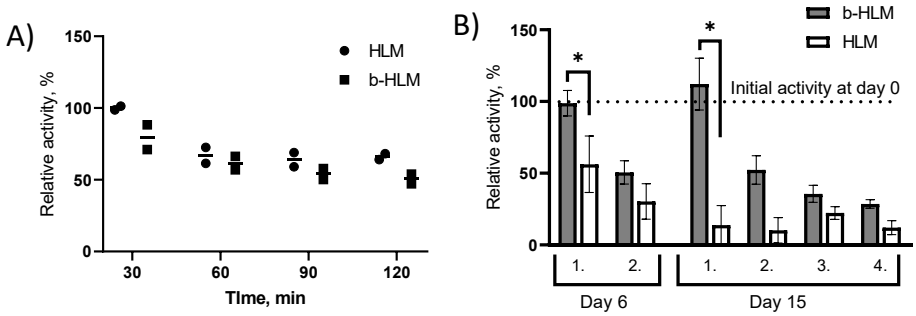

Figure 16. *Effect of biotinylation and immobilization on HLM CYP activity. A) The relative activity of nonimmobilized HLM and nonimmobilized b-HLM as a function of time. The activity normalized with respect to that of native HLM at 30 min. Data from two independent samples is shown. B) Relative activity (% of initial activity on day of immobilization i.e. day 0) of b-HLM and HLM (negative control) immobilized on streptavidin-functionalized magnetic beads on consecutive incubation cycles, after 6 or 15 days of storage at 4 °C. Error bars denote the standard deviation between n=4 batches of beads in each case. *p-value < 0.05.*

When b-HLM was immobilized inside the OSTE microreactors, CYP activity showed a considerable decline over time (halving over in 1-2 h) when assayed with specific probe reactions for both CYP2C9 and CYP2C8. Further investigations indicated that this issue was linked to thiol monomers leaching out of the bulk polymer. These material properties of thiol-enes will be discussed in more detail in Chapter 5.3.

Similar to CYPs, the biotinylation process was shown not to compromise UGT activity (Publication II). In fact, there was a small (ca. 25 %) but statistically significant (p=0.02, Student's t-test) increase in glucuronidation activity with biotinylated HLM compared to native HLM (Figure 17A). This can possibly be explained by the relative increase of long-chain fatty acids in biotinylated HLM, which has been reported to elevate UGT activity.[201] Non-lamellar lipids, such as DOPE, have also been reported to promote the membrane permeation of small molecules.[202] The observed increase in glucuronidation activity was, however, negligible compared to that achieved by pre-incubation with alamethicin, suggesting that biotinylation does not result in physical membrane disruption resembling alamethicin-induced pore formation. The UGT activity of b-HLM immobilized inside OSTE microreactors proved to be highly stable, featuring a negligible decrease in enzyme activity within the first 10 h of continuous use, and a rather minor decrease during the subsequent 5 h period (Figure 17B). This further proves that the immobilization method developed herein is robust and that the inactivation of immobilized CYPs is not a result of immobilized HLM leaching out of the IMER.

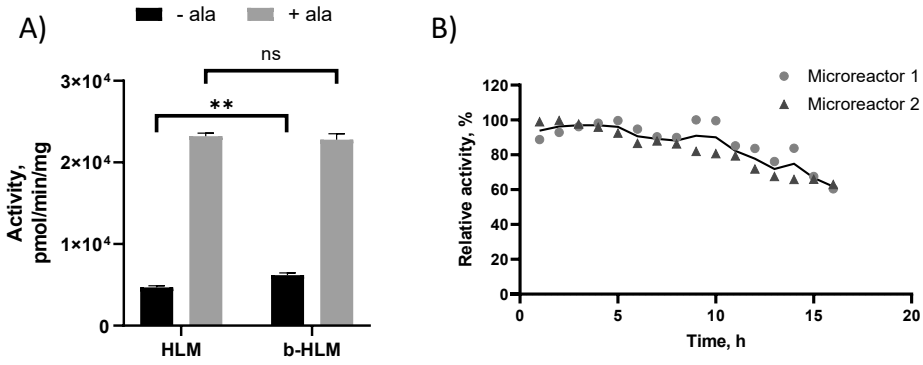

Figure 17. *Effect of biotinylation and immobilization on UGT-activity of HLM. The effect of alamethicin (ala) on the glucuronidation rate in native HLM and biotinylated HLM (b-HLM) in static conditions. Error bars present the variation between n=3 reactors. **p-value < 0.005 (Student's t-test), n.s.=non-significant. B) The stability of the UGT activities of two parallel microreactors over a 15-hour-long experiment at a flow rate of 2.5 µL/min. Activities were normalized with respect to the maximum activity of each reactor. 50 µM 8-hydroxyquinoline was used as the probe substrate in all experiments. Adapted from ref. 203. © 2020, Kiiski et al.; Elsevier, CC-BY-NC-ND 4.0.*

5.3 Material interactions

The leaching of uncrosslinked thiol and allyl monomers from the bulk OSTE polymer has been observed in previous studies[156,204] and was also verified in this thesis by titration (see section 5.5.1). The magnitude of monomer leaching is dependent on the polymer composition used. This study examined the effect of the leaching thiols on CYP- and UGT-mediated reactions in more detail.

5.3.1 CYP metabolism

When CYP metabolism was studied with b-HLM immobilized inside thiol-ene microreactors, considerable decline in the CYP activity was observed with both CYP2C9 and CYP2C8 (Figure 18A). The decline of enzyme activity as a result of issues related to the immobilization procedure (e.g., poorly attached enzymes leaching out of the reactor), could be reliably ruled out based on the UGT activity data (Figure 17B). To study whether instead the leaching thiol monomers could affect CYP metabolism, IC_{50} values were determined for both of the used thiol monomers (tetra- and trithiol) toward CYP2C9 in this study. Both monomers showed similar inhibitory potential that was potentiated by a 30-min preincubation with NADPH, suggesting mechanism-based, irreversible inhibition[205] (Figure 18B-C).

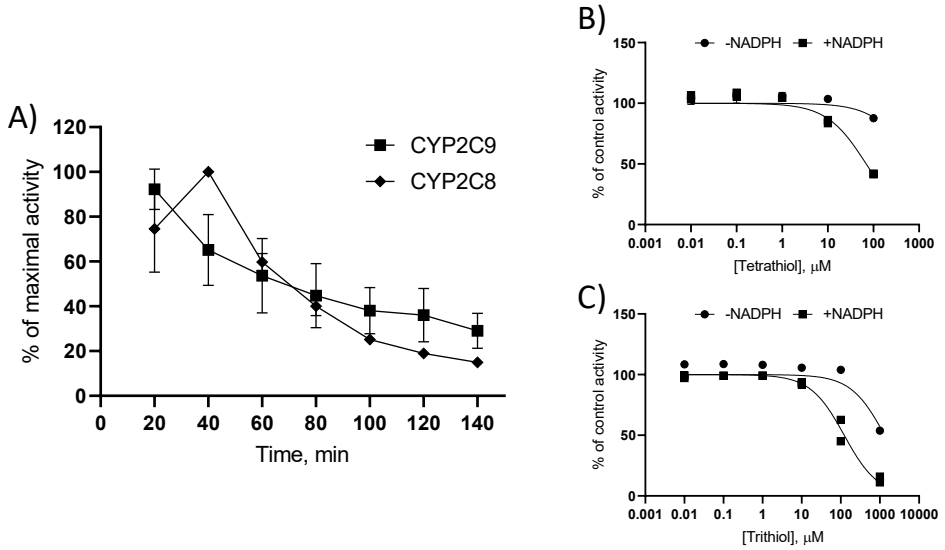

Figure 18. *A) CYP2C9 and CYP2C8 activity of b-HLM immobilized in thiol-ene microreactors as a function of time. Activities were normalized with respect to the maximum activity of each reactor. Luciferin-H (CYP2C9) and paclitaxel (CYP2C8) were used as probe substrates at concentrations of 200 and 5 μM, respectively. Error bars denote the standard deviation between n=4 microreactors in each case. Inhibitory effect of B) tetrathiol and C) trithiol monomers on the metabolic activity of CYP2C9, as assayed using luciferin-H as a probe substrate with or without a 30 min preincubation with NADPH. Activities are expressed as percentages of the inhibitor-free solvent control. All samples were performed in duplicates.*

5.3.2 UGT metabolism

While the leaching thiol monomers were found to inhibit CYP activity in a time-dependent manner even at rather low concentrations, the activity of UGT enzymes immobilized inside thiol-ene microreactors was unaffected by both the tetrathiol and triallyl monomers. This is evidenced by both the long-term stability of UGT activity (Figure 17B) and IC_{50} assays performed with both monomers used in the microreactor fabrication (Figure 19).

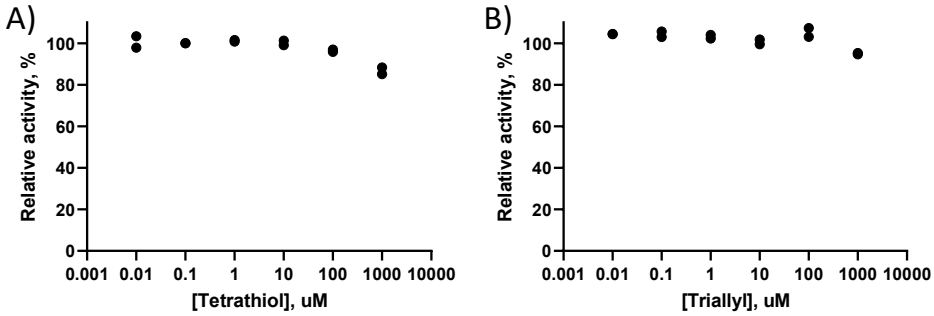

Figure 19. *The impact on UGT activity (8-hydroxyquinoline glucuronidation) in human liver microsomes of A) tetrathiol and B) triallyl monomers dissolved in the incubation matrix. Incubations were performed in duplicate. Adapted from ref. 203. © 2020, Kiiski et al.; Elsevier, CC-BY-NC-ND 4.0*

On the basis of these results, it can be concluded that the detrimental, material-induced effects of leaching monomers is a factor that should be carefully assessed in each specific application. The monomer ratio of thiol and allyl monomers has been shown to affect the amount of leaching monomers.[156] This should be studied further in order to minimize detrimental effects on enzymes, particularly for long-term assays with CYPs. However, alterations to the monomer ratio will also have effects on the surface chemistry of the reactor, impacting the efficiency of surface functionalization. For example, IMERs fabricated from stoichiometric compositions of tetrathiol and triallyl showed only trace amounts of CYP-activity (data not shown), presumably due to the low density of free thiols on the surface.

5.4 Enzyme kinetic determination in flow-through conditions

In the case of UGT enzymes, the determination of enzyme kinetics is complicated by two factors that can result in drastic underestimation of *in vivo* clearances.[43] First, the active site of UGT enzymes resides on the luminal side of the microsomal membranes, meaning that substrates, cosubstrates and metabolites have to cross the membrane. This imposes a mass transfer limitation that has to be eliminated by disrupting the membrane in order to reach maximal enzyme activity.[44,45] Second, free fatty acids leaching from the microsomal matrix have been shown to inhibit some UGT isoforms.[46–48] The mechanisms behind both of these phenomena were studied utilizing flow-through conditions enabled by enzyme immobilization (Publication II).

Under flow conditions, the diffusion of the reaction components across the immobilized microsomal membrane eventually reaches a steady-state (Figure 20A), which is observed as the plateauing of UGT activity to a constant value, regardless of whether the membrane is intact. At high flow rates (15 µL/min), preincubating the microreactor with alamethicin resulted in a 2-fold increase in UGT-activity due to the elimination of diffusional

restrictions. By adding alamethicin to the feed solution, an even greater increase in the UGT activity (ca. 3-fold) was achieved as soon as the steady-state was reached (Figure 20A). However, besides alamethicin, flow rate has a great impact on steady-state formation as it controls the residence time of the substrate within the system. When the residence time of the substrate increases with lower flow rates, the impact of alamethicin becomes negligible. When the amount of metabolite produced per collected fraction was further compared at different flow rates, it was evident that the reaction was not diffusion limited as the amount of metabolite increased linearly with increasing residence times both in the presence and absence of alamethicin (Figure 20B). The reaction velocities (pmol/min/mg protein) determined for the microreactor reactions at steady-state correlated well with the activities in the static assays with alamethicin (see Publication II for details), and were substantially higher than activities in static assays in the absence of alamethicin. In summary, in flow-through conditions, the steady-state velocity can be distinguished from the initial (diffusion-limited) velocity, obviating the need for membrane disruption.

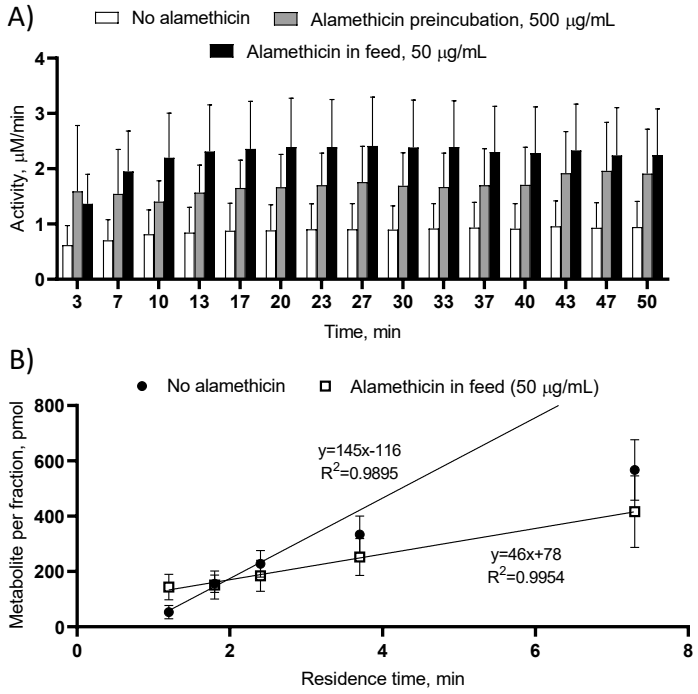

Figure 20. *The effect of alamethicin on UGT activity of immobilized HLM in flow-through conditions. A) The impact of alamethicin on the time for steady-state formation in a microreactor operated at a flow rate of 15 μL/min. Error bars denote the standard deviation between n=4 microreactors in each case. B) The impact of residence time on the amount of 8-hydroxyquinoline-glucuronide formed in the reactor in the absence of alamethicin and with alamethicin included in the feed solution. Error bars denote the standard deviation between n=4 microreactors in each case. Adapted from ref. 203. © 2020, Kiiski et al.; Elsevier, CC-BY-NC-ND 4.0*

The kinetics of immobilized UGTs under flow conditions were further investigated by determining the enzyme kinetic parameters of the antiviral drug zidovudine. Zidovudine is a specific UGT2B7 substrate, whose metabolism is significantly inhibited by free fatty acids and thus typically underestimated in *in vitro* studies[43] unless albumin—capable of binding the inhibitory fatty acids—is added to the *in vitro* enzyme incubations.[46] The effect of albumin on zidovudine glucuronidation kinetics were studied with both non-immobilized, native HLM and immobilized b-HLM. As alamethicin did not have an effect on the steady-state activity of UGT reactions, it was excluded from the enzyme kinetic experiments.

With non-immobilized, native HLM in static conditions, the presence of albumin halved the KM of the enzyme, as expected, but had no effect on Vmax unless the microsomes were pretreated with alamethicin. In the absence of alamethicin, in vitro intrinsic clearance (CLint) increased by 3-fold (from 24 ± 2 nL/min/mg to 73 ± 6 nL/min/mg microsomal protein), while the presence of alamethicin resulted in a 10-fold increase in the CLint (to 268 ± 17 nL/min/mg microsomal protein).

In flow-through conditions, the determination of enzyme kinetics was facilitated by the creation of substrate concentration gradients using two interconnected syringe pumps. At each substrate concentration, three subsequent fractions were collected at a flow rate of 5 μL/min, corresponding to a reaction time of 3.7 min. The last fraction was quantified to ensure that the steady state velocity had been reached and to calculate the kinetic constants. In the absence of albumin, on-chip zidovudine glucuronidation followed Michaelis-Menten kinetics with a slightly higher K_M (2572 ± 718 μM) compared to that obtained for native HLM in similar conditions (1511 ± 146 μM) (Table 9). The presence of albumin reduced the K_M value of on-chip zidovudine glucuronidation by about half (790 ± 190 μM), close to the value determined for native HLM in the presence of albumin. On the other hand, the V_{max} values derived from microreactor experiments were somewhat larger when compared to those determined in static assays with or without added alamethicin. This resulted in comparable CL_{int} values between the microreactors without alamethicin and static assays with alamethicin. These results suggest that conducting drug glucuronidation assays under flow-through conditions could likely improve correlation of microsomal *in vitro* results with *in vivo* drug clearance over static assays, without the need for membrane-disrupting agents such as alamethicin.

Table 9. *Comparison of zidovudine glucuronidation kinetics in static (HLM) and flow-through conditions (b-HLM) (±standard error). For soluble HLM, the samples were assayed in duplicate with and without bovine serum albumin (0.1 % w/v) and/or alamethicin (50 µg/mL). For the microreactors, kinetics were determined with and without albumin by quantifying the metabolite from the third fraction (à 50 µL) collected after the feed composition had been changed (n=3 microreactors).*

Enzyme source	Albumin	Alamethicin	$K_{M,\ \mu M}$	$V_{max,}$ pmol/min/mg	$CL_{int,}$ nL/min/mg
HLM	No	No	1511 ± 146	36 ± 1	24 ± 2
	No	Yes	3430 ± 238	163 ± 5	48 ± 4
	Yes	No	505 ± 40	37 ± 1	73 ± 6
	Yes	Yes	549 ± 33	147 ± 3	268 ± 17
b-HLM	No	No	2572 ± 718	274 ± 35	107 ± 33
	Yes	No	791 ± 190	306 ± 23	387 ± 97

The presence of flow in the microreactor assays was initially thought to remove any inhibitory fatty acid artifacts, thus obviating the need for albumin addition. However, even in flow conditions albumin had a clear lowering effect on $K_{M.}$ This may indicate that inhibitory fatty acid artifacts are accumulated on the luminal side of the membrane as well, and albumin helps sequester the fatty acids upon their partitioning across the microsomal membrane. Interestingly, Horspool et al.[206] recently reported a method for binding HLM on silica-coated magnetic beads, which was shown to lower the K_M of zidovudine glucuronidation. This was hypothesized to be caused by the elimination of free fatty acids during the multiple washing steps in the protocol. Further study is warranted to investigate the possibility that the fatty-acid-eliminating effect of the immobilization procedure could be more prominent if the enzyme kinetics are determined using streptavidin-coated particles similar to CYPs.

5.5 Drug metabolism assays under controlled oxygen environment

5.5.1 Oxygen scavenging of thiol-enes

The oxygen scavenging capability of OSTEs has been previously characterized using OSTE+ formulations, which include a heat-curable epoxy component in addition to thiol and allyl (ene) monomers.[180] The oxygen scavenging capability of OSTE+ was associated with the oxidation of thioether-linkages in the polymer bulk. Heat treatment of the polymer was shown to significantly decrease the oxygen scavenging rate, which was associated with increased T_g and thus decreased oxygen permeability to the bulk.[180]

In this study, the impact of bulk polymer composition on the oxygen depletion rate of pure thiol-enes was studied in more detail by varying the monomer ratio in the bulk from a 50 % molar excess of thiols to a stoichiometric ratio of thiols (tri- or tetrathiol) and allyls (triallyl). The impact of heat treatment (110 °C) and degree of cross-linking was also studied.

In microchannels fabricated using both tetrathiol (Figure 21A) and trithiol (Figure 21B) monomers, the oxygen depletion rate followed first order kinetics and was dependent on the relative amount of thiol and allyl components in the bulk polymer. The reaction constant (k) was shown to be greater for tetrathiol-containing polymers than trithiol-containing polymers and increased along with increasing excess of the thiol component in the bulk (see Publication III for details). Heat-treating the microchannels after curing (110 °C overnight) markedly slowed the oxygen depletion rate for both thiol monomers. Contrary to previous reports,[180] the effect of heat-treatment could not be explained by changes in the polymer T_g, which reflects the oxygen permeability of the bulk polymer.[207] T_g was practically unaffected by heat treatment in the case of both trithiol-containing (2.2→3.1 °C, n=1 measurement) and tetrathiol-containing (25.9→26.6 °C, n=1 measurement) compositions. Furthermore, the oxygen permeability determined for polymers fabricated using trithiol (3.0 ± 0.6 cc cm/m^2 day atm) was approximately 3-fold higher than that of the polymer fabricated from tetrathiol (1.0 ± 0.007 cc cm/m^2 day atm) using the same molar excess of thiol groups (50%) in the bulk. If oxygen permeability from solution to the bulk was the rate determining step in oxygen depletion, the use of trithiols should have accelerated the speed of the depletion, contrary to observations. However, differences in permeability might explain the plateauing of the oxygen partial pressure inside the more permeable trithiol channels.

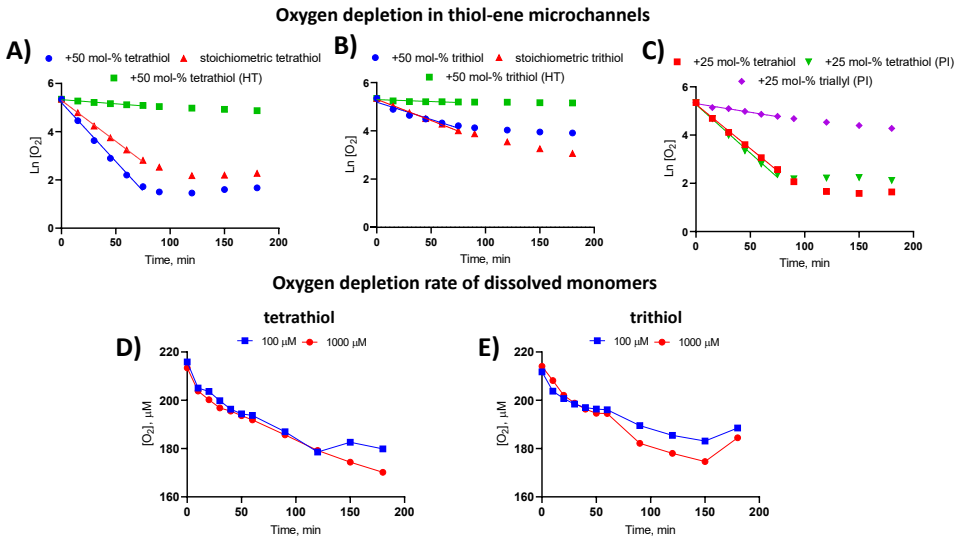

Figure 21. *Oxygen depletion as a function of time in thiol-ene microchannels (30×2×0.2 mm) fabricated with different monomer ratios using A) tetrathiol or B) trithiol as the thiol-containing monomer. n=4–8 microreactors in each sample group. HT = heat treatment (110 °C overnight) C) Oxygen depletion in either thiol-rich (+25 mol-%) or allyl-rich (+25 mol-%) bulk compositions made using tetrathiol. PI refers to added photoinitiator (Irgacure® TPO-L, 0.1 % m/v) in the bulk composition. D & E: Oxygen scavenging by dissolved D) tetrathiol and E) trithiol monomers (in water) as a function of time.*

The mechanism of oxygen depletion in thiol-ene channels was traced back to the oxidation of uncrosslinked thiol monomers leaching from the bulk polymer. In this case, the oxygen depletion rate should correlate with the amount of free (uncrosslinked) monomers in the bulk. This hypothesis was tested by manipulating the amount of the uncrosslinked tetrathiol monomer with the help of a photoinitiator and by using opposite excess (+25 mol-%) of thiol and allyl functional groups in the bulk. The addition of the photoinitiator to the thiol-rich composition did not visibly affect the oxygen depletion rate constant compared with photoinitiator-free, thiol-rich composition (Figure 21C), even if the T_g was substantially increased with the addition of the photoinitiator (13→42 °C). However, using allyl-excess decreases the amount of free thiol monomer in the bulk, and was shown to decrease the rate constant substantially. These observations confirmed that the oxygen scavenging rate in thiol-ene channels was mostly governed by the chemical composition of the bulk, particularly the amount of uncrosslinked thiol monomers, and was rather independent on the mechanical bulk properties, such as T_g.

When the free trithiol and tetrathiol monomers were dissolved in an aqueous media, both monomers demonstrated an ability to scavenge oxygen from the solution (Figure 21D-E). This experiment was performed at high micromolar concentrations (100 and 1000 µM) and revealed that the oxygen depletion rate does not markedly depend on the thiol monomer concentration, until the thiol component is completely consumed (e.g., at approximately

120 min for tetrathiol, Figure 21D). The omission of a photoinitiator from the polymer fabrication is known to result in incomplete conversion of polymers, even when a stoichiometric ratio of functional groups is used.[153,208] The extent of monomer conversion is also known to decrease as a function of layer depth.[209] In replica molding, this results in a low degree of cross-linking at the channel surface, the point furthest from the UV light source during the curing step. These factors likely explain the effective elimination of oxygen in microchannels made of even stoichiometric thiol-ene compositions. The impact of heat treatment was associated with the evaporation of uncrosslinked thiol monomers from the bulk polymer, rather than changes in the oxygen permeability of the bulk polymer, as reported previously by Sticker et al.[180]

To further confirm that leaching monomers, not surface thiols, were responsible for the oxygen depletion, the amount of thiol monomers leaching out of a micropillar microchannel (25% excess of tetrathiol) was determined. The amount of leaching tetrathiols over time was quantified after surface passivation. This experiment confirmed that the mass transfer of tetrathiol from the bulk follows first-order kinetics (Figure 22A), similar to oxygen depletion in thiol-ene microchannel in static conditions. Thus, it was hypothesized that the diffusion of thiols across the polymer-liquid interface is the rate limiting step for oxygen depletion in OSTE microchannels, and that the diffusion rate is most dependent on the amount of uncrosslinked thiols in the bulk.

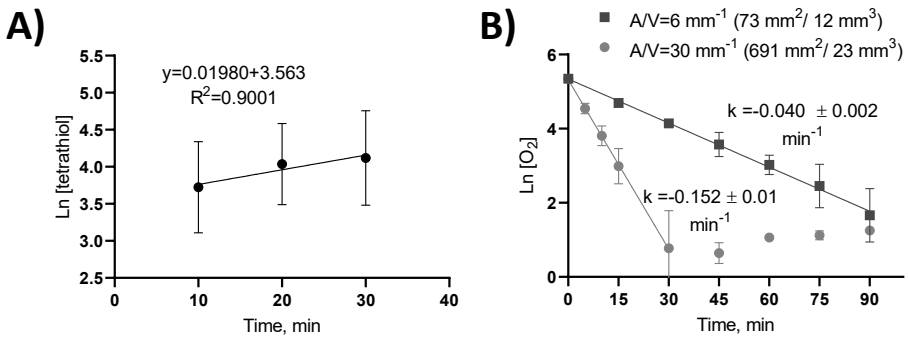

Figure 22. *A) The leaching of tetrathiol monomers inside a thiol-ene micropillar channel quantified using DTNB (5,5'-dithiobis[2-nitrobenzoic acid], "Ellman's reagent"). The free surface thiols were first neutralized by an incubation with 1 mM DTNB for 30 min, followed by consecutive incubations of 10, 20 and 30 min. Error bars denote standard deviation from n = 6 individual micropillar channels. B) The effect of channel surface-to-volume ratio (A/V) on oxygen scavenging kinetics in channels fabricated using thiol-rich (+25 mol-%) tetrathiol-containing polymer. n=3 individual channels.*

Assuming that the diffusion of thiol monomers across the polymer-liquid interface is the rate limiting step for oxygen depletion, the oxygen depletion rate should be dependent on the surface-to-volume ratio of the microreactor. The effect of surface-to-volume ratio was studied by comparing the O_2 consumption rate in a rectangular channel (2×30×0.2 mm, surface-to-volume ratio of 6 mm^{-1}) vs. in a micropillar array channel (Design 1, surface-to-

volume ratio of 30 mm^{-1}), in static conditions. In both cases, oxygen depletion displayed first order kinetics, with the rate coefficient *k* being directly proportional to the surface-to-volume ratio (Figure 22B).

5.5.2 On-chip metabolism assays under controlled oxygen environment

In recent years, numerous approaches for oxygen control in microfluidic systems have been introduced.[210,211] These platforms often rely on multi-compartment designs comprised of a separate cell culture compartments and oxygen control compartments, separated by a gas-permeable membrane. The gas content in the oxygen control compartment is usually regulated by an external gas supply[212,213] or supplemented reducing agents.[214,215] While these approaches permit the precise control of the oxygen microenvironment, they do so at the cost of complex, multicompartmental designs.

The omission of a photoinitiator also facilitates the unique oxygen scavenging property of OSTE, which was linked to leaching thiol monomers due to a lower degree of cross-linking. This property was crucial for the implementation of the on-demand tuning of oxygen partial pressure on-chip studied in Publication III. However, the thiol monomers were also shown to have an inhibitory effect on CYPs, which should be taken into account when carrying out metabolic assays on thiol-ene-based systems. The inherent ability of OSTE materials to scavenge dissolved oxygen from aqueous solutions shows great potential for simple implementation of oxygen control in microfluidic settings. Based on the initial material characterization of thiol-enes (see section 5.5.1), a chip design capable of tuning the oxygen partial pressure inside a microfluidic channel was designed. In this design, the oxygen control was based solely on the geometry of the chip and the tuning of flow rate ratios, obviating the need for supplementary reducing agents or complicated, multi-compartmental chip designs (Design 2, Figure 9, Figure 23A-B).

The design featured six serially connected micropillar channels (responsible for the scavenging of oxygen) junctioning with a second inlet supplying air-saturated fluid. From the junction the flow continues to a seventh micropillar unit comprising immobilized HLM. Based on oxygen scavenging kinetics, the length of the oxygen scavenging unit (defining the reaction time) was scaled to allow near anoxic conditions at the end of the oxygen scavenging channel with flow rates (residence time) up to 5 µL/min (Figure 23C). At this flow rate regime, the drop in oxygen partial pressure inside the final microreactor compartment was confirmed to be negligible (Figure 23D), which ensured that the oxygen content inside the IMER compartment could be reliably tuned by adjusting the flow rate ratio of the oxygen-rich and oxygen-depleted flows.

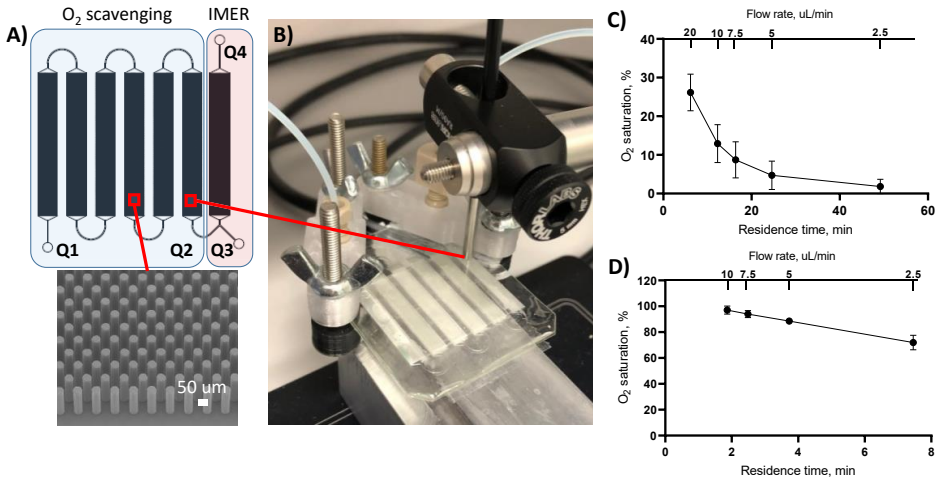

Figure 23. *A) Schematic of the chip design comprising an oxygen scavenging unit (blue), with an inlet Q1 and an outlet Q2, monolithically integrated with an immobilized enzyme microreactor (IMER) unit (red) with Y-junction providing air-saturated feed solution from inlet Q3 and an outlet Q4 for collecting metabolite samples. Oxygen level inside the microreactor was controlled by tuning the flow rate ratio of flows Q2 (oxygen-depleted) and Q3 (air-saturated). B) Photograph of the oxygen level measurement setup. C) Oxygen level (% of air-saturated O_2) at the end of the oxygen scavenging section as function of different residence times. n=3 chips. D) Oxygen level (% of air-saturated O_2) at the end of a single micropillar array channel as a function of different residence times. n=3 chips. Corresponding flow rates are denoted on the upper x-axis.*

The applicability of the platform for performing drug assays under controlled oxygen environment was demonstrated by studying the reductive metabolism of zidovudine. In addition to glucuronidation, zidovudine can also be metabolized to 3'-amino-3'-deoxythymidine (AMT) by the reduction of the drug's azide group into an amine.[69] AMT is a myelotoxic metabolite, hypothesized to play a role in the bone marrow suppression that occurs as a side effect of zidovudine therapy.[216] The specific mechanism of this NADPH-dependent reaction is unresolved, but it is understood to involve POR, cytochrome b_5, and CYPs.[217] The pathway is known to be oxygen-sensitive, with the presence of oxygen inhibiting the production of AMT either partially[218] or completely.[219]

First, the ability of the design to control the oxygen partial pressure inside the channel on-demand with the adjustment of flow rate ratios was verified. As expected, the actual measured oxygen levels inside the microreactor (Figure 24A) were in good agreement with the theoretical values determined based on the applied flow rate ratios (Figure 24B).

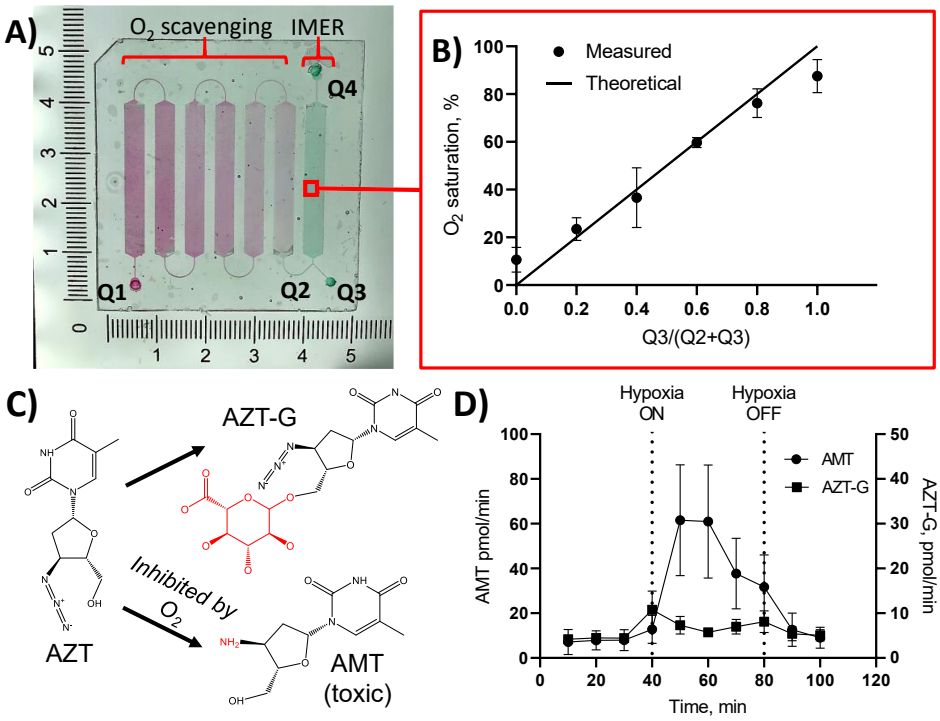

Figure 24. *A) Photograph of the chip design comprising an oxygen scavenging unit (filled with red dye integrated with n microreactor unit (filled with green dye). B) Tuning of oxygen levels inside a microfluidic chip by mixing oxygen-rich (Q3) and oxygen-depleted (Q2) flows (shown as a function of flow rate ratio). n=3 chips. C) Schematic of the oxygen-sensitive metabolism of zidovudine. D) Demonstration of the oxygen-sensitive reductive metabolism of zidovudine on-chip. n=4 chips. Abbreviations: AZT: zidovudine; AMT, 3'-amino-3'-deoxythymidine; AZT-G, zidovudine glucuronide.*

Finally, the oxygen-sensitivity of the reduction of zidovudine to AMT was demonstrated on-chip (Figure 24C-D). The rate of zidovudine reduction increased approximately 10-fold when oxygen was eliminated from the microreactor compartment. When the oxygen saturated flow was switched back on, the rate of zidovudine reduction dropped back to its initial level. On the other hand, the rate of oxygen independent zidovudine glucuronidation, which was also simultaneously monitored, was not markedly affected by the changes in oxygen partial pressure. This simple demonstration showcases the potential of the developed platform to perform biological assays under a controlled oxygen environment.

6 Conclusions

Preclinical drug metabolism research would benefit from assays implemented on microfluidic immobilized enzyme microreactors (IMER), but well-characterized IMERs comprising drug-metabolizing enzymes have been scarcely reported in the literature. This is presumably due to the methodological complexity of immobilizing membrane-bound enzymes. The methodology developed in this thesis addressed this unmet need.

In Publication I, a novel approach for immobilizing membrane-bound enzymes was developed based on 1) the biotinylation of lipid membranes *via* spontaneous fusion with biotin-tagged liposomes with biological membranes and 2) the facile surface functionalization of off-stoichiometric thiol-enes (OSTE). Unlike in previously reported methods, both CYP and UGT enzymes immobilized using this method retained their activity and native enzyme kinetic parameters. This novel method therefore circumvents issues associated with conventional immobilization approaches, such as diffusion-limited kinetics and enzyme inactivation.

In Publication II, the microreactor platform was further characterized with respect to UGT-mediated phase II metabolism. The ability to perform UGT reactions under flow facilitated the determination of enzyme kinetics and the in-depth study of mechanisms behind the latency associated with UGT reactions *in vitro*.

In Publication III, the material-induced oxygen scavenging of OSTE was utilized to enable the performance of metabolic assays under a controlled oxygen environment. The mechanism behind the oxygen scavenging phenomenon of OSTE was studied in detail and linked with thiol monomers leaching out of the polymer bulk. Based on this initial characterization, a chip design was devised that enabled the facile control of oxygen partial pressure inside the microreactor compartment based on the control of flow rate ratio of oxygen-depleted and oxygen-saturated flows. The ability to control the oxygen environment of on-chip metabolic reactions is a novel feature that has not been reported in any other drug-metabolizing enzyme microreactor platforms to-date.

The effect of the leaching thiol monomers responsible for oxygen scavenging on the enzyme activity of both CYPs and UGTs was also studied. UGTs were shown to be unaffected by the monomers, but CYPs exhibited time-dependent inhibition at mid-micromolar concentrations of both tri- and tetrathiol monomers. This suggests that thiol monomers are irreversible inhibitors of CYPs. The consequent decline in CYP activity in IMERs is an issue that should be addressed in the future in order to enable long-term CYP assays.

The methodology developed in this thesis has already has already found use in several subsequent studies by other researchers, highlighting the practical feasibility of the concepts developed here. For example, droplet-based enzyme microreactors have been successfully implemented on digital microfluidic platforms using the enzyme immobilization protocol developed in this thesis and porous thiol-ene monoliths as solid supports.[188,220] The immobilization method developed in this thesis has also been implemented on magnetic particles to study inter-individual differences in drug metabolism using digital microfluidics.[221] Furthermore, the same microreactor platform has been used in the in-depth study of time-dependent inhibition of the CYP system under flow conditions.[222] In addition

to drug metabolism research, the characterization of the material-induced hypoxia of OSTE-based systems carried out in this thesis are likely to find widespread use in many organ-on-a-chip applications, including the ongoing work by the hosting research group.

Moving forward, the technology developed herein could additionally offer significant advantages over conventional *in vitro* assays in the pharmaceutical industry as well. These include increased throughput, intricate study designs in flow-through conditions and streamlined analysis enabled by the integration potential of microfluidic systems, to name a few. However, most microfluidic systems reported to-date have encountered difficulty when it comes to commercial utilization, falling into a sort of limbo between academia and industry often referred to as the "technological valley of death." The work carried out in this thesis contributed to the validation of this novel IMER system in a laboratory setting, and the platform can be used in academic research to good effect. However, in order for the platform to become a viable commercial product, further optimization and standardization of the fabrication protocol are needed. That said, mass production of this microreactor platform could be possible with roll-to-plate fabrication technology.[223]

All in all, the microreactor platform developed in this thesis successfully addressed many of the key shortcomings of current state of the art (i.e., static) *in vitro* assay methodologies and previously reported IMER platforms, and shows great promise as a versatile toolbox for *in vitro* drug metabolism research. The thorough method development and validation of the IMER platform in this thesis paves the way for applications such as the mechanistic study of complex drug-drug interactions. Future work should also focus on further integration of the platform with a view to true total analytical systems for drug metabolism research.

References

1. Wouters, O. J., McKee, M. & Luyten, J. Estimated research and development investment needed to bring a new medicine to market, 2009-2018. *JAMA* **323**, 844–853 (2020).
2. Smietana, K., Siatkowski, M. & Møller, M. Trends in clinical success rates. *Nat. Rev. Drug Discov.* **15**, 379–380 (2016).
3. Hay, M., Thomas, D. W., Craighead, J. L., Economides, C. & Rosenthal, J. Clinical development success rates for investigational drugs. *Nat. Biotechnol.* **32**, 40–51 (2014).
4. Guengerich, F. P. Common and uncommon cytochrome P450 reactions related to metabolism and chemical toxicity. *Chem. Res. Toxicol.* **14**, 611–650 (2001).
5. Zanger, U. M. Introduction to drug metabolism. In *Metabolism of drugs and other xenobiotics* 285–300, John Wiley & Sons, Ltd (2012).
6. Döring, B. & Petzinger, E. Phase 0 and phase III transport in various organs: Combined concept of phases in xenobiotic transport and metabolism. *Drug Metab. Rev.* **46**, 261–282 (2014).
7. Williams, J. A., Hyland, R., Jones, B. C., Smith, D. A., Hurst, S., Goosen, T. C., Peterkin, V., Koup, J. R. & Ball, S. E. Drug-drug interactions for UDP-glucuronosyltransferase substrates: a pharmacokinetic explanation for typically observed low exposure (AUC_i/AUC) ratios. *Drug Metab. Dispos.* **32**, 1201–1208 (2004).
8. Wienkers, L. C. & Heath, T. G. Predicting *in vivo* drug interactions from *in vitro* drug discovery data. *Nat. Rev. Drug Discov.* **4**, 825–833 (2005).
9. Smith, H. S. Opioid metabolism. *Mayo Clin. Proc.* **84**, 613–624 (2009).
10. Klimas, R. & Mikus, G. Morphine-6-glucuronide is responsible for the analgesic effect after morphine administration: a quantitative review of morphine, morphine-6-glucuronide, and morphine-3-glucuronide. *Br. J. Anaesth.* **113**, 935–944 (2014).
11. Zanger, U. M. & Schwab, M. Cytochrome P450 enzymes in drug metabolism: Regulation of gene expression, enzyme activities, and impact of genetic variation. *Pharmacol. Ther.* **138**, 103–141 (2013).
12. Guengerich, F. P. Cytochromes P450. In *Metabolism of Drugs and Other Xenobiotics* 27–66, John Wiley & Sons, Ltd (2012).
13. Munro, A. W., Girvan, H. M., Mason, A. E., Dunford, A. J. & McLean, K. J. What makes a P450 tick? *Trends Biochem. Sci.* **38**, 140–150 (2013).
14. Waskell, L. & Kim, J.-J. P. Electron transfer partners of cytochrome P450. in *Cytochrome P450: Structure, Mechanism, and Biochemistry* (ed. Ortiz de Montellano, P. R.) 33–68, Springer International Publishing (2015).
15. Im, S.-C. & Waskell, L. The interaction of microsomal cytochrome P450 2B4 with its redox partners, cytochrome P450 reductase and cytochrome b5. *Arch. Biochem. Biophys.* **507**, 144–153 (2011).

16. Šrejber, M., Navrátilová, V., Paloncýová, M., Bazgier, V., Berka, K., Anzenbacher, P. & Otyepka, M. Membrane-attached mammalian cytochromes P450: An overview of the membrane's effects on structure, drug binding, and interactions with redox partners. *J. Inorg. Biochem.* **183**, 117–136 (2018).
17. Tukey, R. H. & Strassburg, C. P. Human UDP-Glucuronosyltransferases: Metabolism, Expression, and Disease. *Annu. Rev. Pharmacol. Toxicol.* **40**, 581–616 (2000).
18. Pelkonen, O., Turpeinen, M., Uusitalo, J., Rautio, A. & Raunio, H. Prediction of drug metabolism and interactions on the basis of *in vitro* investigations. *Basic Clin. Pharmacol. Toxicol.* **96**, 167–175 (2005).
19. Issa, N. T., Wathieu, H., Ojo, A., Byers, S. W. & Dakshanamurthy, S. Drug metabolism in preclinical drug development: a survey of the discovery process, toxicology, and computational tools. *Curr. Drug Metab.* **18**, 556–565 (2017).
20. Seibert, E. & Tracy, T. S. Fundamentals of enzyme kinetics. in *Enzyme Kinetics in Drug Metabolism: Fundamentals and Applications* (eds. Nagar, S., Argikar, U. A. & Tweedie, D. J.) 9–22, Humana Press (2014).
21. Ito, K., Iwatsubo, T., Kanamitsu, S., Nakajima, Y. & Sugiyama, Y. Quantitative prediction of *in vivo* drug clearance and drug interactions from *in vitro* data on metabolism, together with binding and transport. *Annu. Rev. Pharmacol. Toxicol.* **38**, 461–499 (1998).
22. Houston, J. B. & Carlile, D. J. Prediction of hepatic clearance from microsomes, hepatocytes, and liver slices. *Drug Metab. Rev.* **29**, 891–922 (1997).
23. Pelkonen, O. & Turpeinen, M. In vitro-in vivo extrapolation of hepatic clearance: biological tools, scaling factors, model assumptions and correct concentrations. *Xenobiotica* **37**, 1066–1089 (2007).
24. Sproule, B. A., Naranjo, C. A., Brenmer, K. E. & Hassan, P. C. Selective serotonin reuptake inhibitors and CNS drug interactions. A critical review of the evidence. *Clin. Pharmacokinet.* **33**, 454–471 (1997).
25. Patsalos, P. N. & Perucca, E. Clinically important drug interactions in epilepsy: general features and interactions between antiepileptic drugs. *Lancet Neurol.* **2**, 347–356 (2003).
26. Guengerich, F. P. Role of cytochrome P450 enzymes in drug-drug interactions. in *Advances in Pharmacology* (ed. Li, A. P.) vol. 43 7–35, Academic Press (1997).
27. Friedman, M. A., Woodcock, J., Lumpkin, M. M., Shuren, J. E., Hass, A. E. & Thompson, L. J. The safety of newly approved medicines: do recent market removals mean there is a problem? *JAMA* **281**, 1728–1734 (1999).
28. Lasser, K. E., Allen, P. D., Woolhandler, S. J., Himmelstein, D. U., Wolfe, S. M. & Bor, D. H. Timing of new black box warnings and withdrawals for prescription medications. *JAMA* **287**, 2215–2220 (2002).
29. Ito, K., Iwatsubo, T., Kanamitsu, S., Ueda, K., Suzuki, H. & Sugiyama, Y. Prediction of pharmacokinetic alterations caused by drug-drug interactions: metabolic interaction in the liver. *Pharmacol. Rev.* **50**, 387–412 (1998).

30. Tien, E. S. & Negishi, M. Nuclear receptors CAR and PXR in the regulation of hepatic metabolism. *Xenobiotica* **36**, 1152–1163 (2006).
31. Fowler, S. & Zhang, H. *In vitro* evaluation of reversible and irreversible cytochrome p450 inhibition: current status on methodologies and their utility for predicting drug–drug interactions. *AAPS J.* **10**, 410–424 (2008).
32. Fasinu, P., Bouic, P. J. & Rosenkranz, B. Liver-based *in vitro* technologies for drug biotransformation studies - a review. *Curr. Drug Metab.* **13**, 215–224 (2012).
33. Yung-Chi, C. & Prusoff, W. H. Relationship between the inhibition constant (K_I) and the concentration of inhibitor which causes 50 per cent inhibition (I_{50}) of an enzymatic reaction. *Biochem. Pharmacol.* **22**, 3099–3108 (1973).
34. Ghanbari, F., Rowland-Yeo, K., Bloomer, J., Clarke, S., Lennard, M., Tucker, G. & Rostami-Hodjegan, A. A critical evaluation of the experimental design of studies of mechanism based enzyme inhibition, with implications for *in vitro-in vivo* extrapolation. *Curr. Drug Metab.* **7**, 315–334 (2006).
35. Silverman, R. B. Mechanism-based enzyme inactivators. in *Methods in Enzymology* vol. 249 240–283, Academic Press (1995).
36. Pelkonen, O. & Breimer, D. D. Role of environmental factors in the pharmacokinetics of drugs: considerations with respect to animal models, P-450 enzymes, and probe drugs. in *Pharmacokinetics of Drugs* (eds. Welling, P. G. & Balant, L. P.) 289–332, Springer (1994).
37. van Midwoud, P. M., Verpoorte, E. & Groothuis, G. M. M. Microfluidic devices for *in vitro* studies on liver drug metabolism and toxicity. *Integr. Biol.* **3**, 509–521 (2011).
38. Krishna, D. R. & Klotz, U. Extrahepatic metabolism of drugs in humans. *Clin. Pharmacokinet.* **26**, 144–160 (1994).
39. Brandon, E. F. A., Raap, C. D., Meijerman, I., Beijnen, J. H. & Schellens, J. H. M. An update on *in vitro* test methods in human hepatic drug biotransformation research: pros and cons. *Toxicol. Appl. Pharmacol.* **189**, 233–246 (2003).
40. Bjornsson, T. D. *et al.* The conduct of *in vitro* and *in vivo* drug-drug interaction studies: a pharmaceutical research and manufacturers of America (PhRMA) perspective. *Drug Metab. Dispos.* **31**, 815–832 (2003).
41. Raucy, J. L. & Lasker, J. M. Isolation of P450 enzymes from human liver. in *Methods in Enzymology* vol. 206 577–587, Academic Press (1991).
42. Soars, M. G., Burchell, B. & Riley, R. J. *In vitro* analysis of human drug glucuronidation and prediction of *in vivo* metabolic clearance. *J. Pharmacol. Exp. Ther.* **301**, 382–390 (2002).
43. Boase, S. & Miners, J. O. *In vitro–in vivo* correlations for drugs eliminated by glucuronidation: Investigations with the model substrate zidovudine. *Br. J. Clin. Pharmacol.* **54**, 493–503 (2002).
44. Liu, Y. & Coughtrie, M. W. H. Revisiting the latency of uridine diphosphate-glucuronosyltransferases (UGTs)—How does the endoplasmic reticulum membrane influence their function? *Pharmaceutics* **9**, 32 (2017).

45. Fisher, M. B., Campanale, K., Ackermann, B. L., VandenBranden, M. & Wrighton, S. A. *In vitro* glucuronidation using human liver microsomes and the pore-forming peptide alamethicin. *Drug Metab. Dispos.* **28**, 560–566 (2000).
46. Rowland, A., Gaganis, P., Elliot, D. J., Mackenzie, P. I., Knights, K. M. & Miners, J. O. Binding of inhibitory fatty acids is responsible for the enhancement of UDP-glucuronosyltransferase 2B7 activity by albumin: Implications for *in vitro-in vivo* extrapolation. *J. Pharmacol. Exp. Ther.* **321**, 137–147 (2007).
47. Rowland, A., Knights, K. M., Mackenzie, P. I. & Miners, J. O. The 'albumin effect' and drug glucuronidation: bovine serum albumin and fatty acid-free human serum albumin enhance the glucuronidation of UDP-glucuronosyltransferase (UGT) 1A9 substrates but not UGT1A1 and UGT1A6 activities. *Drug Metab. Dispos. Biol. Fate Chem.* **36**, 1056–1062 (2008).
48. Manevski, N., Moreolo, P. S., Yli-Kauhaluoma, J. & Finel, M. Bovine serum albumin decreases K_M values of human UDP-glucuronosyltransferases 1A9 and 2B7 and increases V_{MAX} values of UGT1A9. *Drug Metab. Dispos.* **39**, 2117–2129 (2011).
49. Engtrakul, J. J., Foti, R. S., Strelevitz, T. J. & Fisher, M. B. Altered Azt (3′-azido-3′-deoxythymidine) glucuronidation kinetics in liver microsomes as an explanation for underprediction of *in vivo* clearance: comparison to hepatocytes and effect of incubation environment. *Drug Metab. Dispos.* **33**, 1621–1627 (2005).
50. Rodríguez-Antona, C., Donato, M. T., Boobis, A., Edwards, R. J., Watts, P. S., Castell, J. V. & Gómez-Lechón, M.-J. Cytochrome P450 expression in human hepatocytes and hepatoma cell lines: molecular mechanisms that determine lower expression in cultured cells. *Xenobiotica Fate Foreign Compd. Biol. Syst.* **32**, 505–520 (2002).
51. Bell, C. C., Lauschke, V. M., Vorrink, S. U., Palmgren, H., Duffin, R., Andersson, T. B. & Ingelman-Sundberg, M. Transcriptional, functional, and mechanistic comparisons of stem cell–derived hepatocytes, HepaRG cells, and three-dimensional human hepatocyte spheroids as predictive *in vitro* systems for drug-induced liver injury. *Drug Metab. Dispos.* **45**, 419–429 (2017).
52. Ma, L.-D., Wang, Y.-T., Wang, J.-R., Wu, J.-L., Meng, X.-S., Hu, P., Mu, X., Liang, Q.-L. & Luo, G.-A. Design and fabrication of a liver-on-a-chip platform for convenient, highly efficient, and safe in situ perfusion culture of 3D hepatic spheroids. *Lab. Chip* **18**, 2547–2562 (2018).
53. Esch, M. B., Ueno, H., Applegate, D. R. & Shuler, M. L. Modular, pumpless body-on-a-chip platform for the co-culture of GI tract epithelium and 3D primary liver tissue. *Lab. Chip* **16**, 2719–2729 (2016).
54. Laskin, D. L. Parenchymal and nonparenchymal cell interactions in hepatotoxicity. in *Biological Reactive Intermediates IV: Molecular and Cellular Effects and Their Impact on Human Health* (eds. Witmer, C. M., Snyder, R. R., Jollow, D. J., Kalf, G. F., Kocsis, J. J. & Sipes, I. G.) 499–505, Springer New York (1991).
55. Edwards, R. J., Price, R. J., Watts, P. S., Renwick, A. B., Tredger, J. M., Boobis, A. R. & Lake, B. G. Induction of cytochrome P450 enzymes in cultured precision-cut human liver slices. *Drug Metab. Dispos.* **31**, 282–288 (2003).

56. Martin, H., Sarsat, J.-P., de Waziers, I., Housset, C., Balladur, P., Beaune, P., Albaladejo, V. & Lerche-Langrand, C. Induction of cytochrome P450 2B6 and 3A4 expression by phenobarbital and cyclophosphamide in cultured human liver slices. *Pharm. Res.* **20**, 557–568 (2003).
57. Lu, C., Li, P., Gallegos, R., Uttamsingh, V., Xia, C. Q., Miwa, G. T., Balani, S. K. & Gan, L.-S. Comparison of intrinsic clearance in liver microsomes and hepatocytes from rats and humans: Evaluation of free fraction and uptake in hepatocytes. *Drug Metab. Dispos.* **34**, 1600–1605 (2006).
58. Stringer, R., Nicklin, P. L. & Houston, J. B. Reliability of human cryopreserved hepatocytes and liver microsomes as *in vitro* systems to predict metabolic clearance. *Xenobiotica Fate Foreign Compd. Biol. Syst.* **38**, 1313–1329 (2008).
59. Ge, S., Tu, Y. & Hu, M. Challenges and opportunities with predicting *in vivo* phase II metabolism via glucuronidation from *in vitro* data. *Curr. Pharmacol. Rep.* **2**, 326–338 (2016).
60. Carreau, A., Hafny-Rahbi, B. E., Matejuk, A., Grillon, C. & Kieda, C. Why is the partial oxygen pressure of human tissues a crucial parameter? Small molecules and hypoxia. *J. Cell. Mol. Med.* **15**, 1239–1253 (2011).
61. Mohyeldin, A., Garzón-Muvdi, T. & Quiñones-Hinojosa, A. Oxygen in stem cell biology: A critical component of the stem cell niche. *Cell Stem Cell* **7**, 150–161 (2010).
62. Semenza, G. L. Oxygen sensing, homeostasis, and disease. *N. Engl. J. Med.* **365**, 537–547 (2011).
63. Brooks, A. J., Eastwood, J., Beckingham, I. J. & Girling, K. J. Liver tissue partial pressure of oxygen and carbon dioxide during partial hepatectomy. *Br. J. Anaesth.* **92**, 735–737 (2004).
64. Brooks, A. J., Hammond, J. S., Girling, K. & Beckingham, I. J. The effect of hepatic vascular inflow occlusion on liver tissue pH, carbon dioxide, and oxygen partial pressures: defining the optimal clamp/release regime for intermittent portal clamping. *J. Surg. Res.* **141**, 247–251 (2007).
65. Jones, D. P. Hypoxia and drug metabolism. *Biochem. Pharmacol.* **30**, 1019–1023 (1981).
66. Jones, D. P., Aw, T. Y. & Shan, X. Drug metabolism and toxicity during hypoxia. *Drug Metab. Rev.* **20**, 247–260 (1989).
67. Jones, D. P. & Mason, H. S. Gradients of O_2 concentration in hepatocytes. *J. Biol. Chem.* **253**, 4874–4880 (1978).
68. Le Couteur, D. G. & McLean, A. J. The aging liver: Drug clearance and an oxygen diffusion barrier hypothesis. *Clin. Pharmacokinet.* **34**, 359–373 (1998).
69. Veal, G. J. & Back, D. J. Metabolism of zidovudine. *Gen. Pharmacol. Vasc. Syst.* **26**, 1469–1475 (1995).
70. Urban, P. L., Goodall, D. M. & Bruce, N. C. Enzymatic microreactors in chemical analysis and kinetic studies. *Biotechnol. Adv.* **24**, 42–57 (2006).
71. Cohen, C. B., Chin-Dixon, E., Jeong, S. & Nikiforov, T. T. A microchip-based enzyme assay for protein kinase a. *Anal. Biochem.* **273**, 89–97 (1999).

72. Mao, H., Yang, T. & Cremer, P. S. Design and characterization of immobilized enzymes in microfluidic systems. *Anal. Chem.* **74**, 379–385 (2002).
73. Hadd, A. G., Raymond, D. E., Halliwell, J. W., Jacobson, S. C. & Ramsey, J. M. Microchip device for performing enzyme assays. *Anal. Chem.* **69**, 3407–3412 (1997).
74. Mao, S., Gao, D., Liu, W., Wei, H. & Lin, J.-M. Imitation of drug metabolism in human liver and cytotoxicity assay using a microfluidic device coupled to mass spectrometric detection. *Lab. Chip* **12**, 219–226 (2011).
75. Ma, B., Zhang, G., Qin, J. & Lin, B. Characterization of drug metabolites and cytotoxicity assay simultaneously using an integrated microfluidic device. *Lab. Chip* **9**, 232–238 (2009).
76. Baess, D., Jänig, G. R. & Ruckpaul, K. Interaction of the components of the cytochrome P-450 monooxygenase system from liver microsomes. I. Immobilization of the solubilized and partially purified protein components. *Acta Biol. Med. Ger.* **34**, 1745–1754 (1975).
77. Eremin, A. N., Usanov, S. A. & Mterlitsa, D. I. Immobilization of highly purified cytochrome P-450 from microsomes of rabbit liver. *Prikl. Biokhim. Mikrobiol.* **15**, 861–868 (1979).
78. Sheldon, R. A. Enzyme immobilization: The quest for optimum performance. *Adv. Synth. Catal.* **349**, 1289–1307 (2007).
79. Wong, L. S., Khan, F. & Micklefield, J. Selective covalent protein immobilization: strategies and applications. *Chem. Rev.* **109**, 4025–4053 (2009).
80. Jesionowski, T., Zdarta, J. & Krajewska, B. Enzyme immobilization by adsorption: a review. *Adsorption* **20**, 801–821 (2014).
81. Mattiasson, B. Affinity immobilization. In *Methods in Enzymology* 647–656, Academic Press (1988).
82. Green, N. M. Avidin. *Adv. Protein Chem.* **29**, 85–133 (1975).
83. Hermanson, G. T. Chapter 1 - Functional targets. In *Bioconjugate Techniques (Second Edition)* (ed. Hermanson, G. T.) 1–168, Academic Press (2008).
84. Hermanson, G. T. Chapter 3 - The reactions of bioconjugation. in *Bioconjugate Techniques (Third Edition)* (ed. Hermanson, G. T.) 229–258, Academic Press (2013).
85. Luo, Q., Mao, X., Kong, L., Huang, X. & Zou, H. High-performance affinity chromatography for characterization of human immunoglobulin G digestion with papain. *J. Chromatogr. B* **776**, 139–147 (2002).
86. Datta, S., Christena, L. R. & Rajaram, Y. R. S. Enzyme immobilization: an overview on techniques and support materials. *3 Biotech* **3**, 1–9 (2013).
87. Kim, D. & Herr, A. E. Protein immobilization techniques for microfluidic assays. *Biomicrofluidics* **7**, 041501 (2013).
88. Sheldon, R. A. & Pelt, S. van. Enzyme immobilisation in biocatalysis: Why, what and how. *Chem. Soc. Rev.* **42**, 6223–6235 (2013).
89. Zguris, J. C., Itle, L. J., Hayes, D. & Pishko, M. V. Microreactor microfluidic systems with human microsomes and hepatocytes for use in metabolite studies. *Biomed. Microdevices* **7**, 117–125 (2005).

90. Sakai-Kato, K., Kato, M., Homma, H., Toyo'oka, T. & Utsunomiya-Tate, N. Creation of a P450 array toward high-throughput analysis. *Anal. Chem.* **77**, 7080–7083 (2005).
91. Yang, H., Zheng, Y., Zhao, B., Shao, T., Shi, Q., Zhou, N. & Cai, W. Encapsulation of liver microsomes into a thermosensitive hydrogel for characterization of drug metabolism and toxicity. *Biomaterials* **34**, 9770–9778 (2013).
92. Lee, J., Kim, S. H., Kim, Y.-C., Choi, I. & Sung, J. H. Fabrication and characterization of microfluidic liver-on-a-chip using microsomal enzymes. *Enzyme Microb. Technol.* **53**, 159–164 (2013).
93. Wu, Q., Gao, D., Wei, J., Jin, F., Xie, W., Jiang, Y. & Liu, H. Development of a novel multi-layer microfluidic device towards characterization of drug metabolism and cytotoxicity for drug screening. *Chem. Commun.* **50**, 2762–2764 (2014).
94. Lee, J., Choi, J., Ha, S. K., Choi, I., Lee, S. H., Kim, D., Choi, N. & Sung, J. H. A microfluidic device for evaluating the dynamics of the metabolism-dependent antioxidant activity of nutrients. *Lab. Chip* **14**, 2948–2957 (2014).
95. Ueda, Y., Morigaki, K., Tatsu, Y., Yumoto, N. & Imaishi, H. Immobilization and activity assay of cytochrome P450 on patterned lipid membranes. *Biochem. Biophys. Res. Commun.* **355**, 926–931 (2007).
96. Schejbal, J., Řemínek, R., Zeman, L., Mádr, A. & Glatz, Z. On-line coupling of immobilized cytochrome P450 microreactor and capillary electrophoresis: A promising tool for drug development. *J. Chromatogr. A* **1437**, 234–240 (2016).
97. Nicoli, R., Bartolini, M., Rudaz, S., Andrisano, V. & Veuthey, J.-L. Development of immobilized enzyme reactors based on human recombinant cytochrome P450 enzymes for phase I drug metabolism studies. *J. Chromatogr. A* **1206**, 2–10 (2008).
98. Früh, V., IJzerman, A. P. & Siegal, G. How to catch a membrane protein in action: A review of functional membrane protein immobilization strategies and their applications. *Chem. Rev.* **111**, 640–656 (2011).
99. Wollenberg, L. A., Kabulski, J. L., Powell, M. J., Chen, J., Flora, D. R., Tracy, T. S. & Gannett, P. M. The use of immobilized cytochrome P4502C9 in PMMA-based plug flow bioreactors for the production of drug metabolites. *Appl. Biochem. Biotechnol.* **172**, 1293–1306 (2014).
100. Ménard, A., Huang, Y., Karam, P., Cosa, G. & Auclair, K. Site-specific fluorescent labeling and oriented immobilization of a triple mutant of CYP3A4 via c64. *Bioconjug. Chem.* **23**, 826–836 (2012).
101. Gannett, P. M., Kabulski, J., Perez, F. A., Liu, Z., Lederman, D., Locuson, C. W., Ayscue, R. R., Thomsen, N. M. & Tracy, T. S. Preparation, characterization, and substrate metabolism of gold-immobilized cytochrome P450 2C9. *J. Am. Chem. Soc.* **128**, 8374–8375 (2006).
102. Tan, C. Y., Hirakawa, H. & Nagamune, T. Supramolecular protein assembly supports immobilization of a cytochrome P450 monooxygenase system as water-insoluble gel. *Sci. Rep.* **5**, 8648 (2015).
103. Schneider, E. & Clark, D. S. Cytochrome P450 (CYP) enzymes and the development of CYP biosensors. *Biosens. Bioelectron.* **39**, 1–13 (2013).

104. Manz, A., Graber, N. & Widmer, H. M. Miniaturized total chemical analysis systems: A novel concept for chemical sensing. *Sens. Actuators B Chem.* **1**, 244–248 (1990).
105. Pandey, C. M., Augustine, S., Kumar, S., Kumar, S., Nara, S., Srivastava, S. & Malhotra, B. D. Microfluidics based point-of-care diagnostics. *Biotechnol. J.* **13**, (2018).
106. Sung, J. H., Wang, Y. I., Sriram, N. N., Jackson, M., Long, C., Hickman, J. J. & Shuler, M. L. Recent advances in body-on-a-chip systems. *Anal. Chem.* **91**, 330–351 (2019).
107. Nys, G. & Fillet, M. Microfluidics contribution to pharmaceutical sciences: From drug discovery to post marketing product management. *J. Pharm. Biomed. Anal.* **159**, 348–362 (2018).
108. Dittrich, P. S. & Manz, A. Lab-on-a-chip: microfluidics in drug discovery. *Nat. Rev. Drug Discov.* **5**, 210–218 (2006).
109. Culbertson, C. T., Mickleburgh, T. G., Stewart-James, S. A., Sellens, K. A. & Pressnall, M. Micro total analysis systems: fundamental advances and biological applications. *Anal. Chem.* **86**, 95–118 (2014).
110. Reyes, D. R., Iossifidis, D., Auroux, P.-A. & Manz, A. Micro total analysis systems. 1. Introduction, theory, and technology. *Anal. Chem.* **74**, 2623–2636 (2002).
111. Becker, H. & Gärtner, C. Polymer microfabrication technologies for microfluidic systems. *Anal. Bioanal. Chem.* **390**, 89–111 (2008).
112. Xia, Y. & Whitesides, G. M. Soft lithography. *Annu. Rev. Mater. Sci.* **28**, 153–184 (1998).
113. Duffy, D. C., McDonald, J. C., Schueller, O. J. A. & Whitesides, G. M. Rapid prototyping of microfluidic systems in poly(dimethylsiloxane). *Anal. Chem.* **70**, 4974–4984 (1998).
114. Franssila, S. Optical Lithography. In *Introduction to Microfabrication* 103–113, John Wiley & Sons, Ltd (2010).
115. Lin, C.-H., Lee, G.-B., Chang, B.-W. & Chang, G.-L. A new fabrication process for ultra-thick microfluidic microstructures utilizing SU-8 photoresist. *J. Micromechanics Microengineering* **12**, 590–597 (2002).
116. Sikanen, T., Tuomikoski, S., Ketola, R. A., Kostiainen, R., Franssila, S. & Kotiaho, T. Characterization of SU-8 for electrokinetic microfluidic applications. *Lab. Chip* **5**, 888–896 (2005).
117. Yang, L., Hao, X., Wang, C., Zhang, B. & Wang, W. Rapid and low cost replication of complex microfluidic structures with PDMS double casting technology. *Microsyst. Technol.* **20**, 1933–1940 (2014).
118. McCormick, R. M., Nelson, R. J., Alonso-Amigo, M. G., Benvegnu, D. J. & Hooper, H. H. Microchannel electrophoretic separations of DNA in injection-molded plastic substrates. *Anal. Chem.* **69**, 2626–2630 (1997).
119. Becker, H. & Heim, U. Hot embossing as a method for the fabrication of polymer high aspect ratio structures. *Sens. Actuators Phys.* **83**, 130–135 (2000).

120. McDonald, J. C., Duffy, D. C., Anderson, J. R., Chiu, D. T., Wu, H., Schueller, O. J. A. & Whitesides, G. M. Fabrication of microfluidic systems in poly(dimethylsiloxane). *Electrophoresis* **21**, 27–40 (2000).
121. Tähkä, S., Sarfraz, J., Urvas, L., Provenzani, R., Wiedmer, S. K., Peltonen, J., Jokinen, V. & Sikanen, T. Immobilization of proteolytic enzymes on replica-molded thiol-ene micropillar reactors via thiol-gold interaction. *Anal. Bioanal. Chem.* **411**, 2339–2349 (2019).
122. Ren, K., Zhou, J. & Wu, H. Materials for microfluidic chip fabrication. *Acc. Chem. Res.* **46**, 2396–2406 (2013).
123. Lee, J. N., Park, C. & Whitesides, G. M. Solvent compatibility of poly(dimethylsiloxane)-based microfluidic devices. *Anal. Chem.* **75**, 6544–6554 (2003).
124. Toepke, M. W. & Beebe, D. J. PDMS absorption of small molecules and consequences in microfluidic applications. *Lab. Chip* **6**, 1484–1486 (2006).
125. van Midwoud, P. M., Janse, A., Merema, M. T., Groothuis, G. M. M. & Verpoorte, E. Comparison of biocompatibility and adsorption properties of different plastics for advanced microfluidic cell and tissue culture models. *Anal. Chem.* **84**, 3938–3944 (2012).
126. Morra, M., Occhiello, E., Marola, R., Garbassi, F., Humphrey, P. & Johnson, D. On the aging of oxygen plasma-treated polydimethylsiloxane surfaces. *J. Colloid Interface Sci.* **137**, 11–24 (1990).
127. Chen, Y., Zhang, L. & Chen, G. Fabrication, modification, and application of poly(methyl methacrylate) microfluidic chips. *Electrophoresis* **29**, 1801–1814 (2008).
128. Shadpour, H., Hupert, M. L., Patterson, D., Liu, C., Galloway, M., Stryjewski, W., Goettert, J. & Soper, S. A. Multichannel microchip electrophoresis device fabricated in polycarbonate with an integrated contact conductivity sensor array. *Anal. Chem.* **79**, 870–878 (2007).
129. Sticker, D., Geczy, R., Häfeli, U. O. & Kutter, J. P. Thiol–ene based polymers as versatile materials for microfluidic devices for life sciences applications. *ACS Appl. Mater. Interfaces* **12**, 10080–10095 (2020).
130. Goddard, J. M. & Hotchkiss, J. H. Polymer surface modification for the attachment of bioactive compounds. *Prog. Polym. Sci.* **32**, 698–725 (2007).
131. Makamba, H., Kim, J. H., Lim, K., Park, N. & Hahn, J. H. Surface modification of poly(dimethylsiloxane) microchannels. *Electrophoresis* **24**, 3607–3619 (2003).
132. Brown, L., Koerner, T., Horton, J. H. & Oleschuk, R. D. Fabrication and characterization of poly(methylmethacrylate) microfluidic devices bonded using surface modifications and solvents. *Lab. Chip* **6**, 66–73 (2006).
133. Chan, C.-M., Ko, T.-M. & Hiraoka, H. Polymer surface modification by plasmas and photons. *Surf. Sci. Rep.* **24**, 1–54 (1996).
134. Situma, C., Wang, Y., Hupert, M., Barany, F., McCarley, R. L. & Soper, S. A. Fabrication of DNA microarrays onto poly(methyl methacrylate) with ultraviolet

patterning and microfluidics for the detection of low-abundant point mutations. *Anal. Biochem.* **340**, 123–135 (2005).
135. Carlborg, C. F., Haraldsson, T., Öberg, K., Malkoch, M. & Wijngaart, W. van der. Beyond PDMS: off-stoichiometry thiol–ene (OSTE) based soft lithography for rapid prototyping of microfluidic devices. *Lab. Chip* **11**, 3136–3147 (2011).
136. Machado, T. O., Sayer, C. & Araujo, P. H. H. Thiol-ene polymerisation: A promising technique to obtain novel biomaterials. *Eur. Polym. J.* **86**, 200–215 (2017).
137. Hoyle, C. E. & Bowman, C. N. Thiol-ene click chemistry. *Angew. Chem. Int. Ed.* **49**, 1540–1573 (2010).
138. Khire, V. S., Yi, Y., Clark, N. A. & Bowman, C. N. Formation and surface modification of nanopatterned thiol-ene substrates using step and flash imprint lithography. *Adv. Mater.* **20**, 3308–3313 (2008).
139. Ashley, J. F., Cramer, N. B., Davis, R. H. & Bowman, C. N. Soft-lithography fabrication of microfluidic features using thiol-ene formulations. *Lab. Chip* **11**, 2772 (2011).
140. Tähkä, S. M., Bonabi, A., Nordberg, M.-E., Kanerva, M., Jokinen, Ville. P. & Sikanen, T. M. Thiol-ene microfluidic devices for microchip electrophoresis: Effects of curing conditions and monomer composition on surface properties. *J. Chromatogr. A* **1426**, 233–240 (2015).
141. Sticker, D., Rothbauer, M., Lechner, S., Hehenberger, M.-T. & Ertl, P. Multi-layered, membrane-integrated microfluidics based on replica molding of a thiol–ene epoxy thermoset for organ-on-a-chip applications. *Lab. Chip* **15**, 4542–4554 (2015).
142. Jönsson, A., Svejdal, R. R., Bøgelund, N., Nguyen, T. T. T. N., Flindt, H., Kutter, J. P., Rand, K. D. & Lafleur, J. P. Thiol-ene monolithic pepsin microreactor with a 3D-printed interface for efficient UPLC-MS peptide mapping analyses. *Anal. Chem.* **89**, 4573–4580 (2017).
143. Hoffmann, C., Pinelo, M., Woodley, J. M. & Daugaard, A. E. Development of a thiol-ene based screening platform for enzyme immobilization demonstrated using horseradish peroxidase. *Biotechnol. Prog.* **33**, 1267–1277 (2017).
144. Lafleur, J. P., Kwapiszewski, R., Jensen, T. G. & Kutter, J. P. Rapid photochemical surface patterning of proteins in thiol–ene based microfluidic devices. *Analyst* **138**, 845–849 (2013).
145. Feidenhans'l, N. A., Lafleur, J. P., Jensen, T. G. & Kutter, J. P. Surface functionalized thiol-ene waveguides for fluorescence biosensing in microfluidic devices. *Electrophoresis* **35**, 282–288 (2014).
146. Çakmakçi, E., Yuce-Dursun, B. & Demir, S. Maleic anhydride functionalization of OSTE based coatings via thiol-ene "Click" reaction for the covalent immobilization of xylanase. *React. Funct. Polym.* **111**, 38–43 (2017).
147. Jonkheijm, P., Weinrich, D., Köhn, M., Engelkamp, H., Christianen, P. C. M., Kuhlmann, J., Maan, J. C., Nüsse, D., Schroeder, H., Wacker, R., Breinbauer, R., Niemeyer, C. M. & Waldmann, H. Photochemical surface patterning by the thiol-ene reaction. *Angew. Chem. Int. Ed.* **47**, 4421–4424 (2008).

148. Lafleur, J. P., Senkbeil, S., Novotny, J., Nys, G., Bøgelund, N., Rand, K. D., Foret, F. & Kutter, J. P. Rapid and simple preparation of thiol-ene emulsion-templated monoliths and their application as enzymatic microreactors. *Lab. Chip* **15**, 2162–2172 (2015).
149. Bataille, J., Viodé, A., Pereiro, I., Lafleur, J. P., Varenne, F., Descroix, S., Becher, F., Kutter, J. P., Roesch, C., Poüs, C., Taverna, M., Pallandre, A., Smadja, C. & Le Potier, I. On-a-chip tryptic digestion of transthyretin: a step toward an integrated microfluidic system for the follow-up of familial transthyretin amyloidosis. *The Analyst* **143**, 1077–1086 (2018).
150. Temiz, Y., Lovchik, R. D., Kaigala, G. V. & Delamarche, E. Lab-on-a-chip devices: How to close and plug the lab? *Microelectron. Eng.* **132**, 156–175 (2015).
151. Satyanarayana, S., Karnik, R. N. & Majumdar, A. Stamp-and-stick room-temperature bonding technique for microdevices. *J. Microelectromechanical Syst.* **14**, 392–399 (2005).
152. Sandström, N., Shafagh, R. Z., Vastesson, A., Carlborg, C. F., Wijngaart, W. van der & Haraldsson, T. Reaction injection molding and direct covalent bonding of OSTE+ polymer microfluidic devices. *J. Micromechanics Microengineering* **25**, 075002 (2015).
153. Cramer, N. B., Scott, J. P. & Bowman, C. N. Photopolymerizations of thiol−ene polymers without photoinitiators. *Macromolecules* **35**, 5361–5365 (2002).
154. Sikanen, T. M., Lafleur, J. P., Moilanen, M.-E., Zhuang, G., Jensen, T. G. & Kutter, J. P. Fabrication and bonding of thiol-ene-based microfluidic devices. *J. Micromechanics Microengineering* **23**, 037002 (2013).
155. Huikko, K., Östman, P., Grigoras, K., Tuomikoski, S., Tiainen, V.-M., Soininen, A., Puolanne, K., Manz, A., Franssila, S., Kostiainen, R. & Kotiaho, T. Poly(dimethylsiloxane) electrospray devices fabricated with diamond-like carbon–poly(dimethylsiloxane) coated su-8 masters. *Lab. Chip* **3**, 67–72 (2003).
156. Tähkä, S. M., Bonabi, A., Jokinen, V. P. & Sikanen, T. M. Aqueous and non-aqueous microchip electrophoresis with on-chip electrospray ionization mass spectrometry on replica-molded thiol-ene microfluidic devices. *J. Chromatogr. A* **1496**, 150–156 (2017).
157. Kampe, T., König, A., Schroeder, H., Hengstler, J. G. & Niemeyer, C. M. Modular microfluidic system for emulation of human phase I/phase II metabolism. *Anal. Chem.* **86**, 3068–3074 (2014).
158. Peterson, D. S., Rohr, T., Svec, F. & Fréchet, J. M. J. Enzymatic microreactor-on-a-chip: protein mapping using trypsin immobilized on porous polymer monoliths molded in channels of microfluidic devices. *Anal. Chem.* **74**, 4081–4088 (2002).
159. Oliver-Calixte, N. J., Uba, F. I., Battle, K. N., Weerakoon-Ratnayake, K. M. & Soper, S. A. Immobilization of lambda exonuclease onto polymer micropillar arrays for the solid-phase digestion of ds-DNAs. *Anal. Chem.* **86**, 4447–4454 (2014).

160. Slovakova, M., Minc, N., Bilkova, Z., Smadja, C., Faigle, W., Fütterer, C., Taverna, M. & Viovy, J.-L. Use of self assembled magnetic beads for on-chip protein digestion. *Lab. Chip* **5**, 935–942 (2005).
161. Losey, M. W., Jackman, R. J., Firebaugh, S. L., Schmidt, M. A. & Jensen, K. F. Design and fabrication of microfluidic devices for multiphase mixing and reaction. *J. Microelectromechanical Syst.* **11**, 709–717 (2002).
162. Haapala, M., Saarela, V., Pól, J., Kolari, K., Kotiaho, T., Franssila, S. & Kostiainen, R. Integrated liquid chromatography–heated nebulizer microchip for mass spectrometry. *Anal. Chim. Acta* **662**, 163–169 (2010).
163. Vlakh, E. G. & Tennikova, T. B. Flow-through immobilized enzyme reactors based on monoliths: II. Kinetics study and application. *J. Sep. Sci.* **36**, 1149–1167 (2013).
164. Munirathinam, R., Huskens, J. & Verboom, W. Supported catalysis in continuous-flow microreactors. *Adv. Synth. Catal.* **357**, 1093–1123 (2015).
165. Tallarek, U., Rapp, E., Scheenen, T., Bayer, E. & Van As, H. Electroosmotic and pressure-driven flow in open and packed capillaries: velocity distributions and fluid dispersion. *Anal. Chem.* **72**, 2292–2301 (2000).
166. Kutter, J. P., Mogensen, K. B., Klank, H. & Geschke, O. Microfluidics – Components. In *Microsystem Engineering of Lab-on-a-Chip Devices* 39–77, John Wiley & Sons, Ltd (2004).
167. Li, S. F. Y. Chapter 1 Introduction. In *Capillary Electrophoresis* vol. 52 1–30, Elsevier (1992).
168. Miserendino, S. & Tai, Y.-C. Pressure-driven microfluidics. In *Micro/Nano Technology Systems for Biomedical Applications: Microfluidics, Optics, and Surface Chemistry,* Oxford University Press (2010).
169. Wang, Y.-N. & Fu, L.-M. Micropumps and biomedical applications – A review. *Microelectron. Eng.* **195**, 121–138 (2018).
170. Unger, M. A., Chou, H.-P., Thorsen, T., Scherer, A. & Quake, S. R. Monolithic microfabricated valves and pumps by multilayer soft lithography. *Science* **288**, 113–116 (2000).
171. Zhou, J. & Poloyac, S. M. The effect of therapeutic hypothermia on drug metabolism and drug response: cellular mechanisms to organ function. *Expert Opin. Drug Metab. Toxicol.* **7**, 803–816 (2011).
172. Mogensen, K. B. & Kutter, J. P. Optical detection in microfluidic systems. *Electrophoresis* **30**, S92–S100 (2009).
173. Vandaveer, W. R., Pasas-Farmer, S. A., Fischer, D. J., Frankenfeld, C. N. & Lunte, S. M. Recent developments in electrochemical detection for microchip capillary electrophoresis. *Electrophoresis* **25**, 3528–3549 (2004).
174. Kubán, P. & Hauser, P. C. Fundamentals of electrochemical detection techniques for CE and MCE. *Electrophoresis* **30**, 3305–3314 (2009).
175. Sikanen, T., Tuomikoski, S., Ketola, R. A., Kostiainen, R., Franssila, S. & Kotiaho, T. Fully microfabricated and integrated SU-8-based capillary electrophoresis-

electrospray ionization microchips for mass spectrometry. *Anal. Chem.* **79**, 9135–9144 (2007).
176. Nordman, N., Sikanen, T., Moilanen, M.-E., Aura, S., Kotiaho, T., Franssila, S. & Kostiainen, R. Rapid and sensitive drug metabolism studies by SU-8 microchip capillary electrophoresis-electrospray ionization mass spectrometry. *J. Chromatogr. A* **1218**, 739–745 (2011).
177. Sakai-Kato, K., Kato, M. & Toyo'oka, T. Screening of inhibitors of uridine diphosphate glucuronosyltransferase with a miniaturized on-line drug-metabolism system. *J. Chromatogr. A* **1051**, 261–266 (2004).
178. Alebić-Kolbah, T. & Wainer, I. W. Microsomal immobilized-enzyme-reactor for on-line production of glucuronides in a HPLC column. *Chromatographia* **37**, 608–612 (1993).
179. Kim, H. S. & Wainer, I. W. The covalent immobilization of microsomal uridine diphospho-glucuronosyltransferase (UDPGT): Initial synthesis and characterization of an UDPGT immobilized enzyme reactor for the on-line study of glucuronidation. *J. Chromatogr. B* **823**, 158–166 (2005).
180. Sticker, D., Rothbauer, M., Ehgartner, J., Steininger, C., Liske, O., Liska, R., Neuhaus, W., Mayr, T., Haraldsson, T., Kutter, J. P. & Ertl, P. Oxygen management at the microscale: A functional biochip material with long-lasting and tunable oxygen scavenging properties for cell culture applications. *ACS Appl. Mater. Interfaces* **11**, 9730–9739 (2019).
181. Csiszár, A., Hersch, N., Dieluweit, S., Biehl, R., Merkel, R. & Hoffmann, B. Novel fusogenic liposomes for fluorescent cell labeling and membrane modification. *Bioconjug. Chem.* **21**, 537–543 (2010).
182. Hersch, N., Wolters, B., Ungvari, Z., Gautam, T., Deshpande, D., Merkel, R., Csiszar, A., Hoffmann, B. & Csiszár, A. Biotin-conjugated fusogenic liposomes for high-quality cell purification. *J. Biomater. Appl.* **30**, 846–856 (2016).
183. Kiiski, I. M. A., Pihlaja, T., Urvas, L., Witos, J., Wiedmer, S. K., Jokinen, V. P. & Sikanen, T. M. Overcoming the pitfalls of cytochrome P450 immobilization through the use of fusogenic liposomes. *Adv. Biosyst.* **3**, 1800245 (2019).
184. Sikanen, T., Zwinger, T., Tuomikoski, S., Franssila, S., Lehtiniemi, R., Fager, C.-M., Kotiaho, T. & Pursula, A. Temperature modeling and measurement of an electrokinetic separation chip. *Microfluid. Nanofluidics* **5**, 479–491 (2008).
185. Marmur, A. Soft contact: measurement and interpretation of contact angles. *Soft Matter* **2**, 12–17 (2006).
186. Ellman, G. L. Tissue sulfhydryl groups. *Arch. Biochem. Biophys.* **82**, 70–77 (1959).
187. Eyer, P., Worek, F., Kiderlen, D., Sinko, G., Stuglin, A., Simeon-Rudolf, V. & Reiner, E. Molar absorption coefficients for the reduced Ellman reagent: reassessment. *Anal. Biochem.* **312**, 224–227 (2003).
188. Sathyanarayanan, G., Haapala, M., Kiiski, I. & Sikanen, T. Digital microfluidic immobilized cytochrome P450 reactors with integrated inkjet-printed microheaters for

droplet-based drug metabolism research. *Anal. Bioanal. Chem.* **410**, 6677–6687 (2018).
189. Tiggelaar, R. M., Male, P. van, Berenschot, J. W., Gardeniers, J. G. E., Oosterbroek, R. E., Croon, M. H. J. M. de, Schouten, J. C., Berg, A. van den & Elwenspoek, M. C. Fabrication of a high-temperature microreactor with integrated heater and sensor patterns on an ultrathin silicon membrane. *Sens. Actuators Phys.* **119**, 196–205 (2005).
190. Jeon, N. L., Dertinger, S. K. W., Chiu, D. T., Choi, I. S., Stroock, A. D. & Whitesides, G. M. Generation of solution and surface gradients using microfluidic systems. *Langmuir* **16**, 8311–8316 (2000).
191. Cevc, G. & Richardsen, H. Lipid vesicles and membrane fusion. *Adv. Drug Deliv. Rev.* **38**, 207–232 (1999).
192. Chernomordik, L. V. & Kozlov, M. M. Mechanics of membrane fusion. *Nat. Struct. Mol. Biol.* **15**, 675–683 (2008).
193. Naumovska, E., Ludwanowski, S., Hersch, N., Braun, T., Merkel, R., Hoffmann, B. & Csiszár, A. Plasma membrane functionalization using highly fusogenic immune activator liposomes. *Acta Biomater.* **10**, 1403–1411 (2014).
194. Kube, S., Hersch, N., Naumovska, E., Gensch, T., Hendriks, J., Franzen, A., Landvogt, L., Siebrasse, J.-P., Kubitscheck, U., Hoffmann, B., Merkel, R. & Csiszár, A. Fusogenic liposomes as nanocarriers for the delivery of intracellular proteins. *Langmuir* **33**, 1051–1059 (2017).
195. Bailey, A. L. & Cullis, P. R. Membrane fusion with cationic liposomes: effects of target membrane lipid composition. *Biochemistry* **36**, 1628–1634 (1997).
196. Chesnoy, S. & Huang, L. Structure and function of lipid-DNA complexes for gene delivery. *Annu. Rev. Biophys. Biomol. Struct.* **29**, 27–47 (2000).
197. Bajoria, R. & Contractor, S. F. Effect of the size of liposomes on the transfer and uptake of carboxyfluorescein by the perfused human term placenta. *J. Pharm. Pharmacol.* **49**, 675–681 (1997).
198. Malinin, V. S., Frederik, P. & Lentz, B. R. Osmotic and curvature stress affect PEG-induced fusion of lipid vesicles but not mixing of their lipids. *Biophys. J.* **82**, 2090–2100 (2002).
199. Hoekstra, D., De Boer, T., Klappe, K. & Wilschut, J. Fluorescence method for measuring the kinetics of fusion between biological membranes. *Biochemistry* **23**, 5675–5681 (1984).
200. Smith, P. K., Krohn, R. I., Hermanson, G. T., Mallia, A. K., Gartner, F. H., Provenzano, M. D., Fujimoto, E. K., Goeke, N. M., Olson, B. J. & Klenk, D. C. Measurement of protein using bicinchoninic acid. *Anal. Biochem.* **150**, 76–85 (1985).
201. Hochman, Y., Zakim, D. & Vessey, D. A. A kinetic mechanism for modulation of the activity of microsomal UDP-glucuronyltransferase by phospholipids. Effects of lysophosphatidylcholines. *J. Biol. Chem.* **256**, 4783–4788 (1981).
202. Palaiokostas, M., Ding, W., Shahane, G. & Orsi, M. Effects of lipid composition on membrane permeation. *Soft Matter* **14**, 8496–8508 (2018).

203. Kiiski, I., Ollikainen, E., Artes, S., Järvinen, P., Jokinen, V. & Sikanen, T. Drug glucuronidation assays on human liver microsomes immobilized on microfluidic flow-through reactors. *Eur. J. Pharm. Sci.* **158**, 105677 (2021).
204. Ejserholm, F., Stegmayr, J., Bauer, P., Johansson, F., Wallman, L., Bengtsson, M. & Oredsson, S. Biocompatibility of a polymer based on off-stoichiometry thiol-enes + epoxy (OSTE+) for neural implants. *Biomater. Res.* **19**, 19 (2015).
205. Berry, L. M. & Zhao, Z. An examination of IC_{50} and IC_{50}-shift experiments in assessing time-dependent inhibition of CYP3A4, CYP2D6 and CYP2C9 in human liver microsomes. *Drug Metab. Lett.* **2**, 51–59 (2008).
206. Horspool, A. M., Wang, T., Scaringella, Y.-S., Taub, M. E. & Chan, T. S. Human liver microsomes immobilized on magnetizable beads: a novel approach to study *in vitro* drug metabolism. *Drug Metab. Dispos.* **48**, 645–654 (2020).
207. Kwisnek, L., Nazarenko, S. & Hoyle, C. E. Oxygen transport properties of thiol-ene networks. *Macromolecules* **42**, 7031–7041 (2009).
208. Cramer, N. B. & Bowman, C. N. Kinetics of thiol-ene and thiol-acrylate photopolymerizations with real-time fourier transform infrared. *J. Polym. Sci. Part Polym. Chem.* **39**, 3311–3319 (2001).
209. Vitale, A., Hennessy, M. G., Matar, O. K. & Cabral, J. T. A unified approach for patterning via frontal photopolymerization. *Adv. Mater.* **27**, 6118–6124 (2015).
210. Brennan, M. D., Rexius-Hall, M. L., Elgass, L. J. & Eddington, D. T. Oxygen control with microfluidics. *Lab. Chip* **14**, 4305–4318 (2014).
211. Oomen, P. E., Skolimowski, M. D. & Verpoorte, E. Implementing oxygen control in chip-based cell and tissue culture systems. *Lab. Chip* **16**, 3394–3414 (2016).
212. Oppegard, S. C., Blake, A. J., Williams, J. C. & Eddington, D. T. Precise control over the oxygen conditions within the Boyden chamber using a microfabricated insert. *Lab. Chip* **10**, 2366–2373 (2010).
213. Abaci, H. E., Devendra, R., Soman, R., Drazer, G. & Gerecht, S. Microbioreactors to manipulate oxygen tension and shear stress in the microenvironment of vascular stem and progenitor cells. *Biotechnol. Appl. Biochem.* **59**, 97–105 (2012).
214. Skolimowski, M., Nielsen, M. W., Emnéus, J., Molin, S., Taboryski, R., Sternberg, C., Dufva, M. & Geschke, O. Microfluidic dissolved oxygen gradient generator biochip as a useful tool in bacterial biofilm studies. *Lab. Chip* **10**, 2162–2169 (2010).
215. Peng, C.-C., Liao, W.-H., Chen, Y.-H., Wu, C.-Y. & Tung, Y.-C. A microfluidic cell culture array with various oxygen tensions. *Lab. Chip* **13**, 3239–3245 (2013).
216. Cretton, E. M., Xie, M. Y., Bevan, R. J., Goudgaon, N. M., Schinazi, R. F. & Sommadossi, J. P. Catabolism of 3'-azido-3'-deoxythymidine in hepatocytes and liver microsomes, with evidence of formation of 3'-amino-3'-deoxythymidine, a highly toxic catabolite for human bone marrow cells. *Mol. Pharmacol.* **39**, 258–266 (1991).
217. Pan-Zhou, X.-R., Cretton-Scott, E., Zhou, X.-J., Yang, M.-X., Lasker, J. M. & Sommadossi, J.-P. Role of human liver P450s and cytochrome b5 in the reductive metabolism of 3′-azido-3′-deoxythymidine (AZT) to 3′-amino-3′-deoxythymidine. *Biochem. Pharmacol.* **55**, 757–766 (1998).

218. Eagling, V. A., Howe, J. L., Barry, M. J. & Back, D. J. The metabolism of zidovudine by human liver microsomes in vitro: Formation of 3′-amino-3′-deoxythymidine. *Biochem. Pharmacol.* **48**, 267–276 (1994).
219. Fayz, S. & Inaba, T. Zidovudine azido-reductase in human liver microsomes: activation by ethacrynic acid, dipyridamole, and indomethacin and inhibition by human immunodeficiency virus protease inhibitors. *Antimicrob. Agents Chemother.* **42**, 1654–1658 (1998).
220. Sathyanarayanan, G., Haapala, M. & Sikanen, T. Interfacing digital microfluidics with ambient mass spectrometry using SU-8 as dielectric layer. *Micromachines* **9**, 649 (2018).
221. Sathyanarayanan, G., Haapala, M. & Sikanen, T. Digital microfluidics-enabled analysis of individual variation in liver cytochrome P450 activity. *Anal. Chem.* **92**, 14693–14701 (2020).
222. Pihlaja, T., Kiiski, I. & Sikanen, T. Mechanistic study of time-dependent cytochrome P450 inhibition using microfluidic immobilized enzyme assays. In *Nordic POP 1st annual meeting* (2019).
223. Senkbeil, S., Aho, J., Yde, L., Lindvold, L. R., Stensborg, J. F., Rantanen, J., Lafleur, J. P. & Kutter, J. P. Roll-to-plate fabrication of microfluidic devices with rheology-modified thiol-ene resins. *J. Micromechanics Microengineering* **26**, 075014 (2016).